Functional role of small extracellular vesicles associated DNA and chromatin in pediatric acute myeloid leukemia (AML)

Dissertation
for
the doctoral degree of
Dr. rer. nat.

from the Faculty of Biology
University of Duisburg-Essen
Germany

Submitted by

Venkatesh Kumar Chetty, MSc

Born in Coimbatore, India

Date of submission - December 2022

The experiments underlying the present work were conducted at the Cancer Exosomes AG, Department of Pediatrics III, University Hospital Essen, Essen, Germany.

1. Examiner: Priv.-Doz. Dr. Basant Kumar Thakur

2. Examiner: Prof. Dr. Joachim Fandrey

3. Examiner: Prof. Dr. Nikolas H. Stoecklein

4. Chair of the Board of Examiners: Prof. Dr. Bernd Giebel

Date of the oral examination: 29.03.2023

Table of Contents

Summary

Acute myeloid leukemia (AML) is the second most common pediatric leukemia, with relapse in >30% of the patients. Although pediatric AML patients' survival rate has been significantly improved in the last years using innovative and advanced therapeutic strategies, it remains unclear how AML cells evade chemotherapy resulting in relapse. In AML, it is known that there is a crosstalk between AML blasts and critical components in the bone marrow microenvironment (BMM), resulting in abnormal proliferation and differentiation blockage of stem cells, which disrupts the normal hematopoiesis in favor of leukemogenesis. Besides chromosomal abnormalities and clonal disorders, recent studies demonstrated that proteins and RNA cargoes associated with small extracellular vesicles (sEVs) released by AML blasts execute the molecular changes in the BMM and transform it into AML permissive microenvironment. Nevertheless, sEVs also contain other biomolecular cargoes, including DNA. Therefore, the current study aimed to evaluate the functional role of DNA and DNA-protein complex (chromatin) associated with sEVs in pediatric AML.

sEVs are membrane-enclosed nanovesicles (30-200 nm) released by both healthy and tumor cells into the extracellular space. Detailed functional studies of DNA associated with sEVs (EV-DNA) were set back due to the lack of an sEV isolation method that efficiently separates sEVs from cell-free DNA (cfDNA) and apoptotic bodies. In this regard, using controlled culture conditions, we have established and optimized an efficient sEV isolation method suitable for EV-DNA functional studies by combining tangential flow filtration, size-exclusion chromatography, and ultrafiltration, which we have termed "TSU". Our results demonstrated that TSU provides sEV-enriched fractions F2 and F3 with only EV-DNA without cell-free DNA and apoptotic bodies. Interestingly, we found that EV-DNA derived from AML-sEVs interacts with healthy bone marrow-derived mesenchymal stromal cells (BM-MSCs), a predominant component of BMM that has a pivotal role in clonal hematopoiesis and leukemogenesis.

Next, three-dimensional (3D) confocal imaging analysis using Imaris software intriguingly revealed that most foreign EV-DNA is restricted at the recipient cell membrane barrier. At the same time, the remaining EV-DNA overcomes this barrier and localizes in the cytoplasm and nucleus. In the cytoplasm, we found that EV-DNA interacts with cytoplasmic DNA sensors (cGAS/STING) and endosomal proteins that direct towards lysosomal degradation (Rab5/Rab7). At this point, this finding raises the question of whether EV-DNA is alone or bound with DNA-binding proteins.

Although many studies showed that histones are abundant in sEVs, they have not shown their direct association with EV-DNA. For the first time, using atomic force microscopy, cryo-electron microscopy, and 3D confocal imaging, we revealed that sEVs contain DNA and protein complexes resembling chromatin-like structures, which we termed EV-chromatin or Exogenotin. Mass spectrometry analysis of AML-derived EV-DNA-associated proteins showed that in addition to histones, desmosome proteins and S100 proteins were also abundant in EV-chromatin. Direct EV-DNA association or bound with histones is further confirmed by Western blot. Additionally, we revealed that healthy BM-MSCs treated with AML-sEVs downregulated p53 expression and its cell cycle (p21) and apoptosis-related proteins (BAX and PUMA). To further demonstrate whether the observed effect could be due to EV-DNA or EV-chromatin, engineered polymersomes were utilized for the EV-DNA or EV-chromatin packaging. Surprisingly, we found that EV-chromatin, but not EV-DNA, regulates the proliferation of the BM-MSC cells by suppressing the p53-mediated transcription of p21. On the other hand, EV-chromatin apparently upregulated canonical p53 inhibitor (MDM2) in BM-MSCs. Nevertheless, inhibition of MDM2 either by using inhibitor Siremadlin or by siRNA restored p53 activity in BM-MSCs. Altogether, our results indicate that AML-derived EV-chromatin causes p53 dysfunction in healthy BM-MSCs through MDM2. In the future, revealing the role of additional proteins like S100 associated with EV-chromatin in BMM would enable the development of promising therapeutics to treat pediatric AML patients.

Zusammenfassung

Die akute myeloische Leukämie (AML) ist die zweithäufigste pädiatrische Leukämie, die bei mehr als 30 % der Patienten zu einem Rückfall führt. Obwohl die Überlebensrate pädiatrischer AML-Patienten in den letzten Jahren durch innovative und fortschrittliche Therapiestrategien erheblich verbessert werden konnte, ist nach wie vor unklar, wie AML-Zellen der Chemotherapie entgehen können, was zu einem Rückfall führen kann. Es ist bekannt, dass es bei der AML eine Wechselwirkung zwischen AML-Blasten und kritischen Komponenten in der Mikroumgebung des Knochenmarks (BMM) gibt, die zu einer abnormalen Proliferation und einer Differenzierungsblockade der Stammzellen führt, wodurch die normale Hämatopoese zugunsten der Leukämogenese gestört wird. Neben Chromosomenanomalien und klonalen Aberrationen haben jüngste Studien gezeigt, dass kleine extrazelluläre Vesikel (sEVs), die mit Proteinen und RNA beladen sind, und die von AML-Blasten freigesetzt werden, diese molekularen Veränderungen im BMM bewirken und es in eine permissive Mikroumgebung für AML verwandeln. Allerdings enthalten sEVs auch andere biomolekulare Strukturen, einschließlich DNA. Ziel der aktuellen Studie war es daher, die funktionelle Rolle der DNA und des DNA-Protein-Komplexes (Chromatin) in Verbindung mit sEVs bei pädiatrischer AML zu untersuchen.

sEVs sind membranumschlossene Nanovesikel (30-200 nm), die sowohl von gesunden Zellen als auch von Tumorzellen in den extrazellulären Raum abgegeben werden. Detaillierte funktionelle Studien mit sEVs assoziierter DNA (EV-DNA) wurden durch das Fehlen einer sEV-Isolierungsmethode, die sEVs effizient von zellfreier DNA (cfDNA) und apoptotischen Vesikeln trennt, zurückgeworfen. In diesem Zusammenhang haben wir unter kontrollierten Kulturbedingungen eine effiziente sEV-Isolierungsmethode etabliert und optimiert, die sich für funktionelle EV-DNA-Studien eignet, indem wir Tangentialflussfiltration, Größenausschlusschromatographie und Ultrafiltration miteinander kombinieren, was wir als "TSU" bezeichnet haben. Unsere Ergebnisse zeigen, dass TSU sEV-angereicherte Fraktionen F2 und F3 mit ausschließlich EV-DNA ohne zellfreie DNA und apoptotische Vesikel liefern. Interessanterweise fanden wir heraus, dass EV-DNA aus AML-sEVs mit aus dem Knochenmark stammenden gesunde mesenchymalen Stromazellen (BM-MSCs) kommuniziert, die eine vorherrschende Komponente des BMM darstellt und eine zentrale Rolle bei der klonalen Hämatopoese und Leukämogenese spielt.

Eine dreidimensionale (3D) konfokale Bildgebungsanalyse mit der Imaris-Software ergab, dass der größte Teil der fremden EV-DNA auf die Membranbarriere der Empfängerzellen

beschränkt ist. Trotzdem überwindet die verbleibende EV-DNA diese Barriere und lokalisiert sich im Zytoplasma und im Zellkern. Im Zytoplasma fanden wir heraus, dass EV-DNA mit zytoplasmatischen DNA-Sensoren (cGAS/STING) und endosomalen Proteinen interagiert, die zum lysosomalen Abbau führen (Rab5/Rab7). Diese Erkenntnis wirft die Frage auf, ob EV-DNA allein oder in Verbindung mit DNA-bindenden Proteinen vorliegt.

Obwohl viele Studien gezeigt haben, dass Histone in sEVs reichlich vorhanden sind, konnten sie keine direkte Verbindung mit der EV-DNA zeigen. Mit Hilfe der Rasterkraftmikroskopie, der Kryo-Elektronenmikroskopie und der konfokalen 3D-Bildgebung konnten wir erstmals zeigen, dass sEVs DNA- und Proteinkomplexe enthalten, die chromatinähnliche Strukturen aufweisen, die wir als EV-Chromatin oder Exogenotin bezeichnet haben. Die massenspektrometrische Analyse von EV-DNA-assoziierten Proteinen zeigte, dass neben Histonen auch Desmosomenproteine und S100-Proteine reichlich im EV-Chromatin vorhanden waren. Die direkte Assoziation von EV-DNA mit Histonen oder deren Bindung an Histone wurde durch Western Blot weiter bestätigt. Darüber hinaus konnten wir zeigen, dass mit AML-sEVs behandelte BM-MSCs die Expression von p53 und dessen Zellzyklus- (p21) und Apoptose-bezogenen Proteinen (BAX und PUMA) herunterregulieren. Um weiter zu zeigen, ob der beobachtete Effekt auf EV-DNA oder EV-Chromatin zurückzuführen ist, wurden für die Verpackung der EV-DNA oder des EV-Chromatins konstruierte Polymersomen verwendet. Überraschenderweise stellten wir fest, dass EV-Chromatin, nicht aber EV-DNA, die Proliferation der BM-MSC-Zellen durch Unterdrückung der p53-vermittelten Transkription von p21 reguliert. Andererseits hat EV-Chromatin offenbar den kanonischen p53-Inhibitor (MDM2) in BM-MSCs hochreguliert. Die Hemmung von MDM2 durch den Inhibitor Siremadlin oder siRNA stellte jedoch die p53-Aktivität in BM-MSCs wieder her. Insgesamt deuten unsere Ergebnisse darauf hin, dass das aus AML stammende EV-Chromatin über MDM2 eine p53-Dysfunktion in gesunde BM-MSCs verursacht. In Zukunft würde die Aufdeckung der Rolle zusätzlicher Proteine wie S100, die mit EV-Chromatin in BMM assoziiert sind, die Entwicklung vielversprechender Therapeutika zur Behandlung pädiatrischer AML-Patienten ermöglichen.

List of abbreviations

AFM	Atomic Force Microscopy
AML	Acute Myeloid Leukemia
BM-HSCs	Bone marrow-derived hematopoietic stem cells
BM-MSCs	Bone marrow-derived mesenchymal stem cells
BMM	Bone marrow microenvironment
cfDNA	Cell-free DNA
cGAS	Cyclic GMP-AMP synthase
CML	Chronic Myeloid Leukemia
EPs	Extracellular Particles
ESCRT	Endosomal sorting complex required for transport
EVs	Extracellular Vesicles
gDNA	Genomic DNA
HSCs	Hematopoietic stem cells
HSPCs	Hematopoietic stromal progenitor cells
ILVs	Intraluminal Vesicles
lEVs	Large Extracellular Vesicles
miRNA	Micro-RNA
MSCs	Mesenchymal stem cells
mtDNA	Mitochondrial DNA
MVBs	Multivesicular Bodies
PBP	Polymer-based precipitation
PEG	Polyethylene glycol
sEVs	Small Extracellular Vesicles
STING	Stimulator of interferon genes
TDSE	Tumor-derived small extracellular vesicles
TFF	Tangential flow filtration
TSU	Tangential flow filtration + Size exclusion chromatography + Ultrafiltration
UC	Ultracentrifugation

1. Introduction

1.1. Pediatric acute myeloid leukemia

Acute myeloid leukemia (AML) is a hematopoietic disorder in which bone marrow makes multitude of immature white blood cells called myeloblasts or leukemic blasts (Huang et al. 2020). AML occurs mainly in adults; however, 15 to 20% of all pediatric acute leukemias correspond to only pediatric AML (Lagunas-Rangel et al. 2017; de Rooij, Zwaan, and van den Heuvel-Eibrink 2015). Over the last decades, the survival rate of pediatric AML patients has been significantly improved by up to 75% using intensive chemotherapy and stem-cell transplantation (Reinhardt, Antoniou, and Waack 2022). However, many pediatric AML patients develop chemoresistance during remission resulting in relapse in more than 30 % of patients, and the mechanism involved in it is not well understood.

Recent advances in the characterization of the molecular and genomic landscapes of pediatric AML have resulted in the development of new treatments, such as molecular-targeted therapy and immunotherapy (Chen and Glasser 2020). The strategy of pediatric AML management adopted by the Department of Pediatrics III, University Hospital of Essen includes, but is not limited to, innovative diagnostic and therapeutic interventions as well as supportive care. In addition to advancing our pediatric AML therapeutic strategy, enhancing our understanding of the biological properties of AML in more detail could open new insights to expand and personalize pediatric AML treatment options in the next few years.

1.2. Bone marrow microenvironment in AML

AML is the most aggressive leukemia, which progresses very rapidly characterized by chromosomal rearrangements and gene mutations leading to aberrant clonal expansion and differentiation blockage of hematopoietic stem cells (HSCs), their progenitor cells (HSPCs) and mesenchymal stem cells (MSCs) in the bone marrow microenvironment (BMM) resulting in bone marrow failure (Asada et al. 2019; Yao et al. 2021; Rubnitz, Gibson, and Smith 2010; Lipner 2022). BMM is known to play a vital role in AML progression and contributes to treatment failure or success (Hanahan and Coussens 2012). BMM is a complex niche that contains various cell populations, including endothelial cells, HSCs, MSCs, fibroblasts, osteoblasts, adipocytes, and many immune cells (Figure 1) (Duarte, Hawkins, and Lo Celso 2018).
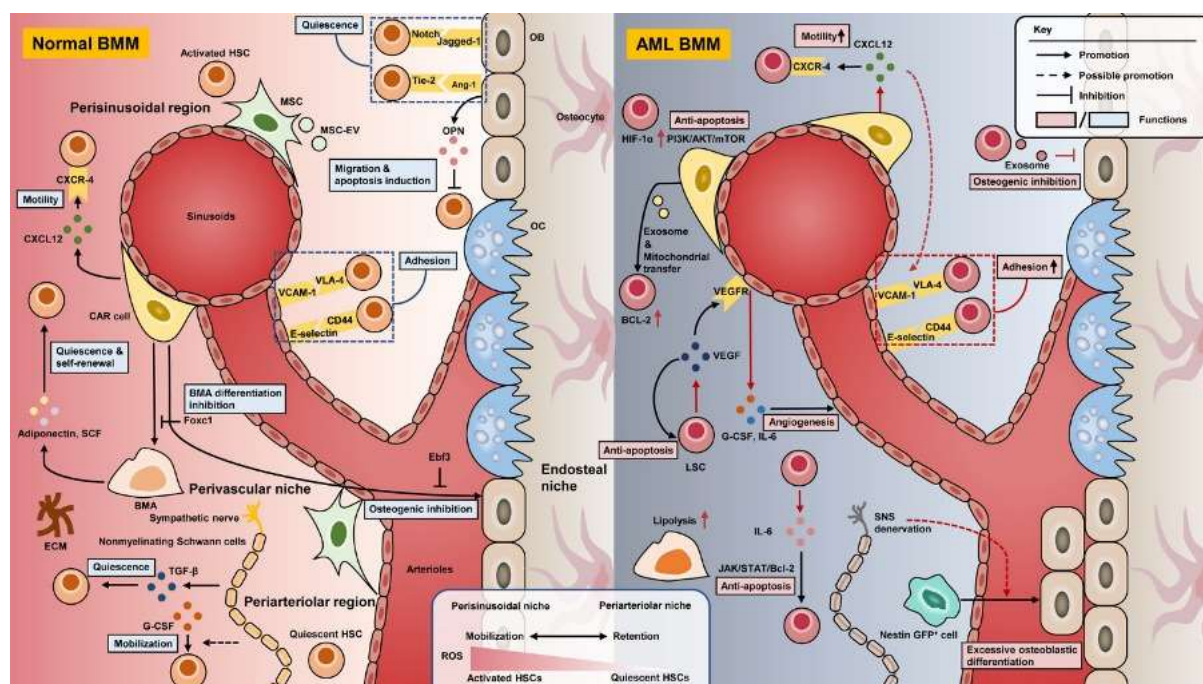
Figure 1: Comparison between the normal and AML BMM. BMM comprises hematopoietic cells, stem cells, endothelial cells, fibroblasts, and extracellular matrix. Compared to normal BMM, AML BMM includes differential remodeling of the vasculature, alteration of cytokines secretion, involvement of hypoxia microenvironment, and maintenance of low ROS, which lead to AML development and further chemoresistance. AML acute myeloid leukemia, BMM bone marrow microenvironment, HSC hematopoietic stem cells, MSC mesenchymal stem cells, MSC-EV MSC-derived extracellular vesicles, TGF-β transforming growth factor-β, HIF hypoxia-inducible factor, ROS reactive oxygen species. Figure adapted from Yao et al. (Yao et al. 2021).

To support normal hematopoiesis, BM-HSCs receive multiple signals from the neighboring cells in BMM to support BM-HSC's self-renewal and differentiation (Greenbaum et al. 2013; Ding et al. 2012). In AML, it is known that AML blasts send various signals to different components in the BMM, which disrupts the normal hematopoiesis maintained by stromal cells and in favor of the development of leukemogenesis or chemoresistance (Schepers et al. 2013; Anderson et al. 2020; Sison and Brown 2011; Sendker, Waack, and Reinhardt 2021; Duarte, Hawkins, and Lo Celso 2018; Waclawiczek et al. 2020). Besides chromosomal abnormalities and clonal disorders, it has been shown recently that the small extracellular vesicles (sEVs) released by leukemia cells induce molecular changes in the BMM and transform BMM into leukemia permissive microenvironment (Kumar et al. 2018; Kumar et al. 2016; Butler, Abdelhamed, and Kurre 2018).

One of the most studied tumor suppressor proteins, p53 is known for its role in cell cycle regulation for preventing the propagation of cells with serious DNA damage through the transactivation of its target genes to induce cell cycle arrest or apoptosis (Ozaki and Nakagawara 2011; Chen 2016). In AML, p53 mutations are prevalent in 5−8% of newly diagnosed patients and 30−40% of therapy-resistant patients (Seifert et al. 2009; Nahi et al.

2008). In addition, p53 function is not only suppressed through mutations but also through the overexpression of canonical p53 negative regulators such as MDM2 or its homolog MDM4 (Kubbutat, Jones, and Vousden 1997; Quintas-Cardama et al. 2017).

It is well known that p53 is highly expressed in one of the critical components of BMM, such as BM-MSCs, which results in the transcriptional activation of the cell cycle arrest protein, p21, required to maintain normal hematopoiesis (Asai et al. 2011; Fei et al. 2014). Also, Boregowda et al. recently demonstrated that $p53^{-/-}$ BM-MSCs are defective in supporting normal hematopoiesis due to the low secretion of various cytokines, including CXCL12 and CSF1 (Boregowda et al. 2018).

1.3. Extracellular vesicles (EVs) and their nomenclature

Extracellular vesicles (EVs) are heterogeneous populations of phospholipid bilayer-surrounded particles ranging from 30–10000 nm released by most cell types into the extracellular space. Unlike eukaryotic cells, EVs do not contain a functional nucleus and, therefore, cannot replicate (Doyle and Wang 2019; Willms et al. 2018; Zaborowski et al. 2015; Thery et al. 2018). The most widely studied EVs, such as exosomes, were first identified in 1983 by Johnstone and Stahl laboratories (Pan and Johnstone 1983; Harding, Heuser, and Stahl 1983). They showed that immature reticulocytes labeled transferrin receptors were repackaged and secreted out as small vesicles (~ 50 nm) containing only mature reticulocytes into the extracellular space. For many years, it was envisioned that cells would release EVs as part of the waste disposal system. Only in recent years, EVs have gained greater attention in scientific research due to their diverse functions in intercellular signaling both in normal and pathophysiological conditions (Yanez-Mo et al. 2015; Admyre et al. 2007).

EVs are very heterogenous in nature due to their different origin, modes of release, sizes and cargoes (Anand, Samuel, and Mathivanan 2021). EVs are commonly found in almost all human body fluids, including blood, urine, saliva, cerebrospinal fluid, and breast milk (Thery et al. 2006; Armstrong and Wildman 2018; Pulliero et al. 2019). EVs contain functional cargoes of biological molecules such as proteins (Logozzi et al. 2009; Kumar et al. 2018), lipids (Ramos-Garcia et al. 2023), metabolites (Zebrowska et al. 2019; Harmati et al. 2021), and nucleic acids including DNA (Thakur et al. 2014; Kahlert et al. 2014), mRNA (Lotvall and Valadi 2007; Valadi et al. 2007), micro RNA (miRNA) (Mittelbrunn et al. 2011; Umezu et al. 2014), and long noncoding RNA (lncRNA) (Lee et al. 2019; Zeng et al. 2019). The composition and secretion level of EVs can be influenced by various environmental factors and health conditions

(Patel et al. 2017; King, Michael, and Gleadle 2012). Based on their size and biogenesis, EVs are currently classified into exosomes (50–150 nm), ectosomes or microvesicles (100–1000 nm), migrasomes (500–3000 nm), large oncosomes (1000–10,000 nm), and apoptotic bodies (1000–5000 nm) (Figure 2) (Hristov et al. 2004; Yanez-Mo et al. 2015; Muller et al. 2014; Ghanam et al. 2022; Anand, Samuel, and Mathivanan 2021).
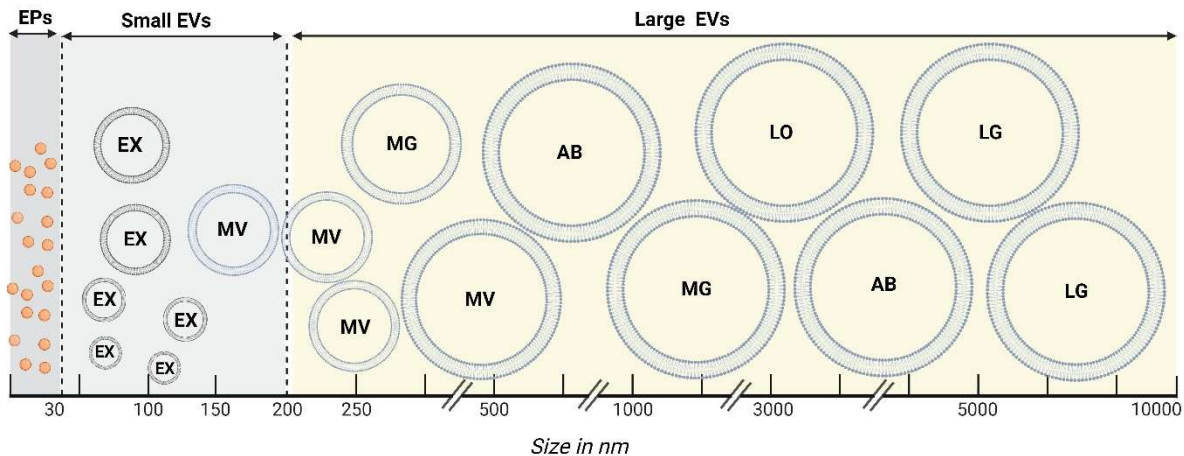

Figure 2. Heterogeneous populations of extracellular vesicles (EVs). Small extracellular vesicles (sEVs) have a size range of 30–200 nm. sEVs population includes both exosomes (EX) and microvesicles (MV). Large extracellular vesicles or lEVs (200–10000 nm) are membrane-enclosed vesicles that are larger than 200 nm. lEVs include migrasomes (MG), large oncosomes (LO), and apoptotic bodies (AB). Recently discovered extracellular particles (EPs) do not contain lipid bilayer enclosed membrane and are less than 30 nm. EPs include exomeres, supermeres, and chromatimeres.

Recently, new 30-nm-sized non-membranous RNA containing extracellular particles (EPs) secreted by cells were revealed and named exomeres and supermeres (Zhang et al. 2018; Zhang et al. 2021). Similarly, another EPs containing DNase-resistant chromatin known as chromatimeres was recently found (Choi et al. 2019). Unlike other EV subtypes, biogenesis and the biological function of exomeres, supermeres, and chromatimeres are still unclear.

1.4. Small extracellular vesicles (sEVs) and their biogenesis

Among the various EV subtypes, exosomes and microvesicles are the most well studied due to their significant impact on health and disease. (Raposo and Stoorvogel 2013). Since there is a size overlap (100–150 nm) and no consensus has yet emerged on specific EV markers of exosomes and microvesicles, MISEV2018 guidelines suggest the EV researchers to use the term small extracellular vesicles (sEVs) for the EVs that are smaller than 200 nm and the large extracellular vesicles (lEVs) for the EVs that are larger than 200 nm (Thery et al. 2018). Initially, exosomes were regarded as cellular debris generated from cell damage that has no biological function on neighboring cells. Only in the past few years, scientists identified that

exosomes contain complex functional cargo of biomolecules that can be delivered to the target cells to reprogram their cellular physiological processes (Kanada et al. 2015).

Exosomes are secreted through unique biogenesis pathway via multivesicular bodies (MVBs) or late endosomes (Figure 3). Exosomes production starts with the process of inward budding of MVBs to generate intraluminal vesicles (ILVs) (Zhang et al. 2019). MVBs were generated through different proposed pathways, and the most well-known is the endosomal sorting complex required for transport (ESCRT) dependent pathway (Wollert and Hurley 2010). We have clearly elaborated the currently known MVBs generation pathways in our recently published review (Ghanam et al. 2022). During the formation of MVBs, certain proteins, including tetraspanins, are incorporated into the invaginating membrane of ILVs. At the same time, some cytosolic proteins, nucleic acids, and lipids are attached and enclosed within the ILVs (Abels and Breakefield 2016). Afterward, most of the MVBs containing ILVs fuse with the plasma membrane, and the ILVs are released as exosomes into the extracellular space (Janas et al. 2016).
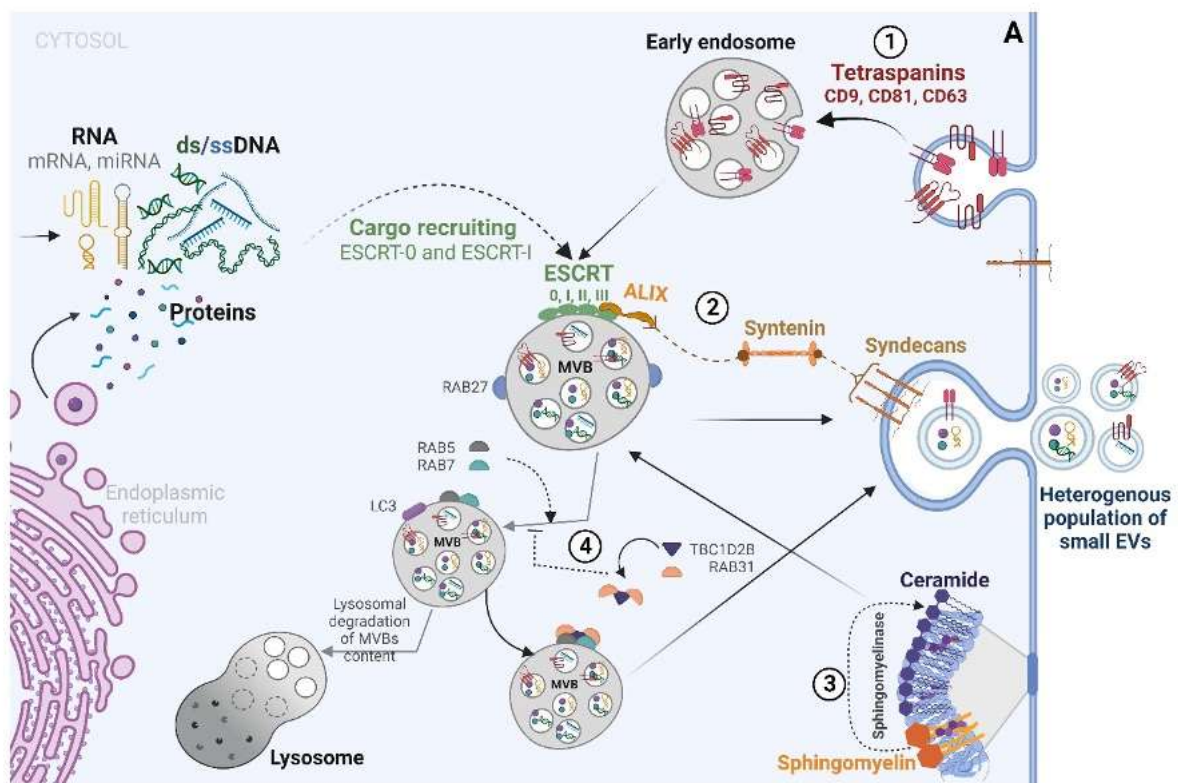
Figure 3. Small extracellular vesicles biogenesis. Cells release heterogeneous population of small extracellular vesicles (sEVs), including exosomes and microvesicles. sEV biogenesis starts from the early endosomes enriched with different tetraspanin microdomains, which then leads to the formation of late endosomes or multivesicular bodies (MVBs) to generate intraluminal vesicles. Various mechanisms have been proposed for the MVBs formation and cargo loading. The most studied and well-known mechanism is the endosomal sorting complex required for transport (ESCRT) dependent pathway. Figure modified from Ghanam et al. (Ghanam et al. 2022).

It is also known that some of the MVBs containing ILVs fuse with the lysosomes/ autophagosomes and undergo subsequent degradation. This process is known as autophagy (Xu, Camfield, and Gorski 2018). On the other hand, the biogenesis of microvesicles is not well characterized compared to exosomes. Microvesicles are plasma membrane-derived sEVs that are released into the extracellular space as a result of the direct outward blebbing of the plasma membrane (Stahl et al. 2019; Raposo and Stoorvogel 2013).

1.5. Internalization of sEVs in the recipient cells

In general, cells communicate with neighboring cells via direct cell-cell contact and through soluble factors such as cytokines and hormones (Camussi et al. 2010). Similarly, sEVs are involved in intercellular communication in various disease contexts, including cancer, by transferring their cargoes from one cell to another (Chetty et al. 2022; Lotvall and Valadi 2007; Valadi et al. 2007; Torralba et al. 2018; Lai et al. 2015). There are different viewpoints by which sEV internalization takes place in the recipient cells. It is not clear yet whether sEV internalization in the target cells occurs with or without immune cells to elicit distinct cellular responses.
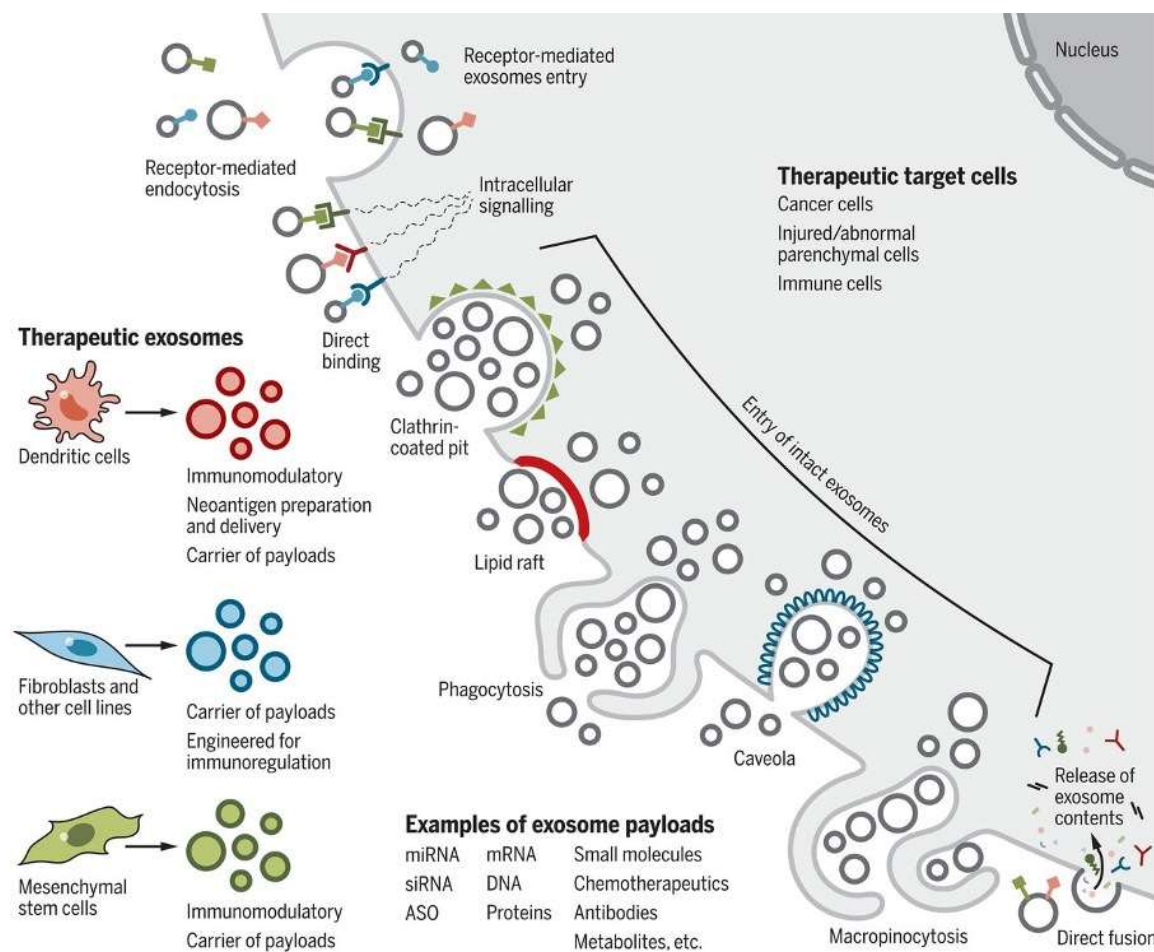
Figure 4. Uptake of exosomes in the recipient cells. Exosomes derived from various sources are known to be involved in cell-cell communication by transferring their cargo from the host to the recipient cells. In general, exosomes enter the recipient cells through receptor-mediated endocytosis, clathrin-coated pits, lipid rafts, phagocytosis, caveolae, and macropinocytosis. Entry of specific cargoes from exosomes can involve ligand-receptor–induced intracellular signaling or fusion to release their contents in the cytoplasm to mediate various cellular physiological effects. Figure adapted from Kalluri et al. (Kalluri and LeBleu 2020).

sEVs secreted by a particular cell type may interact with target cells through its cargo binding with cell surface receptors that specifically recognize them. As a result, sEVs get internalized in the target cells and fuse with endosomes (receptor-mediated endocytosis) to release their cargo contents in the cytosol (Figure 4) (Losche et al. 2004). It is also possible that only specific sEV cargo, not complete sEVs, get internalized in the target cells (soluble signaling) (McKelvey et al. 2015). Clathrin-mediated endocytosis and macropinocytosis are the two most common mechanisms by which sEV internalization occurs in the recipient cells (Tian et al. 2014). Clathrin-mediated endocytosis is a vesicular transport event in which clathrin-coated vesicles bud off from the plasma membrane and are internalized into the target cell (McKelvey et al. 2015), whereas macropinocytosis is a non-specific endocytic pathway characterized by internalization of extracellular materials in eukaryotic cells (McKelvey et al. 2015; Song et al. 2020). Many studies have previously demonstrated that sEVs released from tumor cells were internalized into the recipient or target cells by clathrin-mediated endocytosis and macropinocytosis (Tian et al. 2014; Costa Verdera et al. 2017). On the other hand, following plasma membrane fusion, some of the internalized sEVs are transferred to lysosomes for subsequent degradation (phagocytosis) (Camussi et al. 2010; Cocucci, Racchetti, and Meldolesi 2009; McKelvey et al. 2015).

1.6. Role of sEVs in cancer

sEVs are considered to be a key player involved in cancer development, progression and metastasis in different ways, including the remodeling of tumor microenvironment (TME). Nevertheless, the exact mechanisms involved in these processes remain unclear. In TME, tumor-derived sEVs (TDSE) acts as a signal mediator by transferring their cargo from the tumor to stromal cells to promote tumor progression (Liu et al. 2006), angiogenesis (Umezu et al. 2014; Nazarenko et al. 2010) and metastasis (Hoshino et al. 2015). Due to all these unique functions, sEVs serve as an attractive therapeutic target for different tumors (Campanella et al. 2019).

Many studies reported that TDSE could induce enhanced tumor cell proliferation (Qu et al. 2009; Matsumoto et al. 2017). For instance, it was shown that chronic myeloid leukemia

(CML)-derived exosomes promoted the proliferation and survival of CML cells through the activation of anti-apoptotic pathways (Raimondo et al. 2015). In addition, TDSE plays a role in promoting pro-tumorigenic effect by transferring chemoresistance in the tumor-tumor communication (Maia et al. 2018). In lung cancer, it was shown that TDSE containing low levels of miR-100-5p by donor-resistant cells conferred increased cisplatin resistance to other cancer cells (Qin et al. 2017). TDSE can also alter the invasive potential of various tumors. In nasopharyngeal carcinoma, TDSE containing hypoxia-inducible factor 1 alpha (HIF1α) promoted pro-metastatic effects in the distant recipient cells (Aga et al. 2014). Not only that, sEVs can also suppress the function of the immune cells. In AML patients, it was demonstrated that TDSE decreased natural killer cell cytotoxicity by downregulating the expression of transmembrane protein, NKG2D (Szczepanski et al. 2011).

1.7. Interaction of sEVs with bone marrow microenvironment in AML

It has been known long ago that there is a crosstalk between AML blasts and different components in the BMM, leading to the suppression of normal hematopoiesis (Goulard, Dosquet, and Bonnet 2018). Only in recent years, some studies uncovered the novel features of AML leukemogenesis by showing how AML blasts modulate the BMM through sEV secretion, promoting leukemic cell proliferation and survival while compromising normal hematopoiesis (Bernardi and Farina 2021). Indeed, these studies demonstrated that AML-derived sEVs downregulated the expression of critical retention and supporting factors in BM-HSCs and BM-MSCs, which suppresses the residual hematopoietic function in BMM (Huan et al. 2015; Kumar et al. 2018; Namburi et al. 2021; Hornick et al. 2016; Huan et al. 2013). It's quite challenging to reveal the component present in AML-derived sEVs responsible for the suppression of normal hematopoiesis in BMM since sEVs contain a network of different proteins and nucleic acids cargo.

Huan et al., 2013 showed that primary AML-derived sEVs containing coding and non-coding RNAs were up-taken by BM stromal cells, which altered their secretion of growth factors (Huan et al. 2013). On the other side, Hornick et al., 2016 demonstrated that miR-150 and miR-155 contained in AML-sEVs suppressed normal hematopoiesis by inducing the translational suppression of c-MYB, a transcription factor involved in hematopoietic stromal progenitor cells (HSPCs) differentiation and proliferation (Hornick et al. 2016). Conversely, Namburi and colleagues illustrated that dipeptidylpeptidase4 (DPP4) containing sEVs derived from AML patients' plasma suppressed the proliferation of HSPCs (Namburi et al. 2021). With these findings, we cannot rule out completely that only AML-sEV-associated RNA and protein

cargoes are responsible for AML leukemogenesis in the BMM, since other cargoes including DNA, is also associated with sEVs.

1.8. sEV-derived nucleic acids as cancer biomarkers

Some of the unique properties of sEVs make sEV-derived nucleic acids the exceptional candidate in liquid biopsy as cancer biomarkers. sEVs can be easily obtained from readily available human body fluids with minimal invasion (Liu et al. 2021; Alberro et al. 2021). sEVs are secreted by both healthy and malignant cells, and their secretion level is highly correlated with tumor invasiveness (Boussadia et al. 2018; Xavier et al. 2020). In general, the level of sEVs is always significantly higher in cancer patients compared to healthy controls (Konig et al. 2017; Abhange et al. 2021). In addition, sEV-derived nucleic acids contain molecular signatures, including the mutations reflecting the parental cancer cells from which they were released (Kontopoulou et al. 2020; Kunz et al. 2019; Thakur et al. 2014; Kahlert et al. 2014). Since sEV-derived nucleic acids are mostly enclosed inside the vesicles, they are highly protected from the nucleases degradation (Choi et al. 2013). As a whole, sEV-derived nucleic acids can be utilized as a real-time liquid biopsy monitoring tool for tumor progression or metastasis (Yu et al. 2022).

Many studies focussed on the diagnostic and prognostic potential of sEV-derived nucleic acids for different cancers (Ghanam et al. 2022; Thakur et al. 2014; Kahlert et al. 2014; Maire et al. 2021; Deddens et al. 2016; Hsu et al. 2017; Kunz et al. 2019; Kontopoulou et al. 2020). Compared to other EV nucleic acid cargoes, EV-DNA serves as a superior candidate to depict the pathological state of cancer. Because EV-DNA isolated from tumor-derived sEVs contains abundant biological information reflecting the whole genome of parental tumor cells, including the mutations (Ghanam et al. 2022; Kontopoulou et al. 2020; Chetty et al. 2022). Besides, recent studies revealed the presence of mitochondrial DNA (mtDNA) in addition to chromosomal DNA in sEVs (Guescini et al. 2010; Sansone et al. 2017; Chetty et al. 2022; Tsilioni and Theoharides 2018). Furthermore, EV-DNA contains more reliable biological information than circulating or cell-free DNA (cfDNA) because sEVs are secreted by living cells, and cfDNA is generated by apoptotic or dead tumor cells (Yu et al. 2022). Since cancer-derived sEVs represent only a minor fraction of total EV populations in body fluids, it is a prerequisite to implement or develop an ultrasensitive method using specific markers to detect only cancer-associated sEVs for sEV-based cancer diagnostics.

1.9. Overview of EV-DNA functional studies

For many years, it was well-known that sEV-associated proteins and RNA are transferred to the recipient cells to initiate some biological function. However, this is not the case with EV-DNA. Because it was revealed only recently that DNA is associated with sEVs. Only in 2011, Balaj et al. showed the presence of single stranded DNA (ssDNA) association with exosomes (Balaj et al. 2011). Later in 2014, Thakur et al. and Kahlert et al. proved that the majority of DNA associated with exosomes is indeed double-stranded (dsDNA) (Kahlert et al. 2014; Thakur et al. 2014). Even though sEVs contain both intra- and extra-vesicular DNA (Chetty et al. 2022), the functional studies based on EV-DNA are very limited. This is due to the lack of a suitable sEV isolation method providing efficient separation of sEVs from other non-sEV components such as protein aggregates, lipoproteins, cell-free DNA (cfDNA), and apoptotic bodies. In the next section, we have explained how we addressed this limitation. In this section, a brief overview of prominent EV-DNA functional studies is summarized.

Waldenström et al. were the first ones who showed that EV-DNA derived from cardiomyocytes sEVs was up-taken by fibroblasts and localized in cytoplasm and nucleus (Waldenstrom et al. 2012). However, in this study, they failed to show whether the transferred EV-DNA is functional or not. Later, Cai et al. demonstrated that EV-DNA derived from angiotensin II receptor type 1 (AT$_1$) receptor transfected HEK293 cells can regulate the genomic DNA (gDNA) coding mRNA and protein expressions of AT$_1$ receptor in the recipient non-transfected HEK293 cells (Cai et al. 2013). Similarly, Lee et al. documented the transient expression of H-ras oncogene in the recipient RAT-1 fibroblasts after it was transferred with sEVs generated from a tumorigenic variant of rat epithelial cells such as RAS-3 transfected with the V12 mutant c-H-ras human oncogene (Lee et al. 2014).

Horizontal gene transfer between donor and recipient cells was demonstrated by Fischer et al. by incubating the sEVs derived from lentiviral transduced human BM-MSCs containing *Arabidopsis thaliana*-DNA (*A.t.*-DNA) in the recipient cells. However, in this study, they used human BM-MSCs as both donor and recipient cells (Fischer et al. 2016). Besides, Sansone et al illustrated in hormonal therapy-resistant breast cancer that horizontal transfer of mtDNA from EVs promotes oncogenic potential by increasing the self-renewal potential of cancer stem-like cells leading to an exit from dormancy (Sansone et al. 2017). In the same way, De Carolis showed that Human Papillomavirus-DNA is transferred to breast cancer stromal cells through sEVs (De Carolis et al. 2019). Supporting these findings to some extent, we observed that EV-DNA derived from AML sEVs interacted with healthy BM-MSCs (Chetty et al. 2022).

Cyclic GMP-AMP synthase (cGAS) - stimulator of interferon genes (STING) pathway or cGAS-STING pathway is activated due to the presence of cytosolic DNA as a part of innate immune defense mechanism towards infections, inflammation, and cancer (Motwani, Pesiridis, and Fitzgerald 2019). Interestingly, some studies showed that chemotherapy and irradiation therapy against different cancers increased the sEV secretion containing immunostimulatory EV-DNA, which activates dendritic cells through STING-dependent pathway (Kitai et al. 2017; Diamond et al. 2018). Similarly, Torralba et al. demonstrated that EV-DNA derived from T-cells is involved in priming dendritic cells through the activation of cGAS/STING/IRF3 signaling (Torralba et al. 2018). In concordance with these studies, we also observed that EV-DNA derived from HEK293T cells interacted with cGAS and STING in HeLa recipient cells (Chetty et al. 2022). Despite all these findings, whether the observed function is due to EV-DNA alone or in cooperation with other cofactors remains unclear.

1.10. Limitations of current sEV isolation methods

Until now, most of the published EV-DNA functional studies utilized either ultracentrifugation (UC) method or polymer-based precipitation (PBP) methods for sEV isolation. sEVs obtained by UC or PBP are not well-suitable to perform EV-DNA functional studies since they are known to co-isolate other non-sEV populations mentioned in the previous section. As per MISEV2018 guidelines, we cannot deny the fact that absolute purification of sEVs from other non-sEV populations is currently an unrealistic goal (Thery et al. 2018). However, in contrast to EV-DNA application as a biomarker, highly purified sEVs are needed for EV-DNA-based functional studies. For this purpose, EV researchers tried to combine two or three sEV isolation methods to achieve maximum sEV yield and purity.

Although commercial PBP EV isolation kits provide greater sEV yield than UC, many disputes have been raised regarding their EV purity level (Tian et al. 2020; Lobb et al. 2015). Jeppesen et al. implemented high-resolution multistep density gradient UC to isolate sEVs. Due to the multistep UC, they could not obtain the detectable amount of DNA in sEVs (Jeppesen et al. 2019). Recently, it has been shown that ultrafiltration (UF) combined with size exclusion chromatography (SEC) enabled more EV yield and purity compared to UC. However, they failed to show the percentage of lipoprotein contamination in their EV preparation (Benedikter et al. 2017; Shu et al. 2020). It is quite challenging to completely remove lipoproteins from sEV preparation since the size and density of EVs closely overlap with lipoproteins (Table 1). Additionally, it is important to be noted that sEVs and lipoproteins share some of the common functional characteristics. Therefore, the interpretation of sEV functional data should be

carefully done (Menard, Cerezo-Magana, and Belting 2018). Wu et al. 2019 utilized acoustofluidic-based separation technique to separate sEVs and lipoproteins. However, they could not isolate high and low-density lipoproteins (HDL and LDL) completely from sEVs (Wu et al. 2019).

Table 1. Size and density of sEVs and lipoproteins. Table listing the sizes (in nm) and densities (in g/ml) of sEVs and different classes of lipoproteins.

Name of the particle	Size (nm)	Density (g/ml)
Small extracellular vesicles (sEVs)	30-200nm	1.10-1.18
Very low-density lipoproteins (VLDL)	30-60nm	0.95-1.006
Intermediate density lipoproteins (IDL)	23-27	1.006–1.019
Low density lipoproteins (LDL)	18–25	1.019-1.063
High density lipoproteins (HDL)	5-12	1.063–1.210

By considering all the aspects mentioned above, we have recently established and optimized an efficient sEV isolation method by combining tangential flow filtration (TFF) concentration technique with conventional SEC+UF techniques, together named as TSU. To determine if TSU is a better method for sEV isolation compared to PBP in terms of yield and purity, we also obtained sEVs by combining polyethylene glycol (PEG) precipitation with SEC+UF techniques, collectively known as PSU. Although both TSU and PSU provide good sEVs yield, TSU acts as a better choice for EV-DNA functional studies when it comes to sEVs purity.

2. Aims and scope of the work

Acute myeloid leukemia (AML) is characterized by chromosomal rearrangements and gene mutations leading to an unlimited clonal expansion and differential blockage of stromal cells, thereby suppressing the normal hematopoiesis in bone marrow microenvironment (BMM) resulting in bone marrow failure (Asada et al. 2019; Yao et al. 2021; Rubnitz, Gibson, and Smith 2010; Lipner 2022; Pimenta et al. 2021). Recently, some studies demonstrated that different proteins and RNA cargoes associated with AML-sEVs transform or influence the BMM into AML permissive microenvironment (Huan et al. 2015; Kumar et al. 2018; Namburi et al. 2021; Hornick et al. 2016; Huan et al. 2013). Nonetheless, the functional role of AML-derived EV-DNA and EV-chromatin cargoes in BMM remains unexplored. Since the currently available sEV isolation methods provide enormous non-sEV contaminants, it is indispensable to establish an effective sEV isolation method that provides sEVs free from apoptotic bodies and cfDNA, suitable to perform EV-DNA functional studies. In this regard, we have established an efficient sEV isolation method known as "TSU". We found that the TSU sEV isolation method provides sEVs devoid of apoptotic bodies and cfDNA with good yield and maximum achievable purity. Once the sEVs were isolated using TSU, we focused on the following principal aims or objectives to determine the functional role of EV-DNA and EV-chromatin in pediatric AML,

    I.   Detailed analysis of intra- and extra vesicular DNA associated with sEVs.

   II.   Distribution and functional interaction of foreign EV-DNA in the recipient cells.

  III.   Analysis of proteins associated with AML-derived EV-chromatin.

  IV.   Mechanism involved in inducing non-mutational dysfunction of p53 in healthy BM-MSCs by AML-derived EV-chromatin.

The findings from the current study would enable us to increase our understanding of AML development by revealing the functional role of AML-derived EV-chromatin in BMM. In addition, identifying the role of proteins present in AML-derived EV-chromatin might serve as a potential therapeutic target in the future for pediatric AML treatment.

3. Results

3.1. Publications

All results included in this dissertation were published and are described as follows,

1. **Chetty VK,** Ghanam J, Anchan S, Reinhardt K, Brenzel A, Gelléri M, Cremer C, Grueso-Navarro E, Schneider M, von Neuhoff N, Reinhardt D, Jablonska J, Nazarenko I, Thakur BK. *Efficient Small Extracellular Vesicles (EV) Isolation Method and Evaluation of EV-Associated DNA Role in Cell-Cell Communication in Cancer.* Cancers (Basel). 2022 Apr 20;14(9):2068. doi: 10.3390/cancers14092068.

2. Ghanam J, **Chetty VK**, Anchan S, Reetz L, Yang Q, Rideau E, Liu X, Lieberwirth I, Wrobeln A, Hoyer P, Reinhardt D, Thakur BK. *Extracellular vesicles transfer chromatin-like structures that induce non-mutational dysfunction of p53 in bone marrow stem cells.* Cell Discov. 2023 Jan 31;9(1):12. doi: 10.1038/s41421-022-00505-z.

3.2. Cumulative Thesis/Extent of Contribution

Cumulative thesis of Mr. Venkatesh Kumar Chetty

Author contributions

3.2.1. Efficient Small Extracellular Vesicles (EV) Isolation Method and Evaluation of EV-Associated DNA Role in Cell-Cell Communication in Cancer.
Chetty VK, Ghanam J, Anchan S, Reinhardt K, Brenzel A, Gelléri M, Cremer C, Grueso-Navarro E, Schneider M, von Neuhoff N, Reinhardt D, Jablonska J, Nazarenko I, Thakur BK.

Contributions:

- Conception - 80%

- Conduction of experimental work - 90%: All the experiments except electron microscopy and next-generation sequencing (NGS).

- Data analysis - 90%: All the data analysis involved in the study except NGS.

- Statistical analysis - 100%: All the statistical analysis involved in the study.

- Writing the manuscript - 90%: All parts of the manuscript, including figures.

- Revision of the manuscript - 100%: Revising the manuscript, executing additional experiments suggested by the reviewers, and responding to reviewer comments

3.2.2. Extracellular vesicles transfer chromatin-like structures that induce non-mutational dysfunction of p53 in bone marrow stem cells.
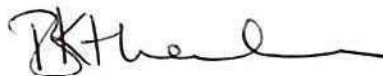
Jamal Ghanam, Venkatesh Kumar Chetty, Srishti Anchan, Laura Reetz, Qiqi Yang, Emeline Rideau, Xiaomin Liu, Ingo Lieberwirth, Anna Wrobeln, Peter Hoyer, Dirk Reinhardt, Basant Kumar Thakur.

Contributions:

- Conception - 35%

- Conduction of experimental work - 40%: Western blot, flow cytometry, confocal microscopy, and real-time PCR.

- Data analysis - 40%: Nanoparticle tracking analysis, mass spectrometry and 3D image analysis using Imaris.

- Writing the manuscript - 30%: Introduction, materials and methods, and discussion.

- Revision of the manuscript - 50%: Executing additional experiments suggested by the reviewers and responding to reviewer comments.

_____
Signature of the Doctoral Candidate

_____
Signature of the Doctoral Supervisor

Efficient Small Extracellular Vesicles (EV) Isolation Method and Evaluation of EV-Associated DNA Role in Cell–Cell Communication in Cancer

Venkatesh Kumar Chetty [1], Jamal Ghanam [1], Srishti Anchan [1], Katarina Reinhardt [1], Alexandra Brenzel [2], Márton Gelléri [3], Christoph Cremer [3,4], Elena Grueso-Navarro [5], Markus Schneider [1], Nils von Neuhoff [1], Dirk Reinhardt [1], Jadwiga Jablonska [6], Irina Nazarenko [5,7] and Basant Kumar Thakur [1,*]

1 Department of Pediatrics III, University Hospital Essen, 45147 Essen, Germany; venkateshkumar.chetty@uk-essen.de (V.K.C.); jamal.ghanam@uk-essen.de (J.G.); anchsana@gmail.com (S.A.); katarina.reinhardt@uk-essen.de (K.R.); markus.schneider@uk-essen.de (M.S.); nils.vonneuhoff@uk-essen.de (N.v.N.); dirk.reinhardt@uk-essen.de (D.R.)
2 Imaging Center Essen (IMCES), University Hospital Essen, 45147 Essen, Germany; alexandra.brenzel@uk-essen.de
3 Institute of Molecular Biology (IMB), 55128 Mainz, Germany; m.gelleri@imb-mainz.de (M.G.); c.cremer@imb-mainz.de (C.C.)
4 Max Planck Institutes for Polymer Research and for Chemistry, 55128 Mainz, Germany
5 Institute for Infection Prevention and Hospital Epidemiology, Medical Center-University of Freiburg, Faculty of Medicine, 79106 Freiburg, Germany; elenagru4@gmail.com (E.G.-N.); irina.nazarenko@uniklinik-freiburg.de (I.N.)
6 Department of Otorhinolaryngology, University Hospital Essen, 45147 Essen, Germany; jadwiga.jablonska@uk-essen.de
7 German Cancer Consortium (DKTK), Partner Site Freiburg and German Cancer Research Center (DKFZ), 69120 Heidelberg, Germany
* Correspondence: basant-kumar.thakur@uk-essen.de; Tel.: +49-201-723-2504

Simple Summary: Small extracellular vesicles (sEVs) released by all cell types function as a mediator in intercellular communication that can promote cell division and survival to remodel the tumor microenvironment to develop tumor invasion and metastasis. Even though dsDNA baggage is associated with all small EV populations, the functional role of EV-DNA in cancer remains poorly understood. This is due to a lack of methods allowing the efficient separation of small EVs (sEVs) from other non-sEV components. The main aim of our study was to develop an efficient sEV isolation method along with EV-associated DNA (EV-DNA) monitoring tool to evaluate the role of EV-DNA as a mediator of cell–cell communication in cancer. Our detailed small EV-DNA characterization confirmed that isolated sEVs using the TSU method (Tangential flow filtration + Size exclusion chromatography + Ultrafiltration) are free from contaminants such as cell-free and apoptotic bodies DNA, making TSU ideal for performing EV-DNA functional studies. Next, we revealed the exact EV-DNA distribution in the recipient cells using 3D image analysis and the association of EV-DNA with key cellular proteins, which may have an essential role in cancer. In the leukemia model, EV-DNA isolated from leukemia cell lines associated with mesenchymal stromal cells (MSCs), a crucial factor in the bone marrow (BM) microenvironment.

Abstract: Small extracellular vesicles (sEVs) play essential roles in intercellular signaling both in normal and pathophysiological conditions. Comprehensive studies of dsDNA associated with sEVs are hampered by a lack of methods, allowing efficient separation of sEVs from free-circulating DNA and apoptotic bodies. In this work, using controlled culture conditions, we enriched the reproducible separation of sEVs from free-circulated components by combining tangential flow filtration, size-exclusion chromatography, and ultrafiltration (TSU). EV-enriched fractions (F2 and F3) obtained using TSU also contained more dsDNA derived from the host genome and mitochondria, predominantly localized inside the vesicles. Three-dimensional reconstruction of high-resolution imaging showed that the recipient cell membrane barrier restricts a portion of EV-DNA. Simultaneously, the remaining EV-DNA overcomes it and enters the cytoplasm and nucleus. In the cytoplasm, EV-DNA associates

with dsDNA-inflammatory sensors (cGAS/STING) and endosomal proteins (Rab5/Rab7). Relevant to cancer, we found that EV-DNA isolated from leukemia cell lines communicates with mesenchymal stromal cells (MSCs), a critical component in the BM microenvironment. Furthermore, we illustrated the arrangement of sEVs and EV-DNA at a single vesicle level using super-resolution microscopy. Altogether, employing TSU isolation, we demonstrated EV-DNA distribution and a tool to evaluate the exact EV-DNA role of cell–cell communication in cancer.

1. Introduction

Extracellular Vesicles (EVs) are lipid bilayer bound vesicles released by all cell types into the extracellular environment, which differ in size, shedding mechanism, and function [1–3]. EVs contain unique biomolecular cargo, consisting of proteins, nucleic acids, and lipids [4–8]. In general, EVs can be classified into three types such as exosomes (30–150 nm), microvesicles (100–1000 nm), and apoptotic bodies (1–5 μm) [1,2,9,10]. Since markers are not well established based on EV origin, MISEV2018 guidelines urged EV researchers to use the term small EVs (sEVs) that are less than 200 nm in diameter and large EVs as the ones that are greater than 200 nm [3]. Small EVs have gained greater scientific research attention than large EVs in recent years. Many researchers have demonstrated that small EVs act as a functional mediator of intercellular communication in various instances, including cancer. In cancer, tumor cell-derived EVs regulate the tumor microenvironment through their cargo delivery promoting tumor progression, metastasis, and angiogenesis [8,11–17]. Although DNA has been associated with sEVs (EV-DNA), it is not extensively studied compared to other EV cargoes. Moreover, very little is known about the molecular mechanisms of EV-DNA packaging and their biological function in the recipient cells [1,5,7,13,18–22].

To demonstrate the presence of cancer biomarkers for liquid biopsy applications, it is not an issue to isolate heterogeneous EVs from blood samples and analyze them for cancer-specific mutations. However, it is very important for functional studies to purify and separate EV populations to discriminate the functional significance of DNA associated with a particular EV subtype [3]. Until now, most studies demonstrating the functional role of EV-DNA in the recipient cells have used classical ultracentrifugation (UC) or polymer-based techniques for EV isolation. However, these studies are still far from conclusive because these isolation methods are known to co-isolate other non-sEV populations, including cell-free DNA and apoptotic bodies, and also, cause morphological changes in the extracted vesicles [23–26]. Recently, Lazaro-Ibanez et al. attempted firstly to distinguish heterogeneous EV subpopulations based on DNA cargo and topology using UC-based iodixanol density gradient separation [27]. Although this method provides pure EVs for molecular characterization, multiple ultracentrifugation steps can result in sample loss affecting EV yield for downstream functional experiments [24].

Furthermore, not all laboratories have access to expensive ultracentrifugation devices; therefore, there is still the need to establish a method that can be performed in a laboratory bench setting yet provides sEVs that are qualified to perform both diagnostics and functional studies. To address these important problems, we have optimized two sEV isolation methods by combining tangential flow filtration (TFF) or PEG-based precipitation with conventional size-exclusion chromatography and ultrafiltration (SEC + UF) techniques, which we named TSU and PSU, respectively. The fractions were characterized according to the MISEV2018 guidelines [3]; the majority of small extracellular vesicles (sEVs) ranging from 30–200 nm were obtained in fraction 2 (F2) and fraction 3 (F3) of TSU and PSU.

As we previously showed, we detected cancer-specific mutations in EV-DNA regardless of the isolation method used [5,21]. However, we found that only sEV fractions obtained from TSU entered the recipient cells and localized in various cell compartments,

whereas sEVs isolated by PSU showed drastically reduced entry into recipient cells. In addition, we applied 3D imaging tools for the first time in the EV field to avoid artifacts obtained from 2D imaging and to accurately quantify the actual amount of EV-DNA entered inside the recipient cells.

Previously, it was shown that EV uptake in the recipient cells occurs through clathrin-mediated endocytosis and micropinocytosis [28]. Moreover, it was recently demonstrated that the accumulation of cytoplasmic DNA arising from genomic DNA undergoing chromosomal duplication activates the cGAS-STING (cyclic GMP-AMP synthase-stimulator of interferon genes) cytosolic DNA-sensing pathway, which results in an innate immune response favoring the spread of cancer cells to distant organs [29]. Furthermore, T-cell-derived EVs carrying DNA can induce antiviral inflammatory responses via the cGAS/STING/IRF3 signaling cascade in priming dendritic cells [30]. Supporting these facts, we found that passenger EV-DNA associates with the endosome–lysosome compartment and cytoplasmic DNA sensors (cGAS/STING) in the recipient cells, which may have an important role in cancer. In addition, we found that EV-DNA derived from leukemia cell lines communicates with the critical component in the BM microenvironment, such as MSCs. Altogether, our work provides an efficient sEV isolation method and new tools to address EV-DNA-associated biology in cancer.

2. Materials and Methods

2.1. Cells and Cell Culture

HeLa and HEK293T cells were cultured in DMEM high glucose media (Gibco, Paisley, UK) in a humidified incubator at 37 °C, 5% CO_2 for 72 h. To perform acute myeloid leukemia (AML) diagnostic studies, MV4−11 and OCI−AML3 cell lines were cultured in RPMI 1640 media (Gibco, Paisley, UK). For EV functional studies, a HEK293T-CD63-GFP-transduced cell line received from Prof. Bernd Giebel (University Hospital Essen, Essen, Germany) was utilized and cultured like HEK293T cells. In this transduced cell line, CD63 is fused to the N-terminus of eGFP and was generated by co-transfection of HEK293T cells with the lentiviral plasmid pCL6-CD63-eGFP, the helper plasmid pCD/NL-BH, and the codon-optimized human foamy virus envelope encoding plasmid pcoPE01 [31].

Growth media was supplemented with 10% EVs-depleted fetal bovine serum (FBS; Gibco, Waltham, MA, USA) and 1% penicillin/streptomycin for all cell lines. EV-depleted FBS (FBS18) was obtained by ultracentrifugation at $100,000 \times g$ for 18 h utilizing a type 45 Ti fixed-angle titanium rotor (Beckmann Coulter, CA, USA). After 72 h, cell conditioned media (CCM) was collected and centrifuged at $500 \times g$ for 10 min followed by $3000 \times g$ for 20 min (4 °C) to remove cells, cell debris, and apoptotic bodies. All cell lines involved in this study were screened for mycoplasma contamination by performing PCR and authenticated using short tandem repeat (STR) DNA fingerprinting through IDEXX BioAnalytics, Germany.

2.2. Isolation of Small EVs by TSU and PSU

To prepare TSU sEVs, CCM was first filtered using a 0.2 μm syringe filter to eliminate large EVs (>200 nm). Filtered CCM was concentrated up to 10 mL using tangential flow filtration (TFF-Easy; Hansa Biomed, Tallin, Estonia). Concentrated CCM was then loaded into a size-exclusion chromatography column (SEC) (qEV10; IZON Science, Christchurch, New Zealand) using 0.2 μm-filtered DPBS (Invitrogen, Waltham, MA, USA) as the running buffer. First, 20 mL was discarded as void volume, and right after, 5 mL fractions (F1–F5) were collected. The SEC fractions were further concentrated to 500 μL final volume using an Amicon Ultra-4 10 kDa centrifugal filter (Merck Millipore, Darmstadt, Germany).

In order to prepare PSU sEVs, CCM was centrifuged at $6800 \times g$ for 45 min and then filtered using a 0.2 μm syringe filter. To the filtered CCM, precipitation agents such as 10% PEG6000 (Sigma, Darmstadt, Germany) along with 0.5% NaCl (Sigma, Darmstadt, Germany) were added and incubated overnight for 16 h at 4 °C. The next day, PEG-treated CCM was centrifuged at $1500 \times g$ for 30 min (40 °C) and the pellets were re-suspended in 2 mL of 0.2 μm-filtered DPBS [31]. Out of 2 mL of the PEG pellet, 100 μL (aliquot) was

stored separately, and the volume was equalized again with filtered DPBS and loaded into the SEC column (qEV2; IZON Science, Christchurch, New Zealand). As mentioned before, 2 mL fractions (F1–F5) were collected and concentrated to 500 µL using an Amicon Ultra-2 10 kDa centrifugal filter (Merck Millipore, Darmstadt, Germany). In parallel, TSU and PSU sEVs were isolated from DMEM containing FBS18 (control without cells) by performing the same steps carried out with CCM.

2.3. Characterization of TSU and PSU sEVs

2.3.1. Measurement of Particle Count and Total Protein Concentration

Firstly, the concentration of particles (particle count) present in various HEK293T and HeLa TSU and PSU sEV fractions (F1–F5) was determined by nanoparticle tracking analysis (NTA) using the ZetaView BASIC PMX-120 instrument (Particle Metrix GmbH, Inning am Ammersee, Germany) equipped with NTA 2.0 analysis software. Using 100 nm standard beads, the instrument was calibrated, and the following settings were used: positions—11, cycles—5, minimum size—5 nm, maximum size—150 nm, trace length—15 s, sensitivity— 75%, shutter speed—75 ms and frame rate—30. Diluted TSU and PSU sEV fractions (100- to 1000-fold) were loaded into the NTA instrument and the values were recorded. Next, micro-BCA assay (Thermo Scientific, Waltham, MA, USA) was performed following the manufacturer's protocol to determine the free protein concentration of various sEV fractions. Then, EV purity was determined by the ratio of particle count determined by NTA and free protein concentration determined by micro-BCA.

2.3.2. Transmission Electron Microscopy (TEM)

Negative staining was performed at the Electron Microscopy Unit (EMU) of the Imaging Center Essen (IMCES) for HEK293T and HeLa TSU and PSU sEV fractions that have more purity (F2 and F3) along with F4 that has less purity. In addition, FBS18 sEV fractions were included as a negative control. Briefly, 3 µL of sEV fractions (F2–F4) was added onto a Formvar- and carbon-coated 200 mesh copper grid (#S162, PLANO GmbH, Wetzlar, Germany) which had a hydrophilic surface due to being exposed to glow discharging for 30 s at 15 mA (easiGlow™, TedPella Inc., Redding, CA, USA). Samples were then negatively stained by placing the grid on the top of the droplet of 1.5% aqueous Phosphotungstic acid solution (*w/v*, 2635.1, Carl Roth, Karlsruhe, Germany) for a minute. Excess liquid was removed using filter paper, and the grids were allowed to dry for at least five minutes under ambient air. Images were acquired using JEOL JEM 1400Plus (JEOL Ltd., Tokyo, Japan) operating at 120 kV and with a 4096 × 4096 pixels CMOS camera (TVIPS, Gauting, Germany). Image acquisition software EMMENU (version 4.09.83) was used for taking 16-bit images. Image post-processing and analysis were carried out using ImageJ (version 1.52a) to determine the average diameter of sEVs.

2.3.3. Western Blot Analysis

Equal amounts (100 µL) of HEK293T, HeLa, and FBS18 TSU and PSU sEVs (F1–F5) were concentrated to 10–12 µL using an Amicon Ultra-0.5 10 kDa centrifugal filter tube (Merck Millipore, Darmstadt, Germany). Both whole-cell lysate (30 µg; prepared using RIPA buffer: ThermoFisher Scientific, Waltham, MA, USA) and EV fractions (F1–F5) were solubilized using 4X Laemmli buffer (Biorad, Feldkirchen, Germany) in reducing conditions at 95 °C for 10 min. Samples were then separated on a NuPAGE 4–12% gel, Bis-Tris, 1.0 mm, (ThermoFisher Scientific, Waltham, MA, USA) along with a pre-stained protein ladder at 100 V for 2 h. Transfer of resolved proteins onto a 0.4 µm PVDF membrane (Merck Millipore, Darmstadt, Germany) was performed following standard semidry conditions. Membranes were blocked in 5% milk blocking solution (Carl Roth, Karlsruhe, Germany) in 1X TBST buffer containing 0.1% Tween20 for 60 min. Membranes were incubated with primary antibodies diluted in 1X TBST containing 0.05% Tween20 (1:1000) overnight at 4 °C [Rabbit-α-TSG101 (Sigma, Cat. No: HPA006161); Rabbit-α-Calnexin (Abcam,

Cat. No: ab22595); Mouse-α-CD81 (Biolegend, Cat. No: 349502); Rabbit-α-Hsp70 (System Biosciences, Cat. No: EXOAB-Hsp70A-1); Rabbit-α-Synthenin (Abcam, Cat No: ab133267).

Unbound antibodies were removed by washing the membranes 4X with 1X TBST and then incubated with the corresponding HRP-conjugated secondary antibody (1:10,000 dilution) at RT for 90 min (anti-mouse IgG, HRP-linked: Cell Signaling Technology, Danvers, MA, USA, Cat. No: 7076; anti-rabbit IgG, HRP-linked: Cell Signaling Technology, Danvers, MA, USA, Cat. No: 7074; goat anti-rabbit for detection of Hsp70: System Biosciences, Cat. No: EXOAB-Hsp70A-1). Proteins were visualized using ECL Prime Western Blotting Detection reagents (ThermoFisher Scientific, Waltham, MA, USA) by scanning the membrane on a Fusion FX machine (Vilber Lourmat GmbH, Eberhardzell, Germany).

2.3.4. Bead-Assisted Flow Cytometry

HEK293T and HeLa TSU and PSU sEV fractions (F1–F5) were analyzed by flow cytometry for semi-quantitative detection of classical EV proteins (CD9 and CD63), apoptotic bodies (phosphatidylserine (PS)), and apolipoprotein (Apo-B). To detect the PS level present in sEVs, annexin-V antibody was employed. A volume of 20 μL of sEV fractions was incubated with 5 μL of aldehyde-sulfate latex beads (4 μM; Invitrogen) for 30 min at RT in a rotating platform shaker. Then 200 μL of 0.1 μm-filtered 1X DPBS was added and incubated for another 30 min at RT. Afterwards, 300 μL of DPBS was added and centrifugation was performed at $2000\times g$ for 5 min to remove the unbound beads in a way that 50 μL of the beads–EV complex was left. To this, 20 μL of a 5% BSA solution in DPBS was added for blocking and incubated for 30 min at RT. DPBS washing and centrifugation were performed as mentioned before. In the last step, staining was carried out using 5 μL of antibody conjugated with different fluorochrome for 30 min at RT (antihuman CD9-PE (MEM61, Exbio, Cat. No: 1P-208-T100); antihuman CD63-APC (Mem259, Exbio, Cat. No: 1A-343-T100); antihuman Apo-B-FITC (polyclonal, Abcam, Cat. No: ab27637); annexin-V-FITC (N/A, BD Biosciences, Cat. No: 560931). A final wash step was performed to remove the unbound antibodies. In addition, various controls were included in the analysis. Beads only and beads with antibody controls were used to select the single beads (monomer) and positive population. Beads with BSA and beads with BSA+ antibody controls were included in determining if BSA bound with any antibodies used. Data were acquired in conventional flow cytometers (BD FACS Aria, BD Biosciences, Heidelberg, Germany, and MACS Quant, Miltenyi Biotech, Bergisch Gladbach, Germany) and analyzed using FlowJo software V10 to determine the mean fluorescence intensity (MFI). MFI relative to the negative control in TSU and PSU sEV fractions was evaluated and depicted on the y-axis. EV purity was also determined based on the values of EV tetraspanins obtained from this method and the free protein concentration was determined by micro-BCA assay.

2.4. Application of TSU and PSU sEVs for Diagnostics and Functional Studies

2.4.1. MV4−11 and OCI−AML3 sEVs for AML Diagnostics

TSU and PSU sEV fractions (F2–F4) obtained from MV4−11 and OCI−AML3 CCM were characterized by performing Western blot with CD81, TSG101, and calnexin. EV-DNA was isolated from these fractions using the QIAamp DNA Micro Kit (#56304, Qiagen) according to the manufacturer's instructions, and the concentration was determined using a Nanodrop 1000 spectrophotometer (ThermoFisher Scientific, Waltham, MA, USA). As shown before, GeneScan-based fragment-length analysis was performed to determine if MV4−11 and OCI−AML3 TSU and PSU sEVs (F2–F4) qualify to detect AML-specific mutations (FLT3 and NPM1 mutations) [21].

2.4.2. Incubation of HEK-CD63-GFP sEVs with HeLa Cells

Around 25,000 HeLa cells were seeded on a 24-well plate containing sterile 12 mm microscopic coverslips (ThermoFisher Scientific, Waltham, MA, USA). After 24 h, normal growth media was replaced with FBS18 media. Thirty microliters of HEK-CD63-GFP TSU and PSU sEV fractions (F1–F5) was added to the corresponding wells and incubated at

37 °C for 48 h. After 48 h, cells were washed once with PBS and 0.01% PBST before being fixed using 4% PFA (Alfa Aesar, Kandel, Germany) for 15 min at RT. Then, 3% BSA in PBS was added and removed, followed by 2X PBS washes. Permeabilization was performed using 0.5% Triton®-X100 (Merck Millipore, Darmstadt, Germany) in PBS for 20 min at RT, after which cells were washed with 3% BSA and PBS as mentioned before. Nucleus staining was performed using DAPI solution (0.2 µg/mL, Biolegend) in PBS for 10 min at RT in the dark, followed by 2X PBS washes. Coverslips were mounted carefully using a few drops of Fluoromount (Southern Biotech, Birmingham, AB, USA) on microscopic glass slides. Images were acquired using a confocal microscope (Leica TCS SP8, Wetzlar, Germany), and the mean GFP fluorescence intensity was measured using ImageJ 1.52a (NIH, Bethesda, MD, USA).

2.4.3. Zeta Potential

Next, we wanted to investigate whether the biophysical property of EVs, such as zeta potential, plays a crucial role in mediating its successful transfer into recipient cells. Using the ZetaView BASIC PMX-120 instrument, the zeta potential of HEK-CD63-GFP TSU and PSU EVs (F1–F5) was measured at 25 °C under the following settings: max size: 200, min size: 5, min brightness: 20.

2.5. Transfer of Foreign EV-DNA in the Recipient Cells
2.5.1. Labelling of EV-DNA with EdU

In order to facilitate EV-DNA-based functional studies, 5 µM of 5-ethynyl-2′-deoxyuridine (EdU; ThermoFisher Scientific) solution was added to HEK-CD63-GFP cells after a few hours of seeding (i.e., when cells had attached to the dishes). EdU is a thymidine analog incorporated into newly synthesized DNA during active DNA synthesis; thereby, cells treated with EdU release EVs in which DNA is labeled with EdU. sEVs were isolated from HEK-CD63-GFP cells treated with EdU using TSU and PSU.

2.5.2. Incubation of sEVs Containing EV-DNA-EdU with HeLa Cells

Thirty microliters of the HEK-CD63-GFP TSU and PSU sEVs (F1–F5) containing EV-DNA-EdU was incubated with HeLa cells seeded on a 24-well plate containing sterile 12 mm microscopic coverslips at 37 °C for 48 h. In parallel, MV4−11 sEVs containing EdU were added to mouse mesenchymal stromal cells (OP9). Fixation and permeabilization were performed as explained before. If cell membrane staining was desired, cells were treated with wheat germ agglutinin (WGA) Alexa Fluor™ 488 conjugate (W11261, Invitrogen) for 10 min well after fixation, before permeabilization. An EdU click-it reaction was carried out using the Click-iT™ EdU Alexa Fluor 647 Imaging Kit (C10640, ThermoFisher Scientific) following the manufacturer's instructions. Images were acquired by confocal microscopy in the corresponding channels (blue—DAPI, green—CD63+ EVs, and red—EdU). Using ImageJ, the red fluorescence signal corresponding to EV-DNA was quantified.

2.5.3. Three-Dimensional (3D) Image Analysis

For 3D analysis, the Leica SP8 confocal system with a 63X objective was used. Z-stack imaging of the cells was performed with Nyquist sampling for subsequent deconvolution of the data set with Huygens. After that, the data were loaded into Imaris for 3D analysis to obtain the exact amount of EV-DNA present inside the cell, inside the nucleus, and those close to the cell membrane, by using the Imaris surface function to distinguish between the cell compartments and the spot function to count the EV-DNA.

2.6. Single EV Imaging

For single-molecule localization measurements, a custom-built inverted microscope equipped with 488 nm, 561 nm, and 640 nm lasers was used [32]. The laser beams were combined by dichroic mirrors and then expanded and focused on the objective's back focal plane (HCX PL APO 100×/NA 1.47 OIL, Leica). Fluorescence light was separated from excitation light using a dichroic mirror (Chroma, zt405/488/561/647rpc). A tube

lens focused the fluorescence light onto an sCMOS camera (PCO edge 4.2, PCO), resulting in an effective pixel size of 65 nm. A cylindrical lens was inserted into the detection path to introduce astigmatism for 3D localization measurements. The detection path was additionally equipped with emission filters (HC520/35 Semrock, ET600/50 Chroma, ET655 Chroma) to reduce bleed-through from different fluorescence channels.

HEK-CD63-GFP TSU EVs (F2 and F3) containing EdU were embedded in Vectashield H-1000 mounting medium (Vector Laboratories, Burlingame, CA, USA) on the day of measurement. CD63-GFP and Edu-Alexa Fluor 647 were excited using 488 nm and 640 nm lasers and imaged with emission filters HC520/35 (GFP) and ET655laser (Alexa647), respectively. Excitation powers were set to 0.8 kW/cm2 to 3 kW/cm^2 for both lasers. A stack of 5000 images with an exposure time of 50 ms was acquired for each channel. For data analysis, reconstruction of SMLM data was performed with the ThunderSTORM plugin [33] in Fiji [34]. A detection threshold of one standard deviation of the applied wavelet filter was used during the detection process. Fluorescence signals visible in consecutive frames within a radius of 20 nm were merged into one detection event to avoid over-counting of molecules. Super-resolution images were then generated as 2D histograms with a pixel size of 20 nm.

2.7. Detailed Characterization of HEK293T TSU EV-DNA

2.7.1. Isolation of EV-DNA before and after dsDNAse Treatment

To determine whether DNA is associated with the outer membrane or inside EVs, we pre-treated 100 µL of HEK293T TSU sEVs (F1–F5) with 6 µL of dsDNAse (ThermoFisher Scientific, Waltham, MA, USA) along with 10X dsDNAse buffer at 37 °C for 5 min and the reaction was stopped by adding 0.5 M EDTA. Then, EV-DNA was extracted from both intact HEK293T TSU sEVs and sEVs pre-treated with dsDNAse (F1–F5) using the QIAamp DNA Micro Kit. Three microliters of these extracted EV-DNA samples was again treated with dsDNAse in the same manner to evaluate if single-stranded DNA is present inside sEVs. Finally, 5 µL of HEK293T EV-DNA samples (four sets) and genomic DNA was loaded on a 2% agarose gel and run at 100 V for one hour. After one hour, the agarose gel was stained with SYBR Gold nucleic acid dye (ThermoFisher Scientific, Waltham, MA, USA) for 30 min and the gel image was acquired.

2.7.2. Next-Generation Sequencing (NGS)

HEK293T TSU sEVs (F1–F5) and HEK293T gDNA samples were divided into two: one was pre-treated with dsDNAse to digest extra vesicular dsDNA and the other one remained untreated prior to DNA extraction and NGS. DNA was extracted in the same way as mentioned before. After DNA extraction, samples were processed for NGS using the NEB Next Ultra II FS DNA Library Prep Kit for Illumina (New England BioLabs, Frankfurt, Germany) following the manufacturer protocols of inputs ≤100 ng for EV-DNA samples; and large fragment sizes (>550 bp) for gDNA. DNA library quality was assessed on an Agilent 2200 TapeStation system using High Sensitivity D1000 ScreenTape (Agilent Technologies, Santa Clara, CA, USA). Once the expected band size based on fragmentation time was confirmed for all the samples, sequencing was performed on an Illumina MiSeqDX Sequencer in research mode with 156 bp paired-end reads using the MiSeq Reagent Kit v2 (300-cycle). After obtaining data, sequencing adapters were removed by Trimmomatic software [35], adapter-free read pairs were mapped to the hg38 genome, and read counts per chromosome were accessed by samtools idxstats [36].

2.8. Immunofluorescence

HeLa cells seeded on a 24-well plate were incubated with 30 µL of HEK293T TSU EVs with EdU (F2 and F3) at 37 °C for 48 h. Fixation, permeabilization, and click-it EdU staining were performed as previously explained. Then, blocking was performed using 1% BSA in PBS for 30 min at RT followed by incubation with primary antibody: rabbit-α-Rab5 (1:250, Abcam, Cambridge, UK); Rab7 (1:1000, Abcam, Cambridge, UK); Lamin (1:1000, Abcam, Cambridge, UK); cGAS (1:500, Cell signaling technology, Danvers, MA,

USA); STING (1:1000, Abcam, Cambridge, UK) at RT for 70 min. Subsequently, 3X PBS washes were performed and then incubated with anti-rabbit Alexa488 (1:500, Abcam, Cambridge, UK) for 45 min at RT. Following 3X PBS washes and DAPI staining, images were obtained by confocal microscopy.

2.9. Statistical Analysis

Statistical analyses were performed using GraphPad Prism 7.0. All data sets were represented as the mean ± S.E.M (shown with error bars) obtained from three independent experiments. One unpaired *t*-test per row was performed to assess the statistical significance, and *p* values were determined using the Holm–Sidak method. *p*-values < 0.05 were considered to be significant. Data that were found to be statistically significant were represented in the graphs as: * for $p < 0.0332$, ** for $p < 0.021$, *** for $p < 0.0002$, and **** for $p < 0.0001$.

3. Results

3.1. Isolation and Characterization of HEK293T TSU and PSU sEVs

Enrichment, fractionation, and isolation of homogenous vesicular and non-vesicular particles were established from HEK293T and HeLa CCM using TSU and PSU methods as explained in Figure 1A. To characterize sEVs as explained in Webber and Clayton, 2013, [37], particle count was determined in each fraction using NTA, and total protein concentration was determined using micro-BCA. We observed that the highest purity of sEV preparations determined by the highest particle number (30–200 nm) and lowest protein content was obtained in both TSU and PSU isolation methods (Figure 1B,C and Supplementary Figure S1A,B). For qualitative characterization, we selected fractions, F2 and F3, with the highest EV purity for negative staining, imaged using TEM, and compared to fraction F4 as the one with the least EV purity, according to our criteria. Indeed, particles present in F2 and F3 possessed an sEVs morphology with an intact membrane with a size ranging from ~30–200 nm in diameter (indicated by red arrows) irrespective of the cell lines or isolation methods used. (Figure 1D and Supplementary Figure S1C). However, some aberrant bubbles were found on the outer surface of PSU sEVs (indicated by blue arrows). Using TEM images, the average size of particles found in fractions (F2–F4) was calculated using ImageJ and is shown in Figure 1E and Supplementary Figure S1D.

Qualitative analysis of TSU and PSU sEV fractions was performed by Western blot analysis with various canonical EV markers (TSG101, CD81, Hsp70, and syntenin). The negative signal of calnexin (an integral endoplasmic reticulum protein) further confirmed the isolation of sEVs. Supporting the TEM data, we found that all canonical EV proteins were enriched in both HEK293T TSU and PSU sEVs (F2, F3). However, the level of canonical protein markers found in HeLa TSU and PSU sEVs (F2, F3) is less compared to HEK293T sEVs. A weak band of calnexin was observed in some PSU sEV fractions. As previously shown [38], we also observed heat shock protein 70 (Hsp70) band in some TSU and PSU sEV fractions isolated from FBS18 media alone (control without cells), thereby suggesting that a small proportion of Hsp70+ sEVs are derived from FBS growth supplement used in the cell culture media (Figure 1F and Supplementary Figure S1E).

Next, we performed bead-assisted flow cytometry for further qualitative characterization of sEV fractions since this method is sensitive and time saving. To do so, we determined the level of surface-EV markers (CD9 and CD63 tetraspanins) and non-small EV contaminants such as phosphatidylserine (PS+) apoptotic bodies and apolipoprotein-B (Apo-B) in all sEV fractions [39]. Positive populations were selected as shown in Supplementary Figure S1F,G. As expected, CD9 and CD63 are primarily present in F2 and F3 of TSU and PSU sEVs from HEK293T cells. In line with the WB results, we observed that CD9 and CD63 signals are weaker in HeLa sEVs irrespective of the isolation method used (Figure 1G). EV purity was also calculated based on the EV tetraspanin value obtained from flow cytometry and free protein concentration determined by micro-BCA. Indeed, we determined that fractions F2 and F3 have more EV purity than other fractions (Supplementary Figure S1H). Interestingly, we found that the level of PS+ apoptotic bodies is close to zero in all TSU and

PSU sEVs (F1–F5), indicating their absence. On the other hand, Apo-B contamination was lower in PSU sEVs than in TSU sEVs (Figure 1H). Overall, our results indicate that both TSU and PSU methods are able to isolate sEVs with high purity.
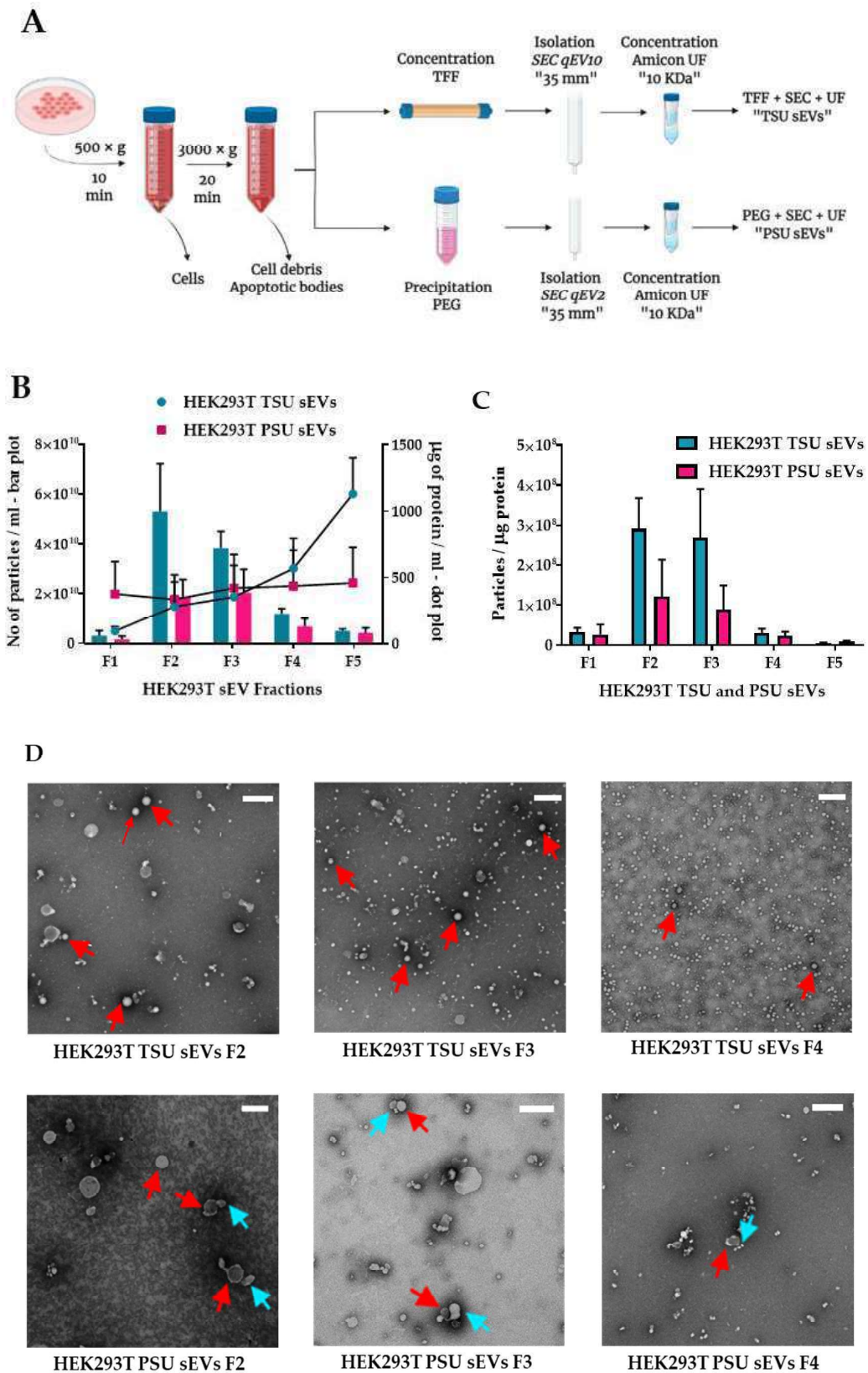
Figure 1. *Cont.*
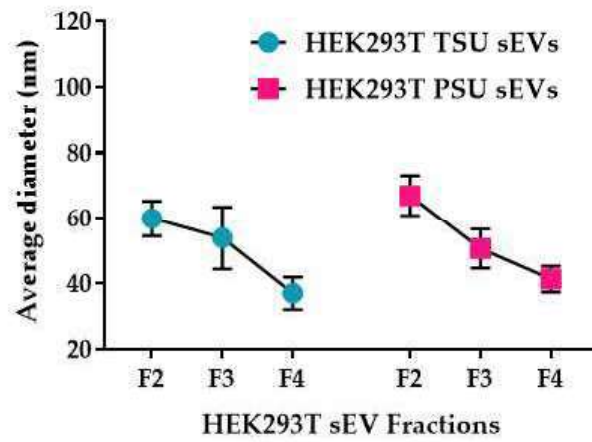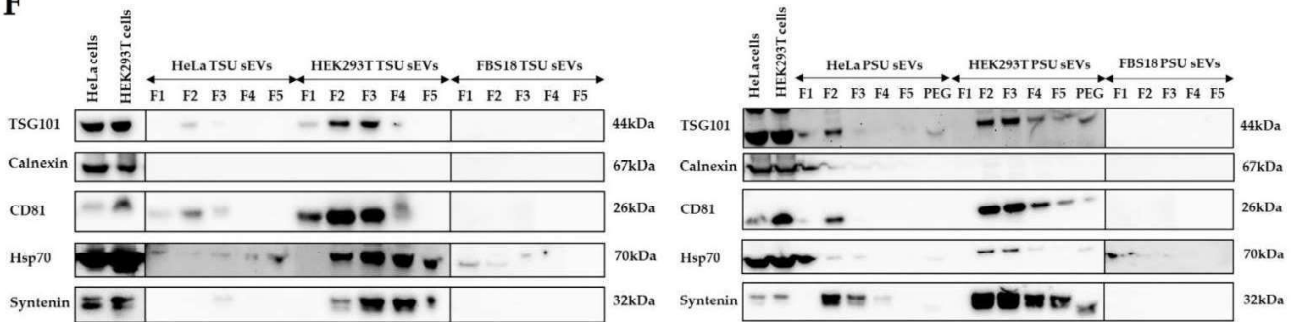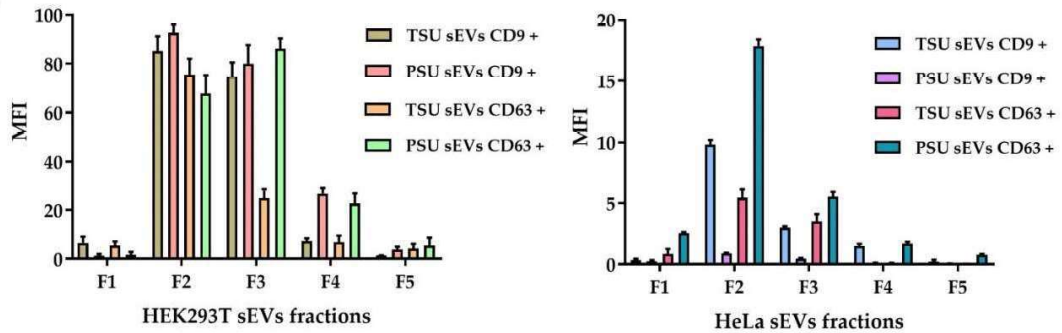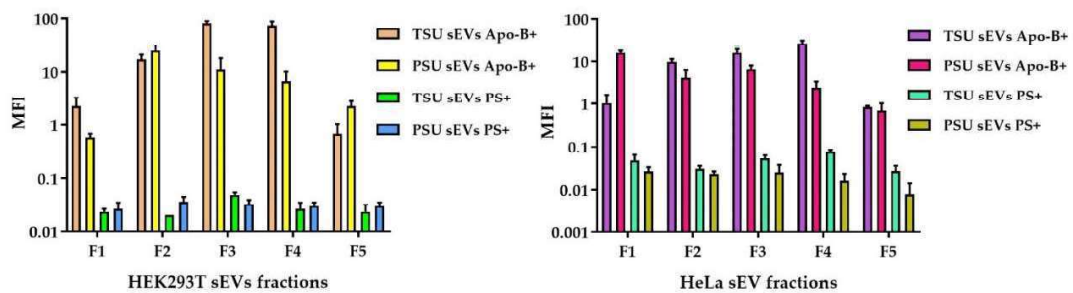
Figure 1. Isolation and characterization of TSU and PSU sEVs. (**A**) Schematic representation of the steps involved in the isolation of sEVs from CCM using TSU and PSU. (**B**) Mean values of particle count and free protein concentration (*n* = 3) in HEK293T TSU and PSU sEV fractions determined by

NTA (left y-axis, bar plot) and micro-BCA (right y-axis, dot plot). (**C**) Measurement of EV purity from the ratio of particle count to free protein concentration. Data correspond to the mean ± S.E.M of different HEK293T TSU and PSU sEV fractions purity values from three independent experiments. (**D**) Imaging of TEM negative staining of HEK293T TSU and PSU sEVs (F2–F4) (6000× magnification). Red arrows indicate sEVs and aberrant bubbles found in PSU sEVs are shown by blue arrows. Scale bars: 200 nm. (**E**) Evaluation of average size diameter of HEK293T sEVs present in TSU and PSU sEV fractions (F2–F4) utilizing TEM negative staining images($n = 3$) using ImageJ. (**F**) Western blot analysis of TSU and PSU sEVs with various EV canonical markers and calnexin. Whole-cell extract (positive control), HeLa, and HEK293T sEV fractions (F1–F5) including FBS18 sEV fractions (negative control) were used. Each black outer line box indicates the samples that were run together. Semi-quantitation of (**G**) EV tetraspanin markers (CD9 and CD63) and (**H**) other non-small EVs contaminants such as apolipoprotein-B [Apo-B] and PS$^+$ apoptotic bodies in TSU and PSU sEV fractions using bead-based flow cytometry. Error bars represent the mean ± S.E.M from three independent experiments.

3.2. Assessment of TSU and PSU sEVs for Diagnostic and Functional Studies

Previously, we [5] and others [7] have shown that tumor-derived exosomes, now known as small EVs, carry double-stranded DNA (dsDNA) that mirrors the mutational status of the donor cancer cells. Nevertheless, whether the EV-DNA derives from apoptotic bodies or dead cells is currently debated. Since TSU and PSU sEVs exhibited low apoptotic markers, we first evaluated if they qualify to perform diagnostic studies in the clinical setting. For this, we selected F2, F3, and F4 of TSU and PSU sEVs derived from AML cell lines (OCI−AML3 cell line bearing NPM1 mutation and MV4−11 cell line bearing FLT3−ITD mutation) to perform mutational analysis as only these fractions revealed the presence of sEVs (Figure 2A). EV-DNA was isolated (Figure 2B) and subjected to GeneScan-based fragment-length analysis to detect AML-specific mutations (FLT3−ITD and NPM1 mutations). The results showed that NPM1 and FLT3−ITD mutations were successfully detected in TSU and PSU sEVs (F2–F4) (Figure 2C). These data are consistent with our previous studies, thereby proving that both TSU and PSU sEVs (F2–F4) qualify to perform diagnostic studies [8].

To evaluate if isolated sEVs enable us to perform EV-based functional studies, we compared the uptake of TSU and PSU sEVs by HeLa cells. For this, a HEK293T-CD63-GFP transfected cell line was used that allowed us to track CD63$^+$ EVs through a GFP signal (Figure 2D). Interestingly, we found TSU, but only to a limited extent F2 and F3 PSU sEVs were taken up by HeLa cells as indicated by the GFP signal detected in the cells by confocal microscopy (Figure 2E). For the quantitative analysis, the level of GFP fluorescence derived from CD63$^+$ TSU and PSU sEVs on HeLa cells was determined using ImageJ and illustrated in Figure 2F. Studies have been focused on the influence of zeta potential in cellular uptake and EV stability, which is the measurement of surface potential that determines the magnitude of the electrical double layer repulsion [40,41]. In this respect, we investigated the zeta potential differences between TSU and PSU sEVs that could explain different up-take rates. No difference in zeta potential was found on both F2 and F3 of TSU and PSU sEVs (Figure 2G). Alternatively, we hypothesized the possibility that the PEG chemical present in PSU sEVs somehow inhibits the entry of sEVs into recipient cells.
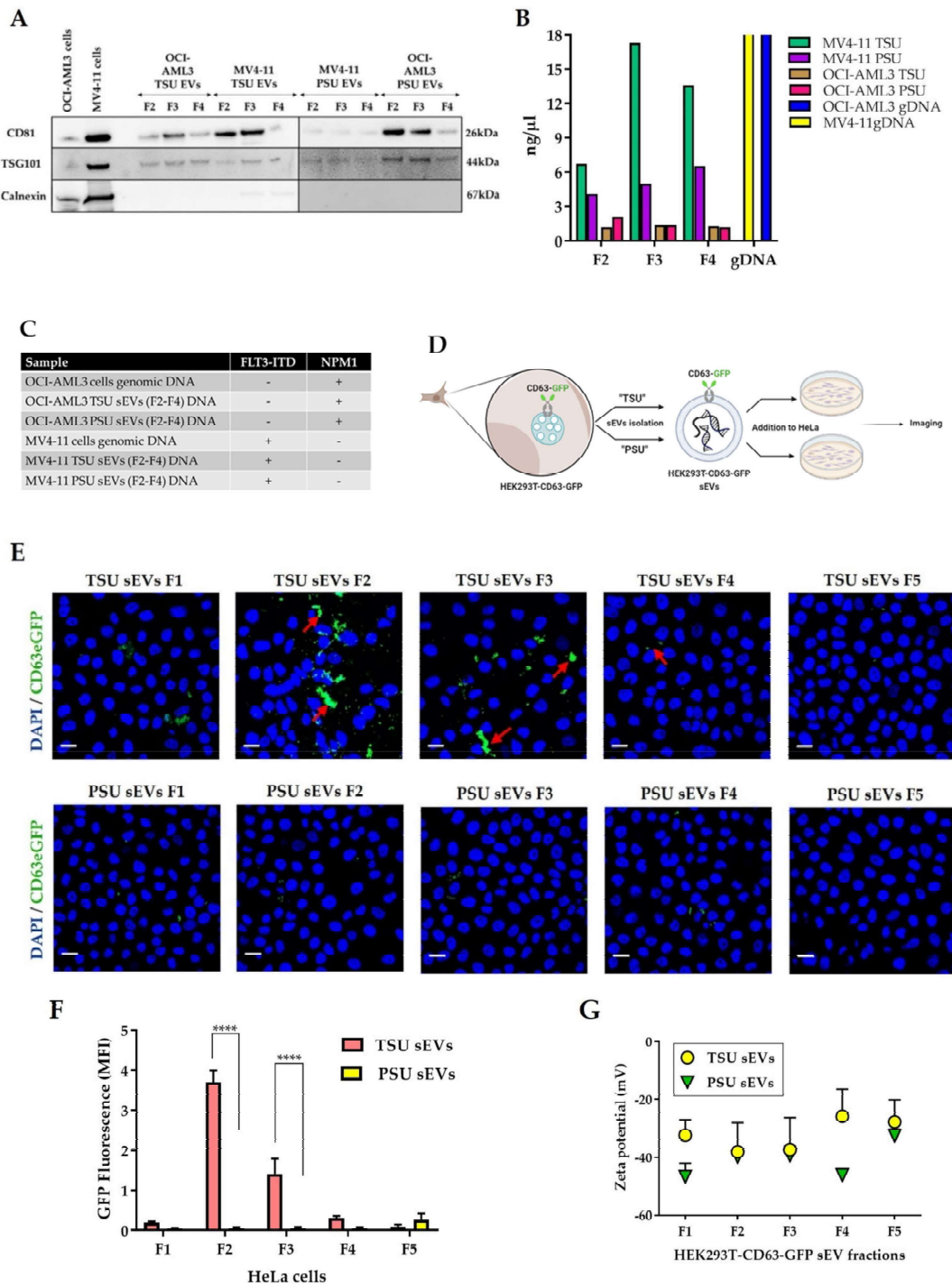
Figure 2. Utilization of sEVs for diagnostic and functional studies. (**A**) Immunoblot analysis of TSU and PSU sEV fractions (F2–F4) obtained from OCI−AML3 and MV4−11 with CD81, TSG101, and calnexin. (**B**) Comparison of EV-DNA concentration of OCI−AML3 and MV4−11 TSU and PSU sEV fractions (F2–F4). (**C**) GeneScan-based fragment-length analyses for detecting FLT3−ITD and NPM1 mutations both in genomic DNA and in their corresponding TSU and PSU sEVs. (**D**) Schematic diagram showing how sEVs obtained from HEK-CD63-GFP stable cell line can be helpful for EV functional studies. (**E**) Immunofluorescence staining of HeLa cells cultured with HEK293T-CD63-GFP TSU and PSU sEVs. Representative confocal images showing cell nuclei stained by DAPI (blue) and GFP fluorescence (green) indicating CD63$^+$ sEVs (shown by red arrows). Scale bar: 10 μm. (**F**) Quantitative analysis of GFP fluorescence derived from CD63$^+$ TSU and PSU sEVs (n = 3). (**G**) Zeta potential of HEK-CD63-GFP TSU and PSU sEVs (n = 3) measured using NTA. Data are shown as the mean ± S.E.M. **** $p < 0.0001$.

3.3. Localization of EV-DNA in the Cell Membrane, Cytoplasm and Nucleus

Horizontal transfer of DNA fragments via EVs from tumor to healthy stromal cells can be a detrimental factor in cell-to-cell communication in cancer. Therefore, we aimed to determine the capability of different sEVs fractions (F1–F5) to transport DNA into recipient cells. For this, the HEK293T-CD63-GFP cell line was incubated with 5-ethynyl-2′-deoxyuridine (EdU) for 72 h to label DNA. As a result, EVs containing DNA were stained with EdU. Later, both genomic DNA and sEVs were isolated from these EdU-treated cells. EdU was detected based on a click-it reaction on HeLa cells incubated with HEK293T-CD63-GFP TSU and PSU sEVs (F1–F5) containing EV-DNA-EdU, the HEK293T-CD63-GFP genomic DNA-EdU (negative control), and imaged using confocal microscopy as illustrated in Figure 3A. As expected, no signal was found on cells incubated with genomic DNA-EdU (data not shown). Comparatively, we found that TSU sEV fractions F2 and F3 could deliver DNA efficiently in HeLa recipient cells both in the cytoplasm and in the nucleus. However, it is negligible in the F1 TSU fraction that contains fewer sEVs and on all PSU sEV fractions (F1–F5) (Figure 3B). Unlike before, we did not observe much GFP fluorescence along with the EdU signal. This could be because the copper ions present in the click-it EdU staining kit might quench the GFP fluorescence, as pointed out by the manufacturer (Figure 3C). In addition, we confirmed that the isolated sEVs are devoid of free EdU since the same effect that we observed in the positive staining control (HeLa cells incubated with EdU for 2 h) was not found in sEV-treated HeLa cells (Figure 3D). To evaluate the efficiency of EV-DNA transfer, we quantified the level of EdU (red fluorescence) derived from various TSU and PSU EV-DNA on HeLa recipient cells, and the data are outlined in Figure 3E. It is apparent that F2 and F3 TSU sEVs are more efficient in delivering DNA into the recipient cells than other fractions.

To precisely visualize and measure the amount of EV-DNA localized in various cell compartments such as the cell membrane, cytoplasm, and nucleus, we analyzed the reconstructed confocal z-stacks of confocal images containing EV-DNA first-ever using Imaris software. Briefly, deconvolution of data sets was performed using Huygens, and the Imaris surface function was used to distinguish different cell compartments, which helped quantify accurately the amount of EV-DNA localized inside the recipient cells, avoiding false-positive results or artifacts generated from 2D microscopy (Figure 3F). Indeed, we observed that only ~50% of EV-DNA from F2 and F3 and 25% from F4 successfully passed through the cell membrane barrier and localized inside the recipient cells, while others were found outside the cells and at the cell membrane. We found nearly the same amount of EV-DNA (F2 and F3) inside the recipient cells both in the cytoplasm and in the nucleus. However, it is significantly less in F4, which explains that there is a different DNA population present in this fraction (Figure 3G). To confirm if the EV-DNA-EdU transfer approach could be used for any disease model, we incubated leukemia cell line MV4-11-derived sEVs containing EV-DNA-EdU with mouse mesenchymal stromal cells, OP9. Indeed, we observed that MV4-11-EV-DNA was transferred into OP9 cells, which shows that this approach could be used to evaluate the EV-DNA role in cell–cell communication in leukemia (Figure 3H). Next, to analyze EV-DNA organization at a single vesicle level, we imaged HEK-CD63-GFP TSU sEVs (F2 and F3) mounted on poly-L lysine coated coverslips using super-resolution microscopy (Figure 3I). Indeed, we observed that most of the EV-DNA (red) signal was found next to CD63+ EVs (green), indicating that these are intravesicular EV-DNA fragments protected inside the vesicles. However, a small proportion of EV-DNA co-localized with CD63 GFP + EVs revealing the possibility that they are extra vesicular DNA.
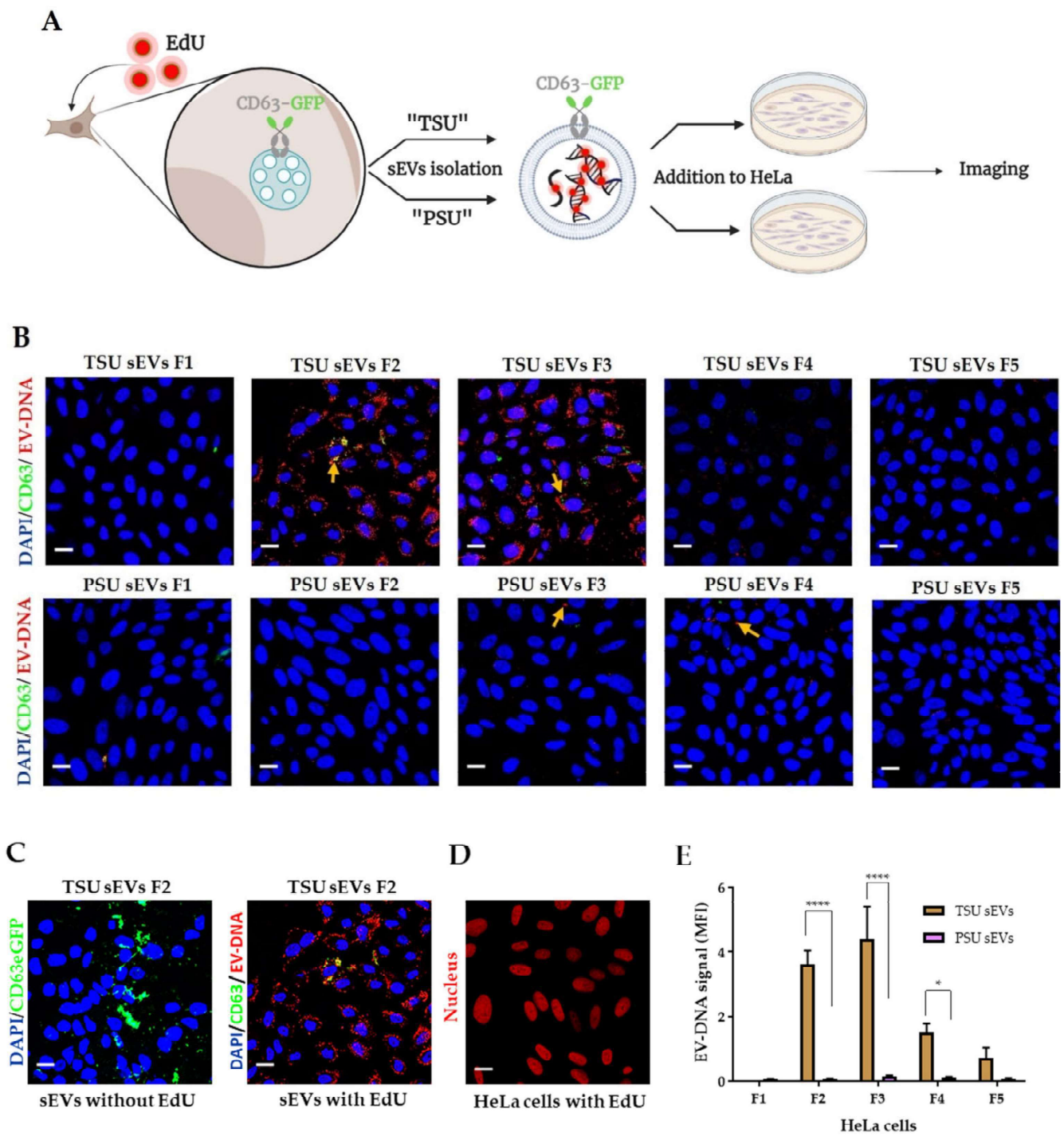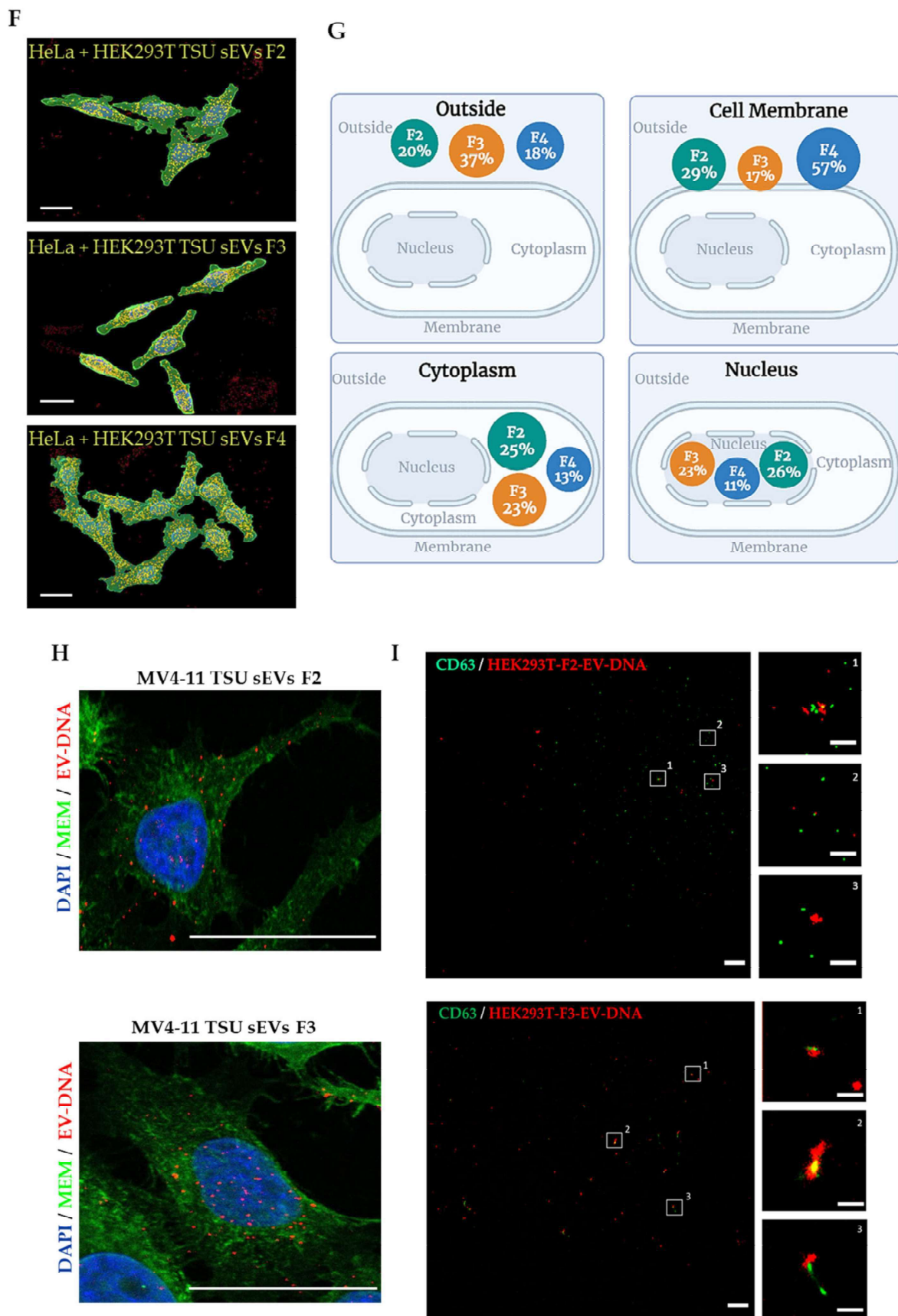
Figure 3. *Cont.*

Figure 3. EV-DNA uptake in the recipient cells. (**A**) Figure explaining the incorporation of EdU into cellular DNA, thereby labeling EV-DNA with EdU for functional studies. (**B**) Immunofluorescence

staining of HeLa cells transferred with HEK293T-CD63-GFP sEVs (F1–F5) containing EV-DNA-EdU. Representative confocal images illustrating cell nuclei (blue) stained by DAPI, GFP (green) derived from transferred CD63+ EVs, and localized foreign EV-DNA inside HeLa cells (red) detected using click-it azide-Alexa647. Yellow arrows show the co-localization of CD63$^+$ EVs (GFP) and transferred EV-DNA (red). (**C**) Quenching of GFP fluorescence due to copper ions derived from click-it EdU staining kit. (**D**) HeLa cells after EdU treatment—positive staining control. Scale bar: 10 μm. (**E**) Quantification of EdU signal to determine EV-DNA transfer efficiency (*n* = 3). (**F**) Three-dimensional image analysis for the accurate quantification of EV-DNA. Representative images obtained from IMARIS showing HeLa cells educated with HEK293T TSU sEVs. Scale bar: 20 μm. (**G**) Measurement of foreign EV-DNA found outside recipient cells and at the cell membrane, cytoplasm, and nucleus. (**H**) Imaging of OP9 cells incubated with MV4−11 sEVs containing EV-DNA-EdU. Representative confocal images showing nuclei staining by DAPI (blue), cell membrane staining by WGA (green), and EV-DNA-EdU staining by click-it kit (red). (**I**) Super-resolution microscopy imaging of HEK293T-CD63-GFP TSU sEVs (F2 and F3) containing EdU. CD63$^+$ EVs-GFP is shown in green, and EV-DNA-Alexa647 is shown in red. Scale bar: 2 μm and Scale bar insets: 0.5 μm. Data are shown as the mean ± S.E.M. * *p* < 0.0332 and **** *p* < 0.0001.

3.4. Characterization of TSU EV-DNA

Knowing that TSU EV-DNA is actively taken up by the recipient cells, we included only TSU sEVs for further downstream analyses. We analyzed the DNA of TSU sEVs (HEK293T) (F1–F5) more elaborately to characterize vesicle protected and exposed non-vesicular DNA either free or sticking on the surface of the EVs using dsDNase digestion as previously published [5] (Figure 4A,B). EV-DNA samples were stained with SYBR green and loaded onto an agarose gel (Figure 4C). We observed in F2 that high molecular weight DNA fragments larger than 2–10 kb were digested after dsDNase exposure that specially digests only dsDNA. However, in F3, some large DNA fragments (2–10 kb) were protected from dsDNase. Conversely, in F4 and F5, we found an apparent decrease in the level of EV-DNA after dsDNase digestion, indicating that mostly extra vesicular EV-DNA is present in these fractions. In addition, the ideal size of circulating or cell-free DNA fragments ranging between 120–220 bp was observed only in non-sEV fractions (F4 and F5) but not in sEV fractions (F2 and F3) before dsDNase treatment [42,43]. Altogether, it suggests that sEV fractions, F2 and F3, are devoid of cell-free DNA, and primarily large DNA fragments 2–10 kb exist on the outer surface of sEVs, and 220 bp- 2 kb DNA fragments are encapsulated inside sEVs.

To further investigate if the intravesicular EV-DNA fragments from various HEK293T TSU sEV fractions are double stranded, we digested them with dsDNase again and analyzed them in the same manner as before (Figure 4D). In line with our previous findings [5], we found that intravesicular EV-DNA present in HEK293T TSU sEV fractions (F2–F5) is completely double stranded. To know the details of vesicle and non-vesicle protected DNA, HEK293T EV-DNA samples pre-treated with and without dsDNase were sequenced using NGS platform. Confirming the previous reports, we observed that both vesicle and non-vesicle-protected EV-DNA fragments are mainly derived from the host cell genome; however, a small proportion is derived from the mitochondria (Figure 4E) [27,44–46]. Furthermore, we observed that there is an increase in the level of mtDNA on the EV-DNA samples pre-treated with dsDNase, which is in accordance with the finding observed by Sansone et al., 2017 [47].
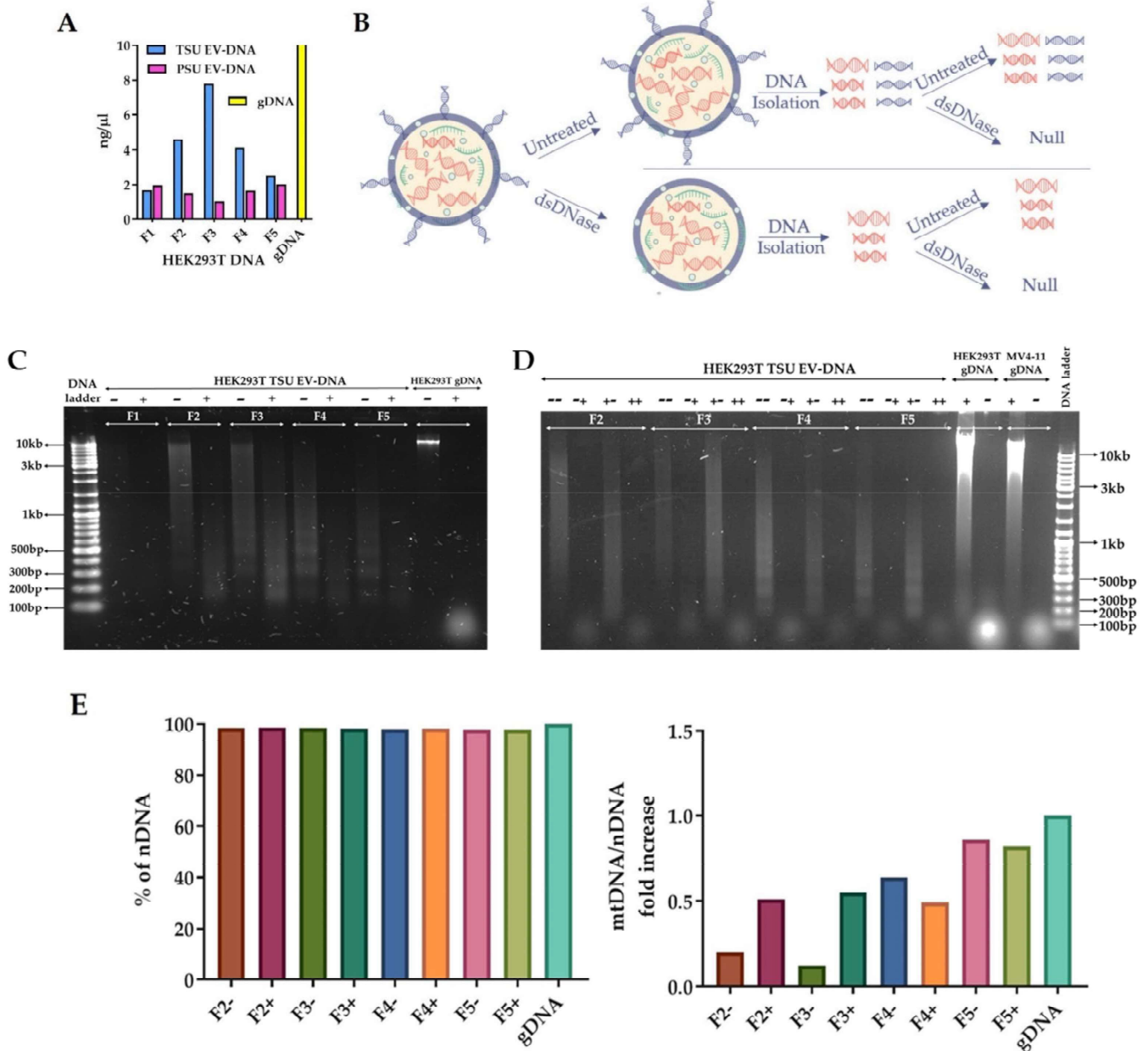
Figure 4. Detailed characterization of EV-DNA. (**A**) Comparison of HEK293T TSU and PSU EV-DNA concentration. (**B**) Scheme displaying the steps involved in the analysis of extravesicular and intravesicular EV-DNA using single and double dsDNAse digestion. (**C**) EV-DNA derived from HEK293T TSU sEVs (F1–F5) pre-treated with and without dsDNAse to demonstrate extravesicular EV-DNA fragments. (**D**) Further treatment of dsDNAse to reveal vesicle protected dsDNA. (**E**) Next-generation sequencing (NGS) analysis of HEK293T-EV-DNA. Percentage of nuclear or genomic DNA and the ratio of host mitochondrial to nuclear DNA fold increase were determined.

3.5. Association of EV-DNA with Cytoplasmic DNA Sensors and Endosomal Proteins

In recent years, it was found that DNA from various sources could enter the cytosol and activate the cGAS-STING pathway: a DNA-driven immune response critical in host defense, inflammation, and tumor immunity [29,30,48]. Interestingly, we observed the co-localization of cGAS and STING with EV-DNA in HeLa cells, suggesting their molecular interaction (Figure 5A).
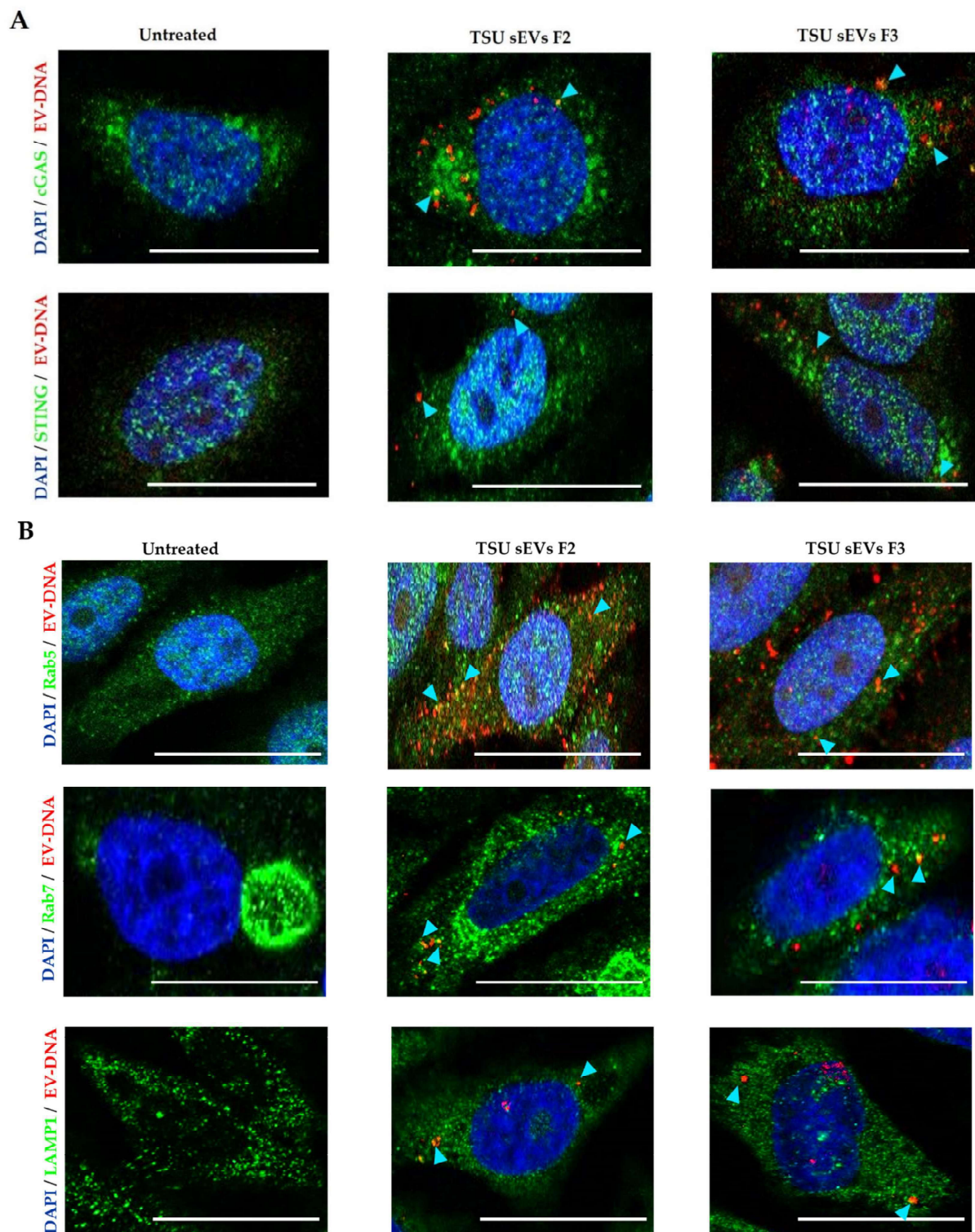
Figure 5. Association of EV-DNA with various cytoplasmic proteins. Staining of HeLa cells with and without HEK293T TSU sEVs (F2 and F3) containing EV-DNA-EdU for (**A**) cGAS and STING (**B**) Rab5, Rab7, and LAMP1. Representative confocal images showing cell nuclei (DAPI- blue), endosomal proteins, and dsDNA sensors (green). Blue arrows show co-localization (yellow) of EV-DNA with various cytoplasmic proteins. Scale bars: 10 μm.

To determine if EV-DNA is considered to be a potential threat inside the recipient cells directing towards endosomal fusion and degradation in the lysosomal compartment, HeLa cells incubated with EdU-labeled F2 and F3 HEK293T TSU sEVs were stained for Rab5

and Rab7 proteins (early and late endosomal markers) and LAMP1 (lysosomal autophagy marker). Further elucidating the previous observations by Rappa et al. [49], we found that a portion of EV-DNA associates with Rab5 and Rab7 (Figure 5B). In addition, the co-localization of EV-DNA with LAMP-1 highlights that they are in the process of degradation.

4. Discussion

Using differential UC and polymer-based EV isolation methods, many studies have demonstrated EV-DNA as a potential biomarker for various diseases [5,7,21,50,51] and the functional role of EV-DNA in cell–cell communication [30,47,52]. Although these EV isolation methods provide good EV yield to perform diagnostic studies, we claim that these isolated EVs are not suitable to perform EV-DNA-based functional studies since these methods are known to co-isolate cell-free DNA (cfDNA) and apoptotic bodies [23–25,37,53]. Because of these obstacles, one cannot illustrate exactly if the observed physiological function in the recipient cells is due to EV-DNA only, not by any other contaminants [3]. To address this problem, we applied a simple benchtop method to enrich sEVs from non-EV particles using a state-of-the-art combination of tangential flow filtration, size-exclusion chromatography, and ultrafiltration (TSU). Out of five TSU sEVs fractions (F1–F5), fractions (F2 and F3) fulfill the EV criteria recommended by MISEV2018 [3]. Further, TSU F2 and F3 provide sEVs qualified to perform EV-DNA functional studies.

To reveal the distribution of EV-DNA in the recipient cells, we employed the 3D reconstruction of confocal z-stacks using Imaris software. Contrary to 2D imaging data, we found through 3D analysis that almost the same amount of EV-DNA from F2 and F3 entered the cytoplasm and the nucleus of recipient cells (Figure 3E,G). In addition, from this analysis, we revealed something unique: the recipient cell membrane barrier prevents almost 50 percent of F3-EV-DNA from getting inside. There may be other cofactors deciding the entry of different EV-DNA fragments into the recipient cells, which requires further investigation. Collectively, 3D image analysis using Imaris helps EV researchers in the future to avoid reporting false-positive results generated from confocal microscopy images taken in a single plane of focus [54]. Next, we utilized CD63+ EVs and EV-DNA-EdU to study the arrangement of EVs and EV-DNA at a single vesicle level employing super-resolution microscopy. As expected, we revealed that not all EV-DNA was associated with the EV surface marker, CD63, since EV-DNA was mainly localized inside the vesicles (Figure 3I).

Lázaro-Ibáñez et al., 2019 isolated sEVs using UC-based iodixanol density separation; however, it is unclear whether radiocontrast agents such as iodixanol used for separation will be entirely removed from EV preparation [27]. In our case, we observed that the PEG used for the precipitation of sEVs influences the EV uptake and EV-DNA entry into the recipient cells. In addition, they showed that DNA isolated from both low-density and high-density fractions possessed nucleosomal patterns [27]. On the other hand, Vagner et al., 2018 showed that large EVs isolated from prostate cancer cells are enriched in chromosomal DNA, suggesting that most genomic DNA detected in large EVs is nucleosomal, most probably originating in the extracellular space from apoptotic or necrotic cells [55]. Supporting these facts only to a limited extent, we found that isolated small EVs are free from apoptotic bodies; however, the cell-free DNA population with a nucleosomal pattern was observed only in fractions, F4 and F5, which contain fewer small EVs (Figure 4C). Besides, NGS analysis confirmed that mitochondria DNA fragments are enriched more in non-EV fraction F5. Taken together, these observations hint that mostly EV-DNA present in F2 and F3 are genomic DNA fragments packaged inside sEVs, not as a circulating cell-free DNA derived from dead cells or cancer cells.

We know that viral dsDNA activates some pathways during active virus infection, hijacking the host defense machinery to support their survival in the human body [56,57]. It is not explored whether EV-DNA communicates in the same way in our human body to drive cancer progression, metastasis, and cancer relapse. Bakhoum et al., 2018 revealed for the first time that there is an unexpected link between chromosome instability and the

release of free DNA in the cytoplasm for the activation of cytosolic DNA sensing pathways and metastasis [29]. Furthermore, only one study has addressed so far that EV-DNA is involved in cell–cell communication between T cells and dendritic cells. In this study, they used UC to isolate EVs that can be contaminated with other non-EV populations. They showed that activation of the cGAS/STING/IRF3 signaling axis in priming the dendritic cells is an exclusive function of EV-DNA released by T-cells [30]. Similarly, we observed that EV-DNA associates with the cytoplasmic sensors cGAS and STING. However, in the future, after obtaining sEVs using TSU, we need to evaluate if EV-DNA association with cGAS-STING plays an essential role in cancer. In addition, whether DNA associated with F2 and F3 is linked with histones needs to be determined. It could be possible that histones associated with EV-DNA and other cofactors collaborated with EV-DNA might be essential for EV-DNA function in the recipient cells, driving towards cancer progression or metastasis.

5. Conclusions

TSU serves as a better choice for EV isolation when EV-DNA functional studies need to be executed since it provides a small EV preparation deficient in cell-free DNA and apoptotic bodies, unlike other commonly used methods. In addition, the TSU-EV-DNA-EdU labeling approach, along with three-dimensional microscope image analysis using Imaris, helps EV researchers to evaluate the EV-DNA role in cell–cell communication in cancer.

Supplementary Materials: The following supporting information can be downloaded at https://www.mdpi.com/article/10.3390/cancers14092068/s1, Figure S1: A: HeLa sEVs NTA and micro BCA data; B: HeLa TSU and PSU sEVs purity; C: HeLa sEVs TEM images; D: HeLa sEVs average diameter; E: Original western blot images; F: Single beads selection; G: CD9+ population selection; H: Purity based on EV tetraspanins and micro BCA value; I: HeLa EV-DNA concentration.

Author Contributions: Conceptualization, V.K.C. and B.K.T.; methodology, V.K.C., J.G., S.A., K.R., M.G., E.G.-N. and M.S.; validation, V.K.C., J.G., S.A., M.S., E.G.-N., N.v.N. and B.K.T.; formal analysis, V.K.C., K.R., A.B., M.G. and C.C.; investigation, V.K.C., J.G., A.B., I.N. and B.K.T.; resources, D.R., N.v.N., J.J., C.C. and B.K.T.; data curation, V.K.C.; writing—original draft preparation, V.K.C. and B.K.T.; writing—review and editing, V.K.C., J.G., D.R., J.J., I.N. and B.K.T.; visualization, V.K.C. and B.K.T.; supervision, B.K.T.; project administration, B.K.T.; funding acquisition, D.R. and B.K.T. All authors have read and agreed to the published version of the manuscript.

Institutional Review Board Statement: Not applicable.

Informed Consent Statement: Not applicable.

Data Availability Statement: All authors declare that the data presented in this study are available within the article and its supplementary information files or upon reasonable requests to the corresponding author.

Conflicts of Interest: The authors declare no conflict of interest.

Abbreviations

EVs	Extracellular vesicles
sEVs	Small extracellular vesicles
dsDNA	Double-stranded DNA

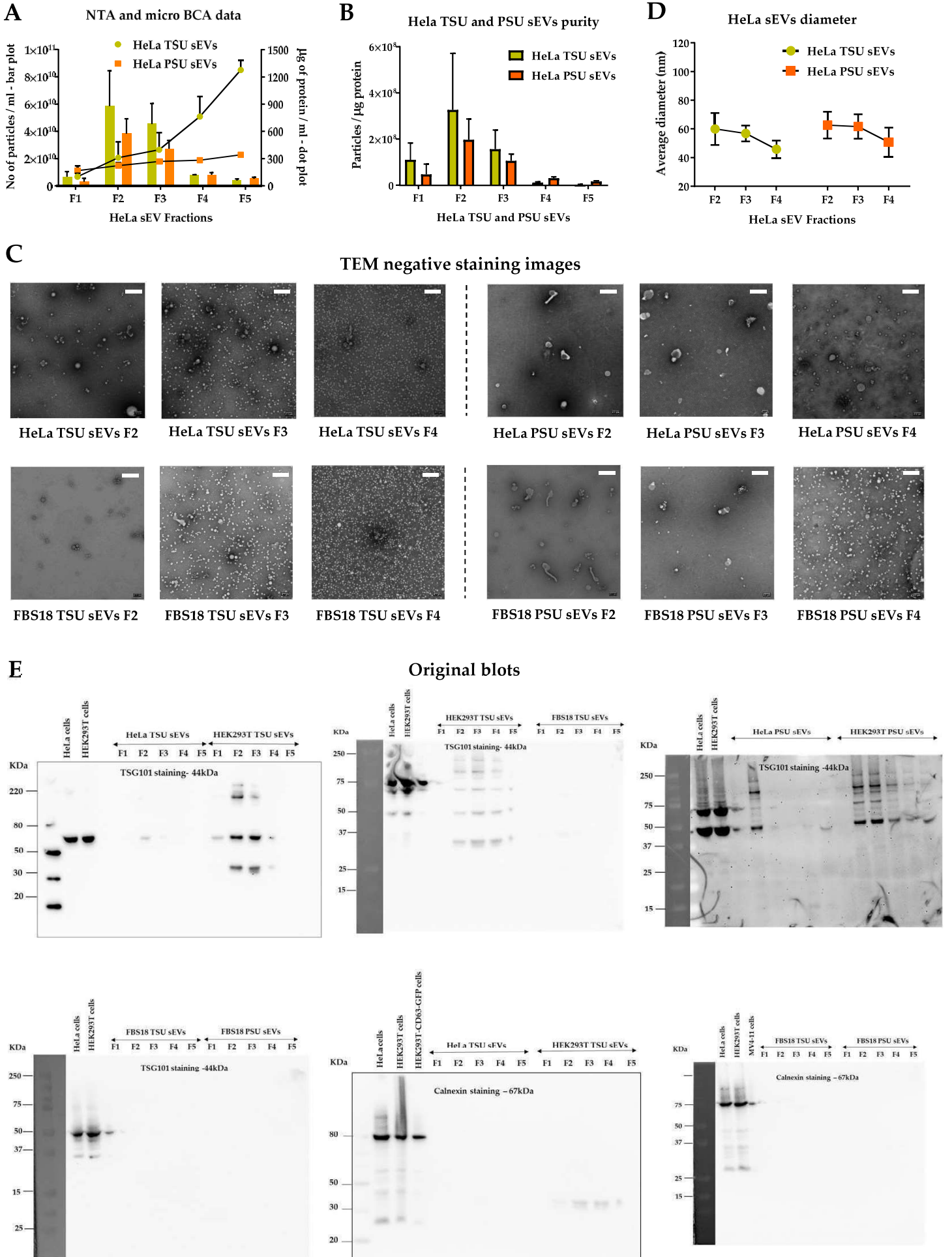|	
EV-DNA	Small extracellular vesicles DNA
cfDNA	Cell-free DNA
TSU	Tangential flow filtration + Size -exclusion chromatography + Ultrafiltration
PSU	Polyethylene glycol precipitation + Size-exclusion chromatography + Ultrafiltration
MSCs	Mesenchymal stromal cells
BM	Bone marrow
cGAS	Cyclic GMP-AMP synthase
STING	Stimulator of interferon genes
UC	Ultracentrifugation
SEC	Size-exclusion chromatography
UF	Ultrafiltration
TFF	Tangential flow filtration
PEG	Polyethylene glycol
IRF3	Interferon regulatory factor 3
AML	Acute myeloid leukemia
GFP	Green fluorescent protein
FBS	Fetal bovine serum
CCM	Cell conditioned media
NTA	Nanoparticle tracking analysis
TEM	Transmission electron microscopy
RT	Room temperature
MFI	Mean fluorescence intensity
FLT3	Fms-like tyrosine kinase 3
NPM1	Nucleophosmin 1
EdU	5-ethynyl-2′-deoxyuridine
WGA	Wheat germ agglutinin
NGS	Next-generation sequencing
SEM	Standard error mean
LAMP1	Lysosomal-associated membrane protein 1
Rab5/7	Ras-related proteins

References

1. Ghanam, J.; Chetty, V.K.; Barthel, L.; Reinhardt, D.; Hoyer, P.F.; Thakur, B.K. DNA in extracellular vesicles: From evolution to its current application in health and disease. *Cell Biosci.* **2022**, *12*, 37. [CrossRef]
2. Elzanowska, J.; Semira, C.; Costa-Silva, B. DNA in extracellular vesicles: Biological and clinical aspects. *Mol. Oncol.* **2021**, *15*, 1701–1714. [CrossRef]
3. Thery, C.; Witwer, K.W.; Aikawa, E.; Alcaraz, M.J.; Anderson, J.D.; Andriantsitohaina, R.; Antoniou, A.; Arab, T.; Archer, F.; Atkin-Smith, G.K.; et al. Minimal information for studies of extracellular vesicles 2018 (MISEV2018): A position statement of the International Society for Extracellular Vesicles and update of the MISEV2014 guidelines. *J. Extracell. Vesicles* **2018**, *7*, 1535750. [CrossRef]
4. Thery, C.; Amigorena, S.; Raposo, G.; Clayton, A. Isolation and characterization of exosomes from cell culture supernatants and biological fluids. *Curr. Protoc. Cell Biol.* **2006**, *3*, 3.22.1–3.22.29. [CrossRef]
5. Thakur, B.K.; Zhang, H.; Becker, A.; Matei, I.; Huang, Y.; Costa-Silva, B.; Zheng, Y.; Hoshino, A.; Brazier, H.; Xiang, J.; et al. Double-stranded DNA in exosomes: A novel biomarker in cancer detection. *Cell Res.* **2014**, *24*, 766–769. [CrossRef]
6. Valadi, H.; Ekstrom, K.; Bossios, A.; Sjostrand, M.; Lee, J.J.; Lotvall, J.O. Exosome-mediated transfer of mRNAs and microRNAs is a novel mechanism of genetic exchange between cells. *Nat. Cell Biol.* **2007**, *9*, 654–659. [CrossRef]
7. Kahlert, C.; Melo, S.A.; Protopopov, A.; Tang, J.; Seth, S.; Koch, M.; Zhang, J.; Weitz, J.; Chin, L.; Futreal, A.; et al. Identification of double-stranded genomic DNA spanning all chromosomes with mutated KRAS and p53 DNA in the serum exosomes of patients with pancreatic cancer. *J. Biol. Chem.* **2014**, *289*, 3869–3875. [CrossRef]
8. Hoshino, A.; Costa-Silva, B.; Shen, T.L.; Rodrigues, G.; Hashimoto, A.; Tesic Mark, M.; Molina, H.; Kohsaka, S.; Di Giannatale, A.; Ceder, S.; et al. Tumour exosome integrins determine organotropic metastasis. *Nature* **2015**, *527*, 329–335. [CrossRef]
9. Gao, Y.; Qin, Y.; Wan, C.; Sun, Y.; Meng, J.; Huang, J.; Hu, Y.; Jin, H.; Yang, K. Small Extracellular Vesicles: A Novel Avenue for Cancer Management. *Front. Oncol.* **2021**, *11*, 638357. [CrossRef]
10. Droste, M.; Thakur, B.K.; Eliceiri, B.P. Tumor-Derived Extracellular Vesicles and the Immune System-Lessons From Immune-Competent Mouse-Tumor Models. *Front. Immunol.* **2020**, *11*, 606859. [CrossRef]
11. Yanez-Mo, M.; Siljander, P.R.; Andreu, Z.; Zavec, A.B.; Borras, F.E.; Buzas, E.I.; Buzas, K.; Casal, E.; Cappello, F.; Carvalho, J.; et al. Biological properties of extracellular vesicles and their physiological functions. *J. Extracell. Vesicles* **2015**, *4*, 27066. [CrossRef] [PubMed]

12. Admyre, C.; Johansson, S.M.; Qazi, K.R.; Filen, J.J.; Lahesmaa, R.; Norman, M.; Neve, E.P.; Scheynius, A.; Gabrielsson, S. Exosomes with immune modulatory features are present in human breast milk. *J. Immunol.* **2007**, *179*, 1969–1978. [CrossRef] [PubMed]

13. Malkin, E.Z.; Bratman, S.V. Bioactive DNA from extracellular vesicles and particles. *Cell Death Dis.* **2020**, *11*, 584. [CrossRef]

14. Pitt, J.M.; Kroemer, G.; Zitvogel, L. Extracellular vesicles: Masters of intercellular communication and potential clinical interventions. *J. Clin. Investig.* **2016**, *126*, 1139–1143. [CrossRef] [PubMed]

15. Maas, S.L.N.; Breakefield, X.O.; Weaver, A.M. Extracellular Vesicles: Unique Intercellular Delivery Vehicles. *Trends Cell Biol.* **2017**, *27*, 172–188. [CrossRef] [PubMed]

16. Liu, C.; Yu, S.; Zinn, K.; Wang, J.; Zhang, L.; Jia, Y.; Kappes, J.C.; Barnes, S.; Kimberly, R.P.; Grizzle, W.E.; et al. Murine mammary carcinoma exosomes promote tumor growth by suppression of NK cell function. *J. Immunol.* **2006**, *176*, 1375–1385. [CrossRef]

17. Umezu, T.; Tadokoro, H.; Azuma, K.; Yoshizawa, S.; Ohyashiki, K.; Ohyashiki, J.H. Exosomal miR-135b shed from hypoxic multiple myeloma cells enhances angiogenesis by targeting factor-inhibiting HIF-1. *Blood* **2014**, *124*, 3748–3757. [CrossRef]

18. Moore, M.; Davachi, F.; Bongo, L.; Seruvugo, H.; Mushiya, K.; Roy, J.A.; Mambu ma, D. New parameters for evaluating oral rehydration therapy: One year's experience in a major urban hospital in Zaire. *J. Trop. Pediatr.* **1989**, *35*, 179–184. [CrossRef]

19. Hur, J.Y.; Kim, H.J.; Lee, J.S.; Choi, C.M.; Lee, J.C.; Jung, M.K.; Pack, C.G.; Lee, K.Y. Extracellular vesicle-derived DNA for performing EGFR genotyping of NSCLC patients. *Mol. Cancer* **2018**, *17*, 15. [CrossRef]

20. Klump, J.; Phillipp, U.; Follo, M.; Eremin, A.; Lehmann, H.; Nestel, S.; von Bubnoff, N.; Nazarenko, I. Extracellular vesicles or free circulating DNA: Where to search for BRAF and cKIT mutations? *Nanomedicine* **2018**, *14*, 875–882. [CrossRef]

21. Kontopoulou, E.; Strachan, S.; Reinhardt, K.; Kunz, F.; Walter, C.; Walkenfort, B.; Jastrow, H.; Hasenberg, M.; Giebel, B.; von Neuhoff, N.; et al. Evaluation of dsDNA from extracellular vesicles (EVs) in pediatric AML diagnostics. *Ann. Hematol.* **2020**, *99*, 459–475. [CrossRef] [PubMed]

22. Maire, C.L.; Fuh, M.M.; Kaulich, K.; Fita, K.D.; Stevic, I.; Heiland, D.H.; Welsh, J.A.; Jones, J.C.; Gorgens, A.; Ricklefs, T.; et al. Genome-wide methylation profiling of glioblastoma cell-derived extracellular vesicle DNA allows tumor classification. *Neuro-Oncology* **2021**, *23*, 1087–1099. [CrossRef] [PubMed]

23. Sidhom, K.; Obi, P.O.; Saleem, A. A Review of Exosomal Isolation Methods: Is Size Exclusion Chromatography the Best Option? *Int. J. Mol. Sci.* **2020**, *21*, 6466. [CrossRef] [PubMed]

24. Liangsupree, T.; Multia, E.; Riekkola, M.L. Modern isolation and separation techniques for extracellular vesicles. *J. Chromatogr. A* **2021**, *1636*, 461773. [CrossRef] [PubMed]

25. Furi, I.; Momen-Heravi, F.; Szabo, G. Extracellular vesicle isolation: Present and future. *Ann. Transl. Med.* **2017**, *5*, 263. [CrossRef]

26. Lobb, R.J.; Becker, M.; Wen, S.W.; Wong, C.S.; Wiegmans, A.P.; Leimgruber, A.; Moller, A. Optimized exosome isolation protocol for cell culture supernatant and human plasma. *J. Extracell. Vesicles* **2015**, *4*, 27031. [CrossRef]

27. Lazaro-Ibanez, E.; Lasser, C.; Shelke, G.V.; Crescitelli, R.; Jang, S.C.; Cvjetkovic, A.; Garcia-Rodriguez, A.; Lotvall, J. DNA analysis of low- and high-density fractions defines heterogeneous subpopulations of small extracellular vesicles based on their DNA cargo and topology. *J. Extracell. Vesicles* **2019**, *8*, 1656993. [CrossRef]

28. Tian, T.; Zhu, Y.L.; Zhou, Y.Y.; Liang, G.F.; Wang, Y.Y.; Hu, F.H.; Xiao, Z.D. Exosome uptake through clathrin-mediated endocytosis and macropinocytosis and mediating miR-21 delivery. *J. Biol. Chem.* **2014**, *289*, 22258–22267. [CrossRef]

29. Bakhoum, S.F.; Ngo, B.; Laughney, A.M.; Cavallo, J.A.; Murphy, C.J.; Ly, P.; Shah, P.; Sriram, R.K.; Watkins, T.B.K.; Taunk, N.K.; et al. Chromosomal instability drives metastasis through a cytosolic DNA response. *Nature* **2018**, *553*, 467–472. [CrossRef]

30. Torralba, D.; Baixauli, F.; Villarroya-Beltri, C.; Fernandez-Delgado, I.; Latorre-Pellicer, A.; Acin-Perez, R.; Martin-Cofreces, N.B.; Jaso-Tamame, A.L.; Iborra, S.; Jorge, I.; et al. Priming of dendritic cells by DNA-containing extracellular vesicles from activated T cells through antigen-driven contacts. *Nat. Commun.* **2018**, *9*, 2658. [CrossRef]

31. Ludwig, A.K.; De Miroschedji, K.; Doeppner, T.R.; Borger, V.; Ruesing, J.; Rebmann, V.; Durst, S.; Jansen, S.; Bremer, M.; Behrmann, E.; et al. Precipitation with polyethylene glycol followed by washing and pelleting by ultracentrifugation enriches extracellular vesicles from tissue culture supernatants in small and large scales. *J. Extracell. Vesicles* **2018**, *7*, 1528109. [CrossRef] [PubMed]

32. Chen, S.Y.; Bestvater, F.; Schaufler, W.; Heintzmann, R.; Cremer, C. Patterned illumination single molecule localization microscopy (piSMLM): User defined blinking regions of interest. *Opt. Express* **2018**, *26*, 30009–30020. [CrossRef] [PubMed]

33. Ovesny, M.; Krizek, P.; Borkovec, J.; Svindrych, Z.; Hagen, G.M. ThunderSTORM: A comprehensive ImageJ. plug-in for PALM and STORM data analysis and super-resolution imaging. *Bioinformatics* **2014**, *30*, 2389–2390. [CrossRef] [PubMed]

34. Schindelin, J.; Arganda-Carreras, I.; Frise, E.; Kaynig, V.; Longair, M.; Pietzsch, T.; Preibisch, S.; Rueden, C.; Saalfeld, S.; Schmid, B.; et al. Fiji: An open-source platform for biological-image analysis. *Nat. Methods* **2012**, *9*, 676–682. [CrossRef] [PubMed]

35. Bolger, A.M.; Lohse, M.; Usadel, B. Trimmomatic: A flexible trimmer for Illumina sequence data. *Bioinformatics* **2014**, *30*, 2114–2120. [CrossRef] [PubMed]

36. Li, H. A statistical framework for SNP calling, mutation discovery, association mapping and population genetical parameter estimation from sequencing data. *Bioinformatics* **2011**, *27*, 2987–2993. [CrossRef] [PubMed]

37. Webber, J.; Clayton, A. How pure are your vesicles? *J. Extracell. Vesicles* **2013**, *2*, 19861. [CrossRef]

38. Kornilov, R.; Puhka, M.; Mannerstrom, B.; Hiidenmaa, H.; Peltoniemi, H.; Siljander, P.; Seppanen-Kaijansinkko, R.; Kaur, S. Efficient ultrafiltration-based protocol to deplete extracellular vesicles from fetal bovine serum. *J. Extracell. Vesicles* **2018**, *7*, 1422674. [CrossRef]
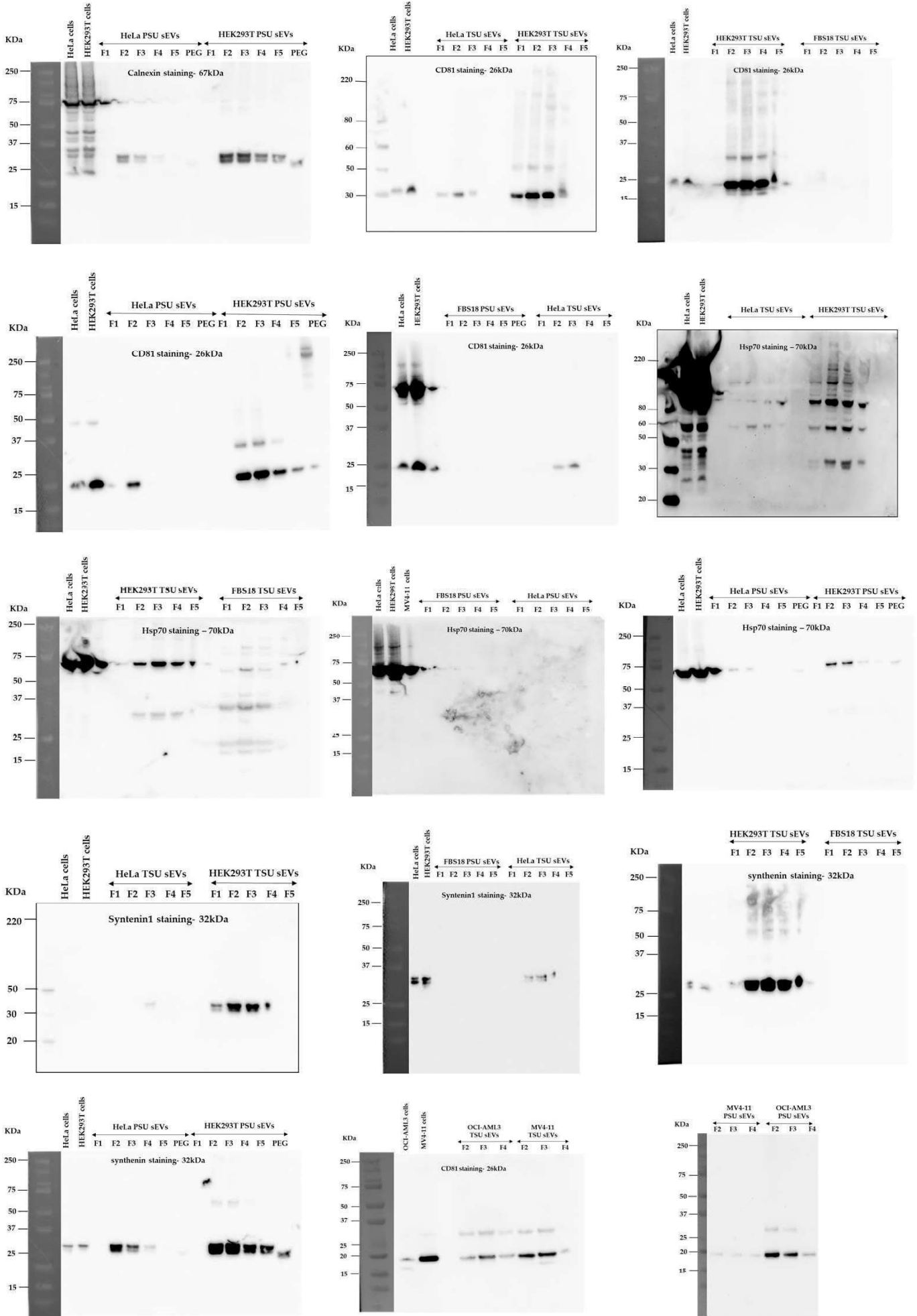
39. Suarez, H.; Gamez-Valero, A.; Reyes, R.; Lopez-Martin, S.; Rodriguez, M.J.; Carrascosa, J.L.; Cabanas, C.; Borras, F.E.; Yanez-Mo, M. A bead-assisted flow cytometry method for the semi-quantitative analysis of Extracellular Vesicles. *Sci. Rep.* **2017**, *7*, 11271. [CrossRef]

40. Midekessa, G.; Godakumara, K.; Ord, J.; Viil, J.; Lattekivi, F.; Dissanayake, K.; Kopanchuk, S.; Rinken, A.; Andronowska, A.; Bhattacharjee, S.; et al. Zeta Potential of Extracellular Vesicles: Toward Understanding the Attributes that Determine Colloidal Stability. *ACS Omega* **2020**, *5*, 16701–16710. [CrossRef]

41. Frohlich, E. The role of surface charge in cellular uptake and cytotoxicity of medical nanoparticles. *Int. J. Nanomed.* **2012**, *7*, 5577–5591. [CrossRef] [PubMed]

42. Chen, E.; Cario, C.L.; Leong, L.; Lopez, K.; Marquez, C.P.; Chu, C.; Li, P.S.; Oropeza, E.; Tenggara, I.; Cowan, J.; et al. Cell-free DNA concentration and fragment size as a biomarker for prostate cancer. *Sci. Rep.* **2021**, *11*, 5040. [CrossRef] [PubMed]

43. Alcaide, M.; Cheung, M.; Hillman, J.; Rassekh, S.R.; Deyell, R.J.; Batist, G.; Karsan, A.; Wyatt, A.W.; Johnson, N.; Scott, D.W.; et al. Evaluating the quantity, quality and size distribution of cell-free DNA by multiplex droplet digital PCR. *Sci. Rep.* **2020**, *10*, 12564. [CrossRef] [PubMed]

44. Soltesz, B.; Urbancsek, R.; Pos, O.; Hajas, O.; Forgacs, I.N.; Szilagyi, E.; Nagy-Balo, E.; Szemes, T.; Csanadi, Z.; Nagy, B. Quantification of peripheral whole blood, cell-free plasma and exosome encapsulated mitochondrial DNA copy numbers in patients with atrial fibrillation. *J. Biotechnol.* **2019**, *299*, 66–71. [CrossRef]

45. Keseru, J.S.; Soltesz, B.; Lukacs, J.; Marton, E.; Szilagyi-Bonizs, M.; Penyige, A.; Poka, R.; Nagy, B. Detection of cell-free, exosomal and whole blood mitochondrial DNA copy number in plasma or whole blood of patients with serous epithelial ovarian cancer. *J. Biotechnol.* **2019**, *298*, 76–81. [CrossRef]

46. Guescini, M.; Genedani, S.; Stocchi, V.; Agnati, L.F. Astrocytes and Glioblastoma cells release exosomes carrying mtDNA. *J. Neural Transm.* **2010**, *117*, 1. [CrossRef]

47. Sansone, P.; Savini, C.; Kurelac, I.; Chang, Q.; Amato, L.B.; Strillacci, A.; Stepanova, A.; Iommarini, L.; Mastroleo, C.; Daly, L.; et al. Packaging and transfer of mitochondrial DNA via exosomes regulate escape from dormancy in hormonal therapy-resistant breast cancer. *Proc. Natl. Acad. Sci. USA* **2017**, *114*, E9066–E9075. [CrossRef]

48. Motwani, M.; Pesiridis, S.; Fitzgerald, K.A. DNA sensing by the cGAS-STING pathway in health and disease. *Nat. Rev. Genet.* **2019**, *20*, 657–674. [CrossRef]

49. Rappa, G.; Santos, M.F.; Green, T.M.; Karbanova, J.; Hassler, J.; Bai, Y.; Barsky, S.H.; Corbeil, D.; Lorico, A. Nuclear transport of cancer extracellular vesicle-derived biomaterials through nuclear envelope invagination-associated late endosomes. *Oncotarget* **2017**, *8*, 14443–14461. [CrossRef]

50. Cambier, L.; Stachelek, K.; Triska, M.; Jubran, R.; Huang, M.; Li, W.; Zhang, J.; Li, J.; Cobrinik, D. Extracellular vesicle-associated repetitive element DNAs as candidate osteosarcoma biomarkers. *Sci. Rep.* **2021**, *11*, 94. [CrossRef]

51. Vaidya, M.; Bacchus, M.; Sugaya, K. Differential sequences of exosomal NANOG DNA as a potential diagnostic cancer marker. *PLoS ONE* **2018**, *13*, e0197782. [CrossRef] [PubMed]

52. Cai, J.; Han, Y.; Ren, H.; Chen, C.; He, D.; Zhou, L.; Eisner, G.M.; Asico, L.D.; Jose, P.A.; Zeng, C. Extracellular vesicle-mediated transfer of donor genomic DNA to recipient cells is a novel mechanism for genetic influence between cells. *J. Mol. Cell Biol.* **2013**, *5*, 227–238. [CrossRef] [PubMed]

53. Gamez-Valero, A.; Monguio-Tortajada, M.; Carreras-Planella, L.; Franquesa, M.; Beyer, K.; Borras, F.E. Size-Exclusion Chromatography-based isolation minimally alters Extracellular Vesicles' characteristics compared to precipitating agents. *Sci. Rep.* **2016**, *6*, 33641. [CrossRef] [PubMed]

54. Gautier, M.K.; Ginsberg, S.D. A method for quantification of vesicular compartments within cells using 3D reconstructed confocal z-stacks: Comparison of ImageJ. and Imaris to count early endosomes within basal forebrain cholinergic neurons. *J. Neurosci. Methods* **2021**, *350*, 109038. [CrossRef]

55. Vagner, T.; Spinelli, C.; Minciacchi, V.R.; Balaj, L.; Zandian, M.; Conley, A.; Zijlstra, A.; Freeman, M.R.; Demichelis, F.; De, S.; et al. Large extracellular vesicles carry most of the tumour DNA circulating in prostate cancer patient plasma. *J. Extracell. Vesicles* **2018**, *7*, 1505403. [CrossRef]

56. Shlomai, A.; Schwartz, R.E.; Ramanan, V.; Bhatta, A.; de Jong, Y.P.; Bhatia, S.N.; Rice, C.M. Modeling host interactions with hepatitis B virus using primary and induced pluripotent stem cell-derived hepatocellular systems. *Proc. Natl. Acad. Sci. USA* **2014**, *111*, 12193–12198. [CrossRef]

57. Morissette, G.; Flamand, L. Herpesviruses and chromosomal integration. *J. Virol.* **2010**, *84*, 12100–12109. [CrossRef]

Supplementary Figure S1

A
NTA and micro BCA data

B
Hela TSU and PSU sEVs purity

D
HeLa sEVs diameter

C
TEM negative staining images

HeLa TSU sEVs F2 · HeLa TSU sEVs F3 · HeLa TSU sEVs F4 · HeLa PSU sEVs F2 · HeLa PSU sEVs F3 · HeLa PSU sEVs F4

FBS18 TSU sEVs F2 · FBS18 TSU sEVs F3 · FBS18 TSU sEVs F4 · FBS18 PSU sEVs F2 · FBS18 PSU sEVs F3 · FBS18 PSU sEVs F4

E
Original blots

E

E
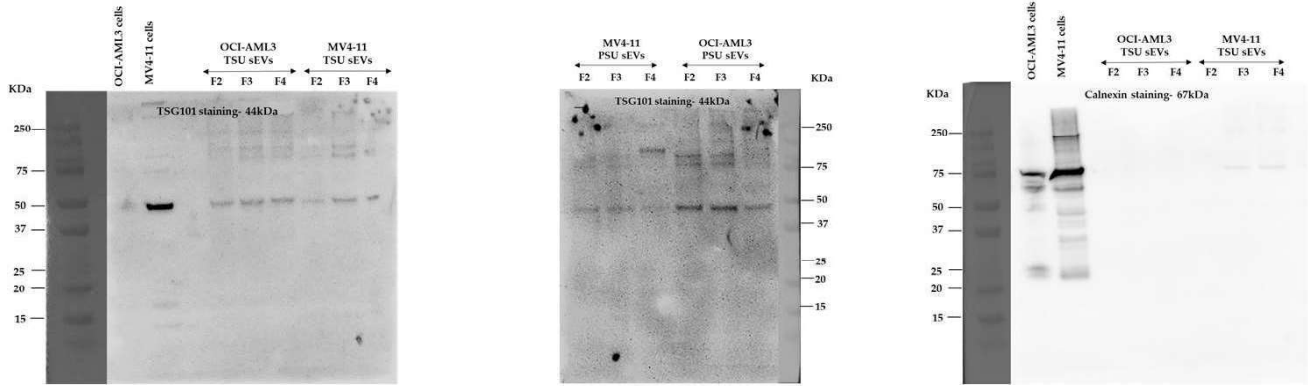
F   Selection of single beads
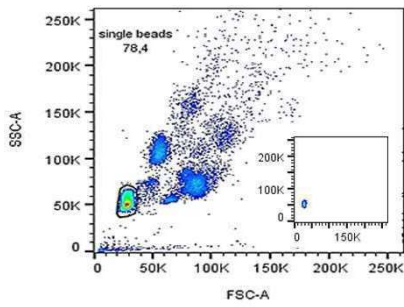
G   Selection of CD9+ population

H   Purity based on EV tetraspanins and micro-BCA value
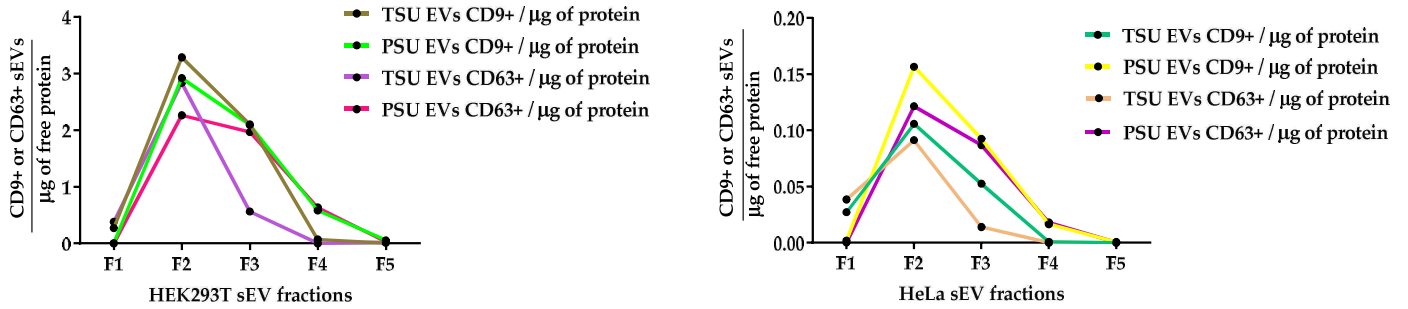
I   DNA concentration
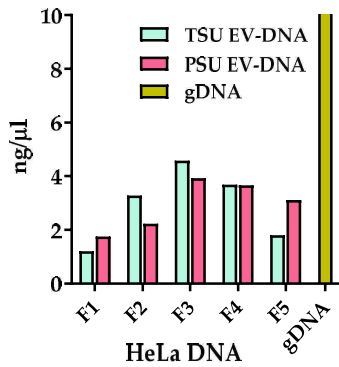
Extracellular vesicles transfer chromatin-like structures that induce non-mutational dysfunction of p53 in bone marrow stem cells

Jamal Ghanam[1], Venkatesh Kumar Chetty[1], Srishti Anchan[1], Laura Reetz[1], Qiqi Yang[2], Emeline Rideau[3], Xiaomin Liu[2], Ingo Lieberwirth[2], Anna Wrobeln[4], Peter Hoyer[5], Dirk Reinhardt[1] and Basant Kumar Thakur [1]✉

Dear Editor,

Small extracellular vesicle (sEV)-DNA has recently emerged as a promising biomarker for cancer diagnosis and prognosis[1]. Despite the growing interest in EV-DNA, many questions related to its nature, loading mechanism, localization, and post-shedding function(s) remain unrevealed. Recently, we have published evidence suggesting an unequal distribution of sEV-DNA between different compartments of the recipient cells, including the nucleus[2]. This finding motivated us to ask whether sEV-DNA is associated with proteins and what is the consequence of this association in the recipient cells. Although histones are abundant in sEVs[3], whether they are free or associated with sEV-DNA and what is the effect of this association is unknown.

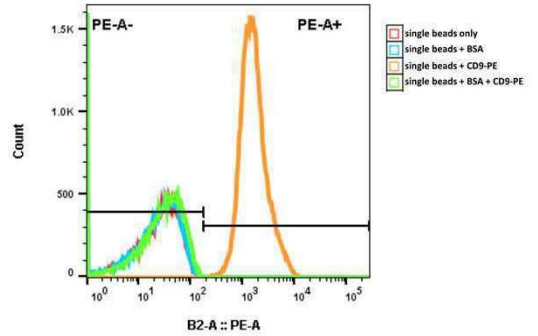Technically, one of the significant limitations in sEV-DNA-related studies is the use of suitable methods to isolate sEVs devoid of non-EV contaminants, such as cell-free DNA (cfDNA) and apoptotic bodies. To address this issue, we employed the combination of Tangential flow filtration, Size exclusion chromatography, and Ultrafiltration known as TSU (Supplementary Fig. S1a). sEVs were isolated from various cell lines and characterized according to MISEV2018 guidelines (Fig. 1a–d; Supplementary Fig. S1b–e). We have previously shown that TSU provides sEVs that are deficient in cfDNA and apoptotic bodies[2]. Additionally, sEVs were isolated from a pediatric AML cell line (MV4-11) cultured in the presence of EdU to label sEV-DNA and DNase I to digest cfDNA or DNA associated with the outer surface of sEVs (Supplementary

Fig. S2a–c). Transfer of these sEVs into bone marrow (BM)-derived mesenchymal stem cells (BM-MSCs) showed that EV-DNA uptake rate was not affected, suggesting that cfDNA or DNA associated with the outer surface of sEVs may not influence EV-DNA uptake (Supplementary Fig. S2d). Further, our results confirmed the presence of histones along with methylated double-stranded DNA (dsDNA) in sEVs (Fig. 1e, f; Supplementary Fig. S3a), as previously reported[4,5]. Using different physical and biochemical methods (Fig. 1g), we have demonstrated that sEVs transfer chromatin-like structures (we termed EV-chromatin), in which many proteins are associated with EV-DNA. With atomic force microscopy (AFM), we documented the presence of EV-chromatin in sEVs derived from MV4-11 (Fig. 1h). Next, we pulled down the sEV-dsDNA and performed non-targeted mass spectrometry to identify the co-precipitated proteins directly interacting with EV-DNA. The data indicate the association of ~30 proteins with EV-DNA, including core histones like H2B and H4, and S100 proteins (Fig. 1i; Supplementary Fig. S3b). The presence of H2B in the pulled-down DNA was further confirmed by western blot against GFP (Supplementary Fig. S3c). This suggests, for the first time, that DNA associated with EVs is directly linked with histones, as the AFM pictures show the existence of chromatin fibers in sEV preparations. Further, confocal images indicate the co-uptake of sEV-DNA and histone H2B, which is identified as an EV-chromatin component (Fig. 1k; Supplementary Fig. S4a–d). Contrariwise, Lázaro-Ibáñez et al.[3] previously reported the presence of nucleosomal patterns in both low- and high-density sEV subgroups. Nonetheless, they have quantified a number of histones in sEVs without characterizing their direct association with EV-DNA[3].

Correspondence: Basant Kumar Thakur (basant-kumar.thakur@uk-essen.de)
[1]Department of Pediatrics III, University Hospital Essen, Essen, Germany
[2]Max Planck Institute for Polymer Research, Mainz, Germany
Full list of author information is available at the end of the article
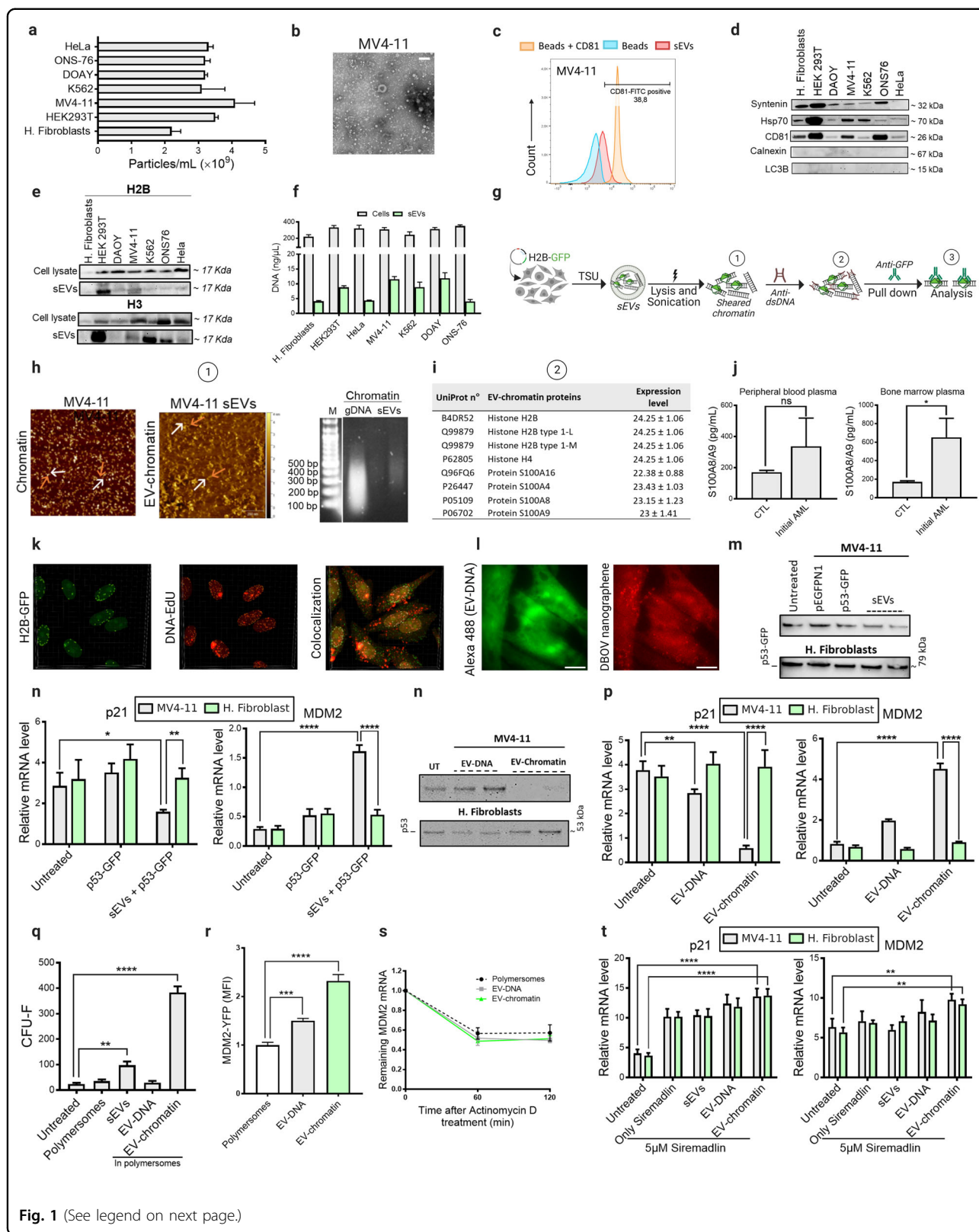
Fig. 1 (See legend on next page.)

(see figure on previous page)

Fig. 1 EV-chromatin induces non-mutational dysfunction of p53 in BM stem cells through overexpression of the E3 ligase MDM2. a Particle number/mL measured by NTA. **b** TEM negative staining images of MV4-11 sEVs. Scale bar, 0.2 μm. **c** FACS analysis showing the expression of CD81 in MV4-11 sEVs. **d** Western blot analysis with various positive (CD81, HSP70, syntenin) and negative (calnexin and LC3B) markers of sEVs. **e** Expression of H2B and H3 histones in the isolated sEVs. **f** EV-DNA and genomic DNA measured by Quantifluor. **g** Workflow for sEV chromatin characterization. **h** AFM imaging of sheared chromatin highlighting the presence of DNA filaments (white arrows) and protein dots (orange arrows) in both cells and sEV preparations. Chromatin and EV-chromatin showed fragments with sizes ranging from 100 bp to 500 bp after shearing by sonication. **i** Mass spec analysis of the pulled-down chromatin, showing histones (H2B and H4) and S100 as the most abundant proteins of EV-Chromatin. **j** S100A8/A9 levels in sEVs isolated from healthy donors and AML patients. **k** 3D confocal images indicating the co-localized and non-co-localized green (H2B-GFP) and red (EV-DNA) signals in different cell compartments. **l** Characterization of polymersome uptake by BM-MSCs. The fluorescence signals of the green channel (EV-DNA, 488 nm laser) and the red channel (polymersomes, 532 nm laser) were detected inside the BM-MSCs. Scale bars, 10 μm. **m** Western blotting analysis revealing a decrease in p53 level upon treatment with MV4-11 sEVs. **n** MV4-11 sEVs but not fibroblast sEVs downregulate p21 expression in BM-MSCs, which was accompanied by an increase in MDM2 level. **o** p53 degradation upon leukemic EV-chromatin treatment. **p** Relative expression levels of p53 target genes (normalized to the internal control), highlighting the downregulating effect of the leukemic EV-chromatin packaged in polymersomes on p21 compared to fibroblast-derived EV-chromatin. **q** BM-MSC colonies were counted after 7 days of treatment with either sEVs, EV-DNA, or EV-chromatin. **r** Mean YFP fluorescent intensity showing an increase in YFP-tagged MDM2 expression after treatment of BM-MSCs by EV-chromatin and EV-DNA. MFI results were normalized to the untreated cells. **s** *MDM2* mRNA decay in BM-MSCs after Actinomycin D treatment demonstrating comparable mRNA levels in the presence of either EV-chromatin, EV-DNA, or empty polymersomes. **t** Relative expression level of p53 target genes after treatment with 5 μM of Siremadlin. Data were all expressed as means ± SD. P value was calculated by one-way or two-way ANOVA. *$P < 0.1$; **$P < 0.01$; ***$P < 0.001$; ****$P < 0.0001$; ns, not significant.

S100 proteins were highly represented in the protein mixture associated with EV-DNA (Fig. 1i). S100 proteins are calcium-binding proteins that interact with target proteins to trigger many biological processes. These proteins are known to localize in different cell compartments, including the nucleus[6]. This suggests that these proteins likely bind to EV-DNA during or after sEV biogenesis and cargo recruitment (post-biogenesis interaction). S100 proteins interfere with different regulators of cell proliferation and differentiation, including p53, that control the integrity and survival of hematopoietic and mesenchymal stem cells in the BM[7,8]. Like histones, we found that S100 proteins were significantly enriched in sEVs derived from MV4-11 and AML patients compared to those obtained from fibroblast sEVs and healthy donors, respectively (Fig. 1j; Supplementary Fig. S5a).

Following this finding, we attempted to determine whether EV-DNA and EV-chromatin derived from MV4-11 affect the p53 activity of BM-MSCs. Physiologically, hematopoietic and mesenchymal stem cells receive multiple signals from BM stroma, where p53 plays a crucial role in regulating their self-renewal and differentiation rates to support hematopoiesis and prevent tumorigenic transformations[7–9]. p53 stabilizes the transcriptional activation of the cyclin-dependent kinase inhibitor p21 that induces cell cycle arrest required to maintain the balance between proliferation, quiescence, and regeneration via interaction with the BM microenvironment. Our data suggest that AML-sEVs downregulated the expression of p53, and its cell cycle (p21) and apoptosis (BAX and PUMA) target genes in BM-MSCs without affecting their viability (Fig. 1m, n; Supplementary Fig. S5c–f). Interestingly, AML-sEVs upregulated the expression of MDM2 in BM-MSCs (Fig. 1n).

We isolated EV-DNA and prepared EV-chromatin as described in Fig. 1g to investigate whether EV-DNA and/or EV-chromatin are responsible for the p21 inhibition. Next, EV-DNA and EV-chromatin were packaged in engineered polymersomes (Supplementary Fig. S6a, c). We used fluorescence imaging to demonstrate that polymersomes can transport EV-DNA and/or EV-chromatin into cells (Fig. 1l). A similar but more intense effect was observed when we treated BM-MSCs with AML-EV-chromatin packaged in polymersomes (Fig. 1o, p; Supplementary Fig. S6d, e). The proliferation rate of BM-MSCs was accelerated after treatment with EV-chromatin, as shown by the colony-forming unit assay (Fig. 1q; Supplementary Fig. S7a). Furthermore, we found an increase in the expression of YFP, which was tagged to *MDM2* promoter in BM-MSCs treated with EV-chromatin and EV-DNA, whereas the *MDM2* mRNA degradation rate remained the same (Fig. 1r, s), suggesting the possible transcriptional regulation of MDM2 by EV-DNA and EV-chromatin in the nucleus.

It is known that reciprocal interactions between BM-MSCs and AML cells can promote AML progression and resistance to chemotherapy[10]. AML-sEVs play a prominent role in this interaction, as BM stromal and endothelial cells are the preferential BM targets for AML-derived exosomes[11]. Moreover, p53$^{-/-}$ MSCs have shown reduced capacity in supporting normal hematopoiesis due to low secretion of cytokines, such as CXCL12 and CSF1[7]. The transcriptional activity of p53 can be dampened in the presence of wild-type (WT) *TP53* alleles through overexpression of canonical inhibitors such as MDM2. Overexpression of MDM2 has been defined as a mechanism by which cancer cells overcome p53's tumor suppressive effects, such as AML, in *TP53* WT cancers[12]. Our data suggest that MDM2 mediates complete and partial degradation of p53 in BM-MSCs treated with

AML-sEV-chromatin and AML-sEVs, respectively. This indicates that EV-chromatin could be the "active component" when AML-sEVs induce MDM2-mediated degradation of p53 in BM-MSCs. Surprisingly, no significant effects were oberved for DNA derived from AML-sEVs when packaged alone in polymersomes. Most EV-DNA in recipient cells colocalizes with endosomal proteins such as RAB5 and RAB7, indicating its future lysosomal degradation[2]. In contrast, EV-chromatin represents a mixture of DNA and nuclear proteins, such as histones and S100 proteins, which might protect the DNA from cytosolic sensing and degradation. Preventing cytosolic degradation of EV-DNA could be one but not the only role of EV-chromatin proteins. Intriguingly, S100A4 and S100B bind to the tetramerization domain of p53 and disturb the tetramerization of p53 necessary for its nuclear translocation[13]. Conversely, MDM2 reduces p53 acetylation by inhibiting CBP/p300 or recruiting HDAC1 (histone deacetylase 1) to deacetylate p53, favoring p53 ubiquitination, which results in reduced p53 levels[14]. Thus, the EV-chromatin-mediated degradation of p53 could culminate in the synergic activity of S100 proteins that prevent p53 nuclear translocation and MDM2 that mediates its ubiquitination. Nonetheless, the Siremadlin HDM201 inhibition of MDM2 rescued the p53 transcriptional activity (Fig. 1t; Supplementary Fig. S7a), which indicates that both EV-chromatin S100 proteins and MDM2 are required for non-mutational inactivation of p53 (Supplementary Fig. S7b). Similarly, p53 transcriptional activity was rescued after using siRNA to induce *MDM2* gene silencing (Supplementary Fig. S8a–c).

How AML-sEVs interfere with BM-MSCs and other stromal cells to transform BM microenvironment into a leukemic niche is still under investigation. We provided proof of the principle of the existence of chromatin-like structures (EV-chromatin) in AML-sEVs, and we have shown that EV-chromatin could communicate with BM-MSCs and modulate their behavior. We identified non-mutational p53 inactivation involving MDM2 and potentially S100 proteins (associated with EV-chromatin) as a mechanism by which AML-EV-chromatin regulates the proliferation of BM-MSCs. Conversely, we re-established the expression of p53 targets in BM-MSCs by inhibiting MDM2 or *MDM2* gene silencing. Our finding delineates a new mechanism of crosstalk between AML and stromal cells via EV-chromatin, which could be one of the reasons for hematopoietic failure during or after AML therapy. Our data emphasized the importance of targeting the interaction between MDM2 and p53 as a promising treatment strategy in *TP53* WT or functional p53 cancers. However, additional basic and clinical investigations are needed to further elucidate how sEVs and EV-chromatin or "Exogenotin" modulate the molecular pathway mediated by the p53-MDM2 axis in the BM niche.

Author details
[1]Department of Pediatrics III, University Hospital Essen, Essen, Germany. [2]Max Planck Institute for Polymer Research, Mainz, Germany. [3]Laboratory for Molecular Engineering of Optoelectronic Nanomaterials, Institute of Chemical Sciences and Engineering (ISIC), École Polytechnique Fédérale de Lausanne (EPFL), Station 6, Lausanne, Switzerland. [4]Institute of Physiology, University Hospital Essen, Essen, Germany. [5]Department of Pediatrics II, University Hospital Essen, Essen, Germany

Author contributions
B.K.T. and J.G. conceived and designed the study; J.G., B.K.T., V.K.C., S.A., L.R., Q.Y., E.R., I.L., and A.W. performed the experiments and analyzed the data; J.G. and B.K.T. wrote the manuscript; J.G., B.K.T., V.K.C., P.H., D.R., and X.L. revised the manuscript. All authors read and approved the final manuscript.

Conflict of interest
The authors declare no competing interests.

Publisher's note
Springer Nature remains neutral with regard to jurisdictional claims in published maps and institutional affiliations.

References
1. Ghanam, J. et al. *Cell Biosci.* **12**, 37 (2022).
2. Chetty, V. K. et al. *Cancers* **14**, 2068 (2022).
3. Lázaro-Ibáñez, E. et al. *J. Extracell. Vesicles* **8**, 1656993 (2019).
4. Thakur, B. K. et al. *Cell Res.* **24**, 766–769 (2014).
5. Kahlert, C. et al. *J. Biol. Chem.* **289**, 3869–3875 (2014).
6. Hsieh, H. L., Schäfer, B. W., Weigle, B. & Heizmann, C. W. *Biochem. Biophys. Res. Commun.* **316**, 949–959 (2004).
7. Boregowda, S. V. et al. *Cell Death Differ.* **25**, 677–690 (2018).
8. Lu, X., Wei, Y. & Liu, F. *Cell Discov.* **1**, 15027 (2015).
9. Greenbaum, A. et al. *Nature* **495**, 227–230 (2013).
10. Jacamo, R. et al. *Blood* **123**, 2691–2702 (2014).
11. Kumar, B. et al. *Leukemia* **32**, 575–587 (2018).
12. Quintás-Cardama, A. et al. *Leukemia* **31**, 1296–1305 (2017).
13. Fernandez-Fernandez, M. R., Veprintsev, D. B. & Fersht, A. R. *Proc. Natl. Acad. Sci. USA* **102**, 4735–4740 (2005).
14. Xia, C., Braunstein, Z., Toomey, A. C., Zhong, J. & Rao, X. *Front. Immunol.* **8**, 1908 (2018).

Supplementary information for

Extracellular vesicles transfer chromatin-like structures that induce non-mutational dysfunction of p53 in bone marrow stem cells.

Authors: Jamal Ghanam[1], Venkatesh Kumar Chetty[1], Srishti Anchan[1], Laura Reetz[1], Qiqi Yang[2], Emeline Rideau[3], Xiaomin Liu[2], Ingo Lieberwirth[2], Anna Wrobeln[4] , Peter Hoyer[5], Dirk Reinhardt[1], Basant Kumar Thakur[1*]

*Correspondance to: basant-kumar.thakur@uk-essen.de

This file includes:

Materials and Methods

Cell culture

Human bone marrow mesenchymal stem cells BM-MSCs (ATCC PCS-500-012) were obtained from American Type Culture Collection (ATCC) and maintained in the Mesenchymal Stem Cell Basal Medium (ATCC PCS-500-030) supplemented with the one Mesenchymal Stem Cell Growth (ATCC PCS-500-041) according to the manufacturer instructions. HeLa (cervical cancer adenocarcinoma), MV4-11 (acute monocytic leukemia), and K562 (chronic myelogenous leukemia) cell lines were maintained in Roswell Park Memorial Institute 1640 (RPMI1640; Gibco® Life Technologies Corp., USA) with 10% fetal bovine serum and 1% penicillin/streptomycin. HEK293T-CD63-GFP (human embryonic kidney with a GFP tag on CD63) and HEK293T (Transformed human embryonic kidney) cell lines were cultivated and maintained in Dulbecco's minimal essential media without pyruvate (DMEM; Gibco® Life Technologies Corp., USA) with 10% fetal bovine serum (Biowest, France) and 1% penicillin/streptomycin (Gibco® Life Technologies Corp., USA). DAOY (desmoplastic cerebellar medulloblastoma), and ONS76 (medulloblastoma) cell lines were cultivated and maintained in Dulbecco's minimal essential media (DMEM; Gibco® Life Technologies Corp., USA) with 10% fetal bovine serum (Biowest, France) and 1% penicillin/streptomycin (Gibco® Life Technologies Corp., USA).

Small extracellular vesicles isolation from conditioned media

One batch (8 x 20 mL) of conditioned culture media (CCM) was used to isolate sEVs. Washed cells were cultured for 72 h in 20 mL of the corresponding media containing 10% EV-depleted FBS, which was obtained by ultracentrifugation at 100,000 x g (Beckmann Coulter, California, USA) for 18 h and filtration through a 0.22 μm filter. First, the media was subjected to a centrifugation step of 500 x g for 10 min to remove cells, and the supernatant was spun again at 3000 x g for 20 min to get rid of cell debris and apoptotic bodies and subsequently frozen at -80°C. The pre-cleared media was then filtrated (0.2 μm) and concentrated (to 10 mL) using a TFF-Easy - tangential flow filtration unit (HansaBioMed, Estonia). Concentrated media was then loaded onto the pre-flushed (with one volume of 0.2 μm filtrated DPBS) size exclusion chromatography (SEC) column (IZON Science, USA) and voided with 10 mL of 0.2 μm filtrated DPBS. Afterward, sEVs fractions (5 mL) were immediately collected, as we have previously described [1]. sEV fractions were then concentrated (to 0.5 mL) using Amicon® Ultra-4 Centrifugal filter unit with Ultracel-10 membrane (MWCO = 10kDa; Merck Millipore, Billerica, MA). sEVs were stored at -80 until further use. To isolate sEVs from DNase I

containing supernatants, cells were cultivated under the same conditions as described above in the presence of 1 ug/mL of cell culture grade DNase I (Roche, Germany).

Isolation of sEVs with EdU labeled EV-DNA

For EV-DNA-based functional uptake studies, 5 µM of 5-ethynyl-2'-deoxyuridine (EdU; Thermofisher Scientific, Germany) solution was added to the CCM a few hours after seeding the cells (i.e., when cells are attached to the dishes). EdU is a thymidine analog incorporated into newly synthesized DNA during active DNA replication; thereby, cells treated with EdU release sEVs in which DNA is metabolically labeled with EdU.

Patient samples

Plasma samples (peripheral blood or bone marrow plasma) were collected from patients initially diagnosed with pediatric acute myeloid leukemia at the University Hospital Essen, Department of Pediatrics III, AML-BFM Reference Lab. Four peripheral blood plasma and four bone marrow plasma samples were used to isolate sEVs. Appropriate informed oral and written consent was obtained from patients and healthy donors before sample collection under the research protocol approved by the ethics committee of the Medical Faculty, University Hospital of Duisburg-Essen (16-7069-BO).

sEVs isolation from patient samples

Samples were first centrifuged for 10 min at 500xg and 4°C to remove red cells. Plasma samples (2 mL) were collected in new tubes, centrifuged at 3000 x g and 4°C for 20 min, and the supernatants were stored at -80°C until use. Samples were concentrated to 500 µL in Amicon (R) Ultra - 2ml centrifugal filters (Merck Millipore, Billerica, MA) at 4000 x g. Samples were washed twice with PBS onto the filter to reduce the protein content and prevent clogging. Samples were then loaded onto a qEV2 column (IZON Science, USA). sEV fractions were then concentrated using an Amicon® Ultra-4 Centrifugal filter unit with Ultracel-10 membrane (Merck Millipore, Billerica, MA) and stored at -80 until further use.

EV-DNA characterization

Genomic DNA (gDNA) and EV-DNA extraction: gDNA and EV-DNA were extracted using the QIAmp DNA kit and QIAmp DNA micro kit respectively, according to the manufacturer's instructions (QIAGEN, Germany). After isolation, EV-DNA samples were eluted in 22 µL nuclease-free water. All DNA samples were stored at −20°C. dsDNA quantification was performed using the sensitive QuantiFluor® ONE dsDNA System (Promega, Germany), providing a fluorescent double-stranded DNA-binding dye (504nmEx/531nmEm).

Characterization of AML-EV-DNA after treatment of MV4-11 cells by DNase I during sEVs biogenesis: DNA was extracted from treated cells and sEVs (Fig. S2a) and loaded onto a 1.5% agarose gel (Sigma Aldrich, Germany) and run for 75 min. DNA was then detected using highly sensitive SYBR Gold nucleic acid staining for 30 min at room temperature (Thermo Fisher Scientific, Germany).

Global DNA methylation

The global methylation profile of EV-DNA and gDNA were determined using the MethylFlash™ Global DNA Methylation (5-mC) ELISA Easy Kit (EpigenTek, Brooklyn, NY, USA) according to the manufacturer's instructions. The absorbance at 450 nm was assayed using a Tecan Infinite 200 Microplate Photometer (Tecan, Switzerland). Results were reported as a percentage (%) of 5-mC methylated DNA relative to the input DNA quantity, according to the following formula:

5-mC% = (Sample OD-Negative control OD) / (Slope × Input DNA) × 100

Immunoblotting

Total cells and sEV protein concentrations were determined using BCA and micro-BCA assay kits respectively (Invitrogen). For sEVs characterization, fractions of 100 μL were first concentrated up to ten times using Amicon® Ultra-4 Centrifugal filter unit with Ultracel-10 membrane (MWCO = 10kDa; Merck Millipore, Billerica, MA). Cell lysates were prepared by digesting cell pellets in RIPA buffer (Thermofisher Scientific). Concentrated vesicle suspensions and cell lysates were then treated with 4X laemmli buffer (Biorad, Germany) in the presence of beta-Mercaptoethanol and protease and phosphatase inhibitors cocktail at 95°C for 10 min. Samples were then loaded on NuPAGE 4-12 % Gel (Invitrogen, Germany), resolved for 2 h (100 V), transferred onto the Immuno-blot PVDF membrane (Merck Millipore), and subsequently blocked with 5% dry milk (Roth, Germany) in TBS-T (Tris Buffered Saline with 0.1% Tween-20) for 1 hour. The membranes were then incubated overnight at 4°C with the primary antibodies listed in Supplementary Table 1. The blots were vigorously washed whit TBS-T and then incubated with the corresponding secondary antibodies for 90 min at room temperature. Membranes were detected with Pierce ECL plus Western blotting substrate (Thermo Fisher Scientific), and images were taken on Fusion FX Machine (Vilber Lourmat Deutschland GmbH).

Nanoparticle tracking analysis

Particle size and concentration were determined by Nanoparticle tracking analysis (NTA) analysis using a Nanosight LM10 instrument (Particle Metrix, Germany) equipped with NTA

2.0 analysis software. sEV fractions were diluted (1:100) and then analyzed according to the following conditions: positions- 11, cycles- 5, minimum size- 5nm, maximum size - 150nm, trace length- 15secs, sensitivity- 75%, shutter speed- 75msecs and frame rate- 30.

Transmission electron microscopy

Negative staining was performed at the Electron Microscopy Unit (EMU) of the Imaging Center Essen (IMCES) for sEVs. In addition, FBS18 sEVs were included as a negative control. Briefly, 3 μl of sEVs were added onto a Formvar-coated 200 mesh copper grid (#SF162, PLANO GmbH) which had a hydrophilic surface due to being exposed to glow discharging for 1.5 minutes (easiGlow™, PELCO). Samples were then negatively stained with 10 μL of 1.5% v/v Phosphotungstic acid (PTA) for 2 min. Excess liquid was removed, and the grids were allowed to dry for at least 2 minutes. Samples were observed using a JEOL JEM-1400 Plus TEM (JEOL) at 120 kV, and the images were processed using ImageJ to determine the average diameter.

Bead-assisted flow cytometry

sEVs were analyzed by flow cytometry for semi-quantitative detection of sEV marker, CD81, according to the protocol we described before [1]. Briefly, sEVs were incubated with aldehyde-sulfate latex beads (4 μM; Invitrogen) for 30 min at RT. After removing the unbound beads, 5% BSA was added for blocking for 30 min at RT. Blocked sSEVs-beads were then stained with CD81-FITC (Beckman Coulter, Marseille, France). Data were acquired in conventional flow cytometers (BD FACS Aria, BD Biosciences, Heidelberg, Germany) and analyzed using FlowJo™ v10.8 Software (BD Life Sciences).

Chromatin Immuno-precipitation followed by deep sequencing (ChIP-Seq)

ChIP assay was performed using the ab500 chromatin immunoprecipitation kit (Abcam Biotechnology, MA, USA). Cells were seeded onto T175 flasks according to the doubling time. Cells were then scraped and washed twice with DPBS, and aliquots of 1×10^7 were considered for the next ChIP steps. Cells and sEVs (100 μL) were cross-linked in 1% of formaldehyde (ThermoFisher, Germany) for 10 min at room temperature and subsequently neutralized with glycine. Cells and EVs were lysed in lysis buffer containing protease inhibitor (Abcam Biotechnology, MA, USA). Only 100 μL of lysis buffer was used for sEVs, and 4 μL of the protease inhibitor was added on the top. Cells and EVs preparations were sonicated at 4°C (eight and four cycles for cells and EVs, respectively) to shear the chromatin to 200-1000 bp fragments using UP400S Bioruptor (Hielscher, Germany). Sonicated lysates were centrifuged for 10 min at 12 000 rpm at 4°C and supernatants were transferred to new tubes. To check the DNA fragment length, 20 μL of sonicated cells and EVs chromatins were mixed with 100 μL

of PCR-grade water (ThermoFisher, Germany), 100 µL of DNA purifying slurry (Abcam Biotechnology, MA, USA), and 1 µL of proteinase K for 30 min at 55°C. 10 µL were then loaded onto a 1.5% agarose gel (Sigma Aldrich), run for 75 min, and detected using SYBR Gold nucleic acid staining for 30 min (Thermo Fisher Scientific, Germany).

Sheared chromatins were then incubated with ChIP grade rabbit polyclonal anti-dsDNA antibody (Abcam Biotechnology, MA, USA) overnight at 4°C on a rotating wheel. The antibody-chromatin mixture was incubated with Protein A beads for 1 h at 4°C, and DNA was purified using the abcam DNA slurry as described before.

ChIP mass spectrometry and data analysis

Sample preparation, LC-MS/MS, data processing, and data analysis were performed at the EMBL Proteomics Core Facility (Heidelberg, Germany) according to the following protocol:

Sample preparation: Reduction of disulfide bridges in cysteine-containing proteins was performed with dithiothreitol (56°C, 30 min, 10 mM in 50 mM HEPES, pH 8.5). Reduced cysteines were alkylated with 2-chloroacetamide (room temperature, in the dark, 30 min, 20 mM in 50 mM HEPES, pH 8.5). Samples were prepared using the SP3 protocol [2,3] and trypsin (sequencing grade, Promega) was added in an enzyme to protein ratio 1:50 for overnight digestion at 37°C. Next day, peptide recovery in HEPES buffer by collecting supernatant on magnet and combining with second elution wash of beads with HEPES buffer. Peptides were further cleaned up using an OASIS® HLB µElution Plate (Waters) according to manufacturer's instructions.

LC-MS/MS: An UltiMate 3000 RSLC nano-LC system (Dionex) fitted with a trapping cartridge (µ-Precolumn C18 PepMap 100, 5µm, 300 µm i.d. x 5 mm, 100 Å) and an analytical column (nanoEase™ M/Z HSS T3 column 75 µm x 250 mm C18, 1.8 µm, 100 Å, Waters). The outlet of the analytical column was coupled directly to an Orbitrap Fusion™ Lumos™ Tribrid™ Mass Spectrometer (Thermofisher) using the Nanospray Flex™ ion source in positive ion mode.

The peptides were introduced into the Orbitrap Fusion Lumos via a Pico-Tip Emitter 360 µm OD x 20 µm ID; 10 µm tip (CoAnn Technologies) and an applied spray voltage of 2.4 kV, instrument was operated in positive mode. The capillary temperature was set at 275°C. Full mass scans were acquired for a mass range 375-1200 m/z in profile mode in the orbitrap with resolution of 120000. The filling time was set to a maximum of 50 ms, the AGC target was set to standard. The instrument was operated in data dependent acquisition (DDA) mode and MSMS scans were acquired in the Orbitrap with a resolution of 15000, with a fill time of up to

54 ms and a limitation of 2e5 ions (AGC target). A normalized collision energy of 34 was applied. MS2 data was acquired in profile mode.

Data processing using MaxQuant: The raw mass spectrometry data were processed with MaxQuant (v1.6.3.4) [4] and searched against the Homo sapiens proteome database (UP000005640) containing common contaminants. The data were searched with the following modifications: Carbamidomethyl (C) (fixed modification), Acetyl (N-term) and Oxidation (M) (variable modifications). A maximum of two missed cleavages was allowed. For protein identification a minimum of 2 unique peptides with a peptide length of at least seven amino acids and a false discovery rate below 0.01 were required on the peptide and protein level. Quantification was performed using iBAQ values [5].

Data analysis: The raw output file of MaxQuant (ProteinGroups.txt – file) was processed using the R programming language (ISBN 3-900051-07-0). As a quality filter, only proteins were allowed that were quantified with at least two unique peptides. Raw iBAQ values were used without normalization. Differential expression was evaluated by computing the respective ratio of raw iBAQ values. To try to annotate the ratio (coming from a single replicate) with a p-value, the ratio distribution was assumed to come from a student's t-distribution from which p-values were estimated using the 'pt' function from R. The degrees of freedom were simplified by the number of observed proteins. The false discovery rates calculated from the p-values using the 'p.adjust' function from R. This method was used to get a quick approximation.

Atomic force microscopy (AFM)

To study DNA-protein association, sheared genomic chromatin and EV-chromatin were analyzed by AFM using Dimension Icon equipped with ScanAsyst FastScann head (Bruker, Germany). Samples were diluted (1:5) in 5 mM Tris pH 8, 12 mM MgCl2, 1 mM EDTA, 5 mM NaCl. 10 μL of diluted samples were dropped on a freshly cleaved mica surface and processed under the following conditions, Experiment: Peak Force QNM in liquid; Cantilever Type: FASTSCAN-C; Resonant Freq.: 300 kHz; Spring Constant: 0.8 N/m; Back side coating: reflective aluminum. The average roughness was calculated using the Gwyddion software to remove the noise and apply the Median Filter on the images as a non-linear digital filtering technique.

Cryo-EM analysis

For cryo-EM examination, samples were vitrified using a Vitrobot Mark V (Thermo Fisher, Hilsboro Oregon) plunging device. 3 μL of the sample dispersion was applied to a Quantifoil or a lacey carbon coated TEM grid that had been glow discharged in an oxygen plasma cleaner (Diener Nano®, Diener electronic, Germany) shortly before. After removing the excess sample

solution with filter paper, the grid is immediately plunged into liquid ethane. The specimen is transferred to a TEM (FEI Titan Krios G4) for the subsequent examination, keeping cryogenic conditions. Conventional TEM imaging was done using an acceleration voltage of 300 kV. Micrographs were acquired with a 4k Direct Electron Detection Camera (Gatan K3) under low-dose conditions.

Packaging EV-DNA and EV-chromatin in polymersomes

The polymersomes preparation was carried out as follows. The block copolymer polybutadiene-b-poly(ethylene ethyl phosphate) (PB-b-PEEP) was prepared as described previously [6]. For the blank polymersomes, 20 µL of a (PB(1,4)73-b-PEEP12) solution in CHCl3 (4 mg/mL) was added to a 2 mL glass vial and concentrated in a desiccator under reduced pressure until the solvent was evaporated. An invisible thin film of the neat polymer was thus obtained. Next, 200 µL of PBS was added quickly, and the reaction was stirred overnight (1250 min-1, 30h) vigorously. The vesicles were prepared as described above for the encapsulation experiments, adding EV-DNA or EV-chromatin to the PBS solution. The prepared vesicles were stored in a refrigerator at 4 °C until the subsequent use.

Treatment of BM-MSCs with sEVs and polymersomes containing EV-DNA or EV-chromatin

For sEVs treatment, BM-MSCs were transiently transfected with p53-wt Cds in pEGPF-N1 vector (Clontech Laboratories, Mountain View, CA, USA) using Lipofectamine 3000 and P3000 reagent according to the manufacturer's instructions (Thermofisher, Germany). Equal numbers of sEVs at an approximately 50:1 ratio (sEVs/recipient cells) were resuspended in FBS18 culture media and added to the transfected BM-MSCs in culture. Cells were incubated for 48 h before being scraped and prepared for qPCR or Western blot experiments. For the treatment with EV-DNA and EV-chromatin packaged in polymersomes, attached BM-MSCs cells have received equal amounts of polymersomes calculated according to the DNA concentration.

Studying EV-DNA uptake in HeLa cells and BM-MSCs

EV-DNA and histone H2B co-uptake by HeLa cells: To generate GFP tagged H2B, HEK293T cells were transiently transfected with H2B-GFP plasmid (Addgene plasmid # 20972 ; http://n2t.net/addgene:20972 ; RRID: Addgene_20972) using lipofectamine RNAiMAX reagent according to the manufacturer's instructions (Thermofisher, Germany) in Opti-MEM media (Gibco® Life Technologies Corp., USA). Transfected HEK293T cells were then incubated for sEVs isolation in the presence of EdU as described above. After isolation from

HEK293T supernatant, sEVs were resuspended in FBS18 culture media and added to HeLa cells in culture at approximately 50:1 ratio (sEVs/recipient cells).

Cells were fixed and permeabilized as we have described before [1]. EdU click-it reaction was carried out using Click-iT™ EdU Alexa Fluor 647 Imaging kit (ThermoFisher, Germany) following the manufacturer's instructions. Images were acquired in confocal microscopy (Leica TCS SP8) in the corresponding channels (blue- DAPI, green- H2B-GFP, and red- EdU). ImageJ was used to quantify red and green mean fluorescence intensity.

EV-DNA uptake by BM-MSCs: After sEVs isolation from MV4-11 supernatants, sEVs were resuspended in FBS18 culture media and added to BM-MSCs in the culture at approximately 50:1 ratio (sEVs/recipient cells). Cells fixation and permeabilization, as well as the click-iT reaction, were performed as we have previously described.

Transcription inhibition by Actinomycin D

For transcription inhibition, BM-MSCs were first incubated with EV-DNA or EV-chromatin for 24h and then treated with 10 μg/mL of Actinomycin D (Sigma-Aldrich, Germany) for 0, 1, and 2 h. Cells were then lysed for RNA extraction, and transcription inhibition was determined using qPCR.

MDM2 reporter assay

To evaluate the ability of AML EV-DNA and EV-chromatin to activate MDM2 promoter, BM-MSCs were transiently transfected with MDM2p-Mdm2-YFP from Uri Alon & Galit Lahav [7] (Addgene plasmid # 53962 ; http://n2t.net/addgene:53962 ; RRID:Addgene_53962) using lipofectamine RNAiMAX reagent according to the manufacturer's instructions (Thermofisher, Germany). Transfected BM-MSCs cells were then incubated with AML EV-DNA and EV-chromatin for 24 h and analyzed by flow cytometry. YFP Data were acquired in conventional flow cytometers (BD FACS Aria, BD Biosciences, Heidelberg, Germany) and analyzed using FlowJo™ v10.8 Software (BD Life Sciences).

MDM2 inhibition

Siremadlin treatment: Siremadlin HDM201 was synthesized by Global Discovery Chemistry at Novartis. For *in vitro* treatment, 2×10^5 BM-MSCs were first cultured in the presence of 5 μM Siremadlin. After 24h, the media was replaced with FBS18 media containing MV4-11 sEVs, EV-DNA, or EV-chromatin for 24h.

siARN against MDM2- For siRNA treatment, 2×10^5 BM-MSCs were first cultured overnight. After 24 h, the media was replaced with FBS18 media containing MV4-11 sEVs, EV-DNA, or EV-chromatin for 24h. Cells were then transfected with 50 nM of siRNA targeting MDM2

(Thermofisher, Germany) using Lipofectamine RNAiMAX Transfection Reagent (Thermofisher, Germany) in Opti-MEM™ medium. Scrambled siRNA was used as a negative control and the knockdown efficiency was assessed by western blotting.

Colony forming unit assay

For colony-forming unit assays, 100 BM-MSCs were seeded in MethoCultTM GF M3434 (Stem Cell Technologies, Canada) with or without sEVs, EV-DNA, and EV-chromatin. Colony numbers were recorded on day 7 after plating.

Reverse transcription-quantitative polymerase chain reaction (RT-qPCR)

BM-MSCs were lysed, and total RNA was extracted using the RNeasy Mini Kit (Qiagen, Germany) according to the manufacturer's instructions. RNA concentration was determined by Nanodrop 1000 Spectrophotometer (Thermofisher, Germany). RNA was reversely transcribed using the Transcriptor First Strand cDNA Synthesis Kit (Roche Applied Science). PCR was performed using FastStart Universal SYBR Green master mix (Roche Applied Science) following the manufacturer's protocols. The reaction was done in StepOnePlus™ Real-Time PCR System (ThermoFisher, Germany). The results were calculated using $\Delta\Delta Ct$ method and normalized to GAPDH. All the measurements were performed in triplicate and repeated for at least three independent sEVs, EV-DNA, and EV-chromatin preparations. Primer sequences are listed in Supplementary Table 2.

Cell viability

Annexin V-FITC Apoptosis Staining: BM-MSCs treated with either leukemic sEVs, EV-DNA, or EV-chromatin were analyzed using an Annexin V-fluorescein isothiocyanate (FITC)/ propidium iodide (PI) apoptosis staining kit according to the manufacturer instructions (Abcam Biotechnology, MA, USA). Cells were resuspended in 500 μL binding buffer, mixed with 5 μL Annexin V-FITC followed by 5 μL PI, and incubated under dark conditions for 10 min at room temperature. A total of 1×10^6 BM-MSCs from each group were collected after 48 h of treatment. Data were acquired in conventional flow cytometers (BD FACS Aria, BD Biosciences, Germany), and results were analyzed using FlowJo™ v10.8 Software (BD Life Sciences, Germany).

MTT assay: BM-MSCs and MV4-11 cell viability was assessed by the reduction 3-(4,5-dimethylthiazol-2-yl)-2,5-diphenyltetrazolium bromide (MTT) (Sigma Aldrich, Germany) measured at 540 nm using a Tecan Infinite 200 Microplate Photometer (Tecan, Switzerland).

Statistical analysis

Data were statistically analyzed using GraphPad Prism 7.0 (GraphPad Software, San Diego, California, USA). Two-tailed student's t-test analyzed the comparisons between two groups, and multiple comparisons were performed by one-way or two-way analysis of variance (ANOVA). All reported results were obtained from at least three independent experiments. The data in the figures are expressed as the mean ± standard deviation (SD). Data that found to be statistically significant were represented in the graphs as * for $p < 0.0332$, ** for $p < 0.021$, *** for $p < 0.0002$ and **** for $p < 0.0001$.

References

1.   Chetty, V. K. *et al.* Efficient Small Extracellular Vesicles (EV) Isolation Method and Evaluation of EV-Associated DNA Role in Cell–Cell Communication in Cancer. *Cancers (Basel).* **14,** (2022).

2.   Hughes, C. S. *et al.* Single-pot, solid-phase-enhanced sample preparation for proteomics experiments. *Nat. Protoc.* **14,** 68–85 (2019).

3.   Hughes, C. S. *et al.* Ultrasensitive proteome analysis using paramagnetic bead technology. *Mol. Syst. Biol.* **10,** 757 (2014).

4.   Cox, J. & Mann, M. MaxQuant enables high peptide identification rates, individualized p.p.b.-range mass accuracies and proteome-wide protein quantification. *Nat. Biotechnol.* **26,** 1367–1372 (2008).

5.   Schwanhäusser, B. *et al.* Global quantification of mammalian gene expression control. *Nature* **473,** 337–342 (2011).

6.   Rideau, E., Wurm, F. R. & Landfester, K. Giant polymersomes from non-assisted film hydration of phosphate-based block copolymers. *Polym. Chem.* **9,** 5385–5394 (2018).

7.   Lahav, G. *et al.* Dynamics of the p53-Mdm2 feedback loop in individual cells. *Nat. Genet.* **36,** 147–150 (2004).
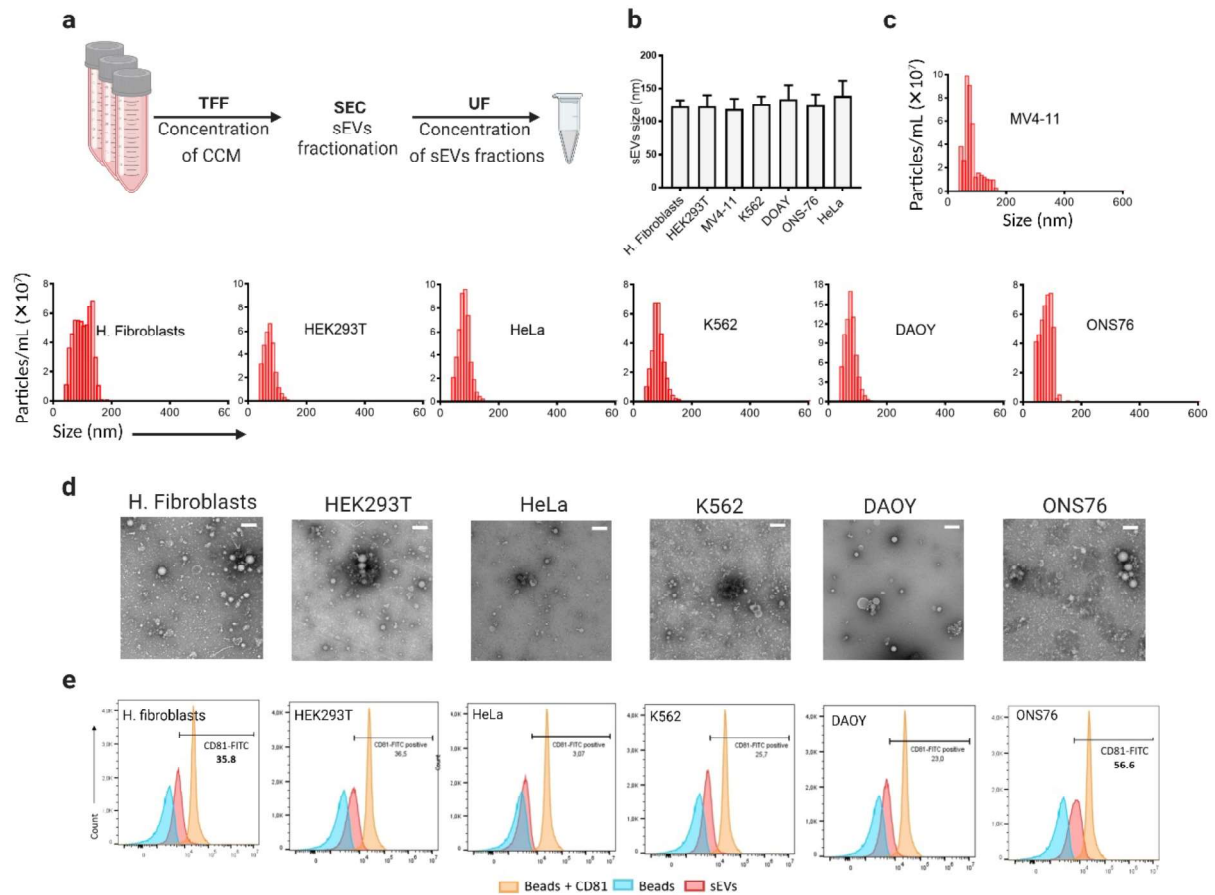
Supplementary Figure S1. Characterization of cancer and non-cancer small EVs. **(a)** Overview of sEVs isolation procedure from CCM. **(b)** sEVs size in nm, measured by NTA. Data are shown as mean ± SD. **(c)** sEVs distribution according to the size, determined by NTA. **(d)** Images of TEM negative staining of sEVs. Scale bars- 0.2 μm. **(e)** Flow cytometry analysis showing the percentage of sEV surface marker, CD81.
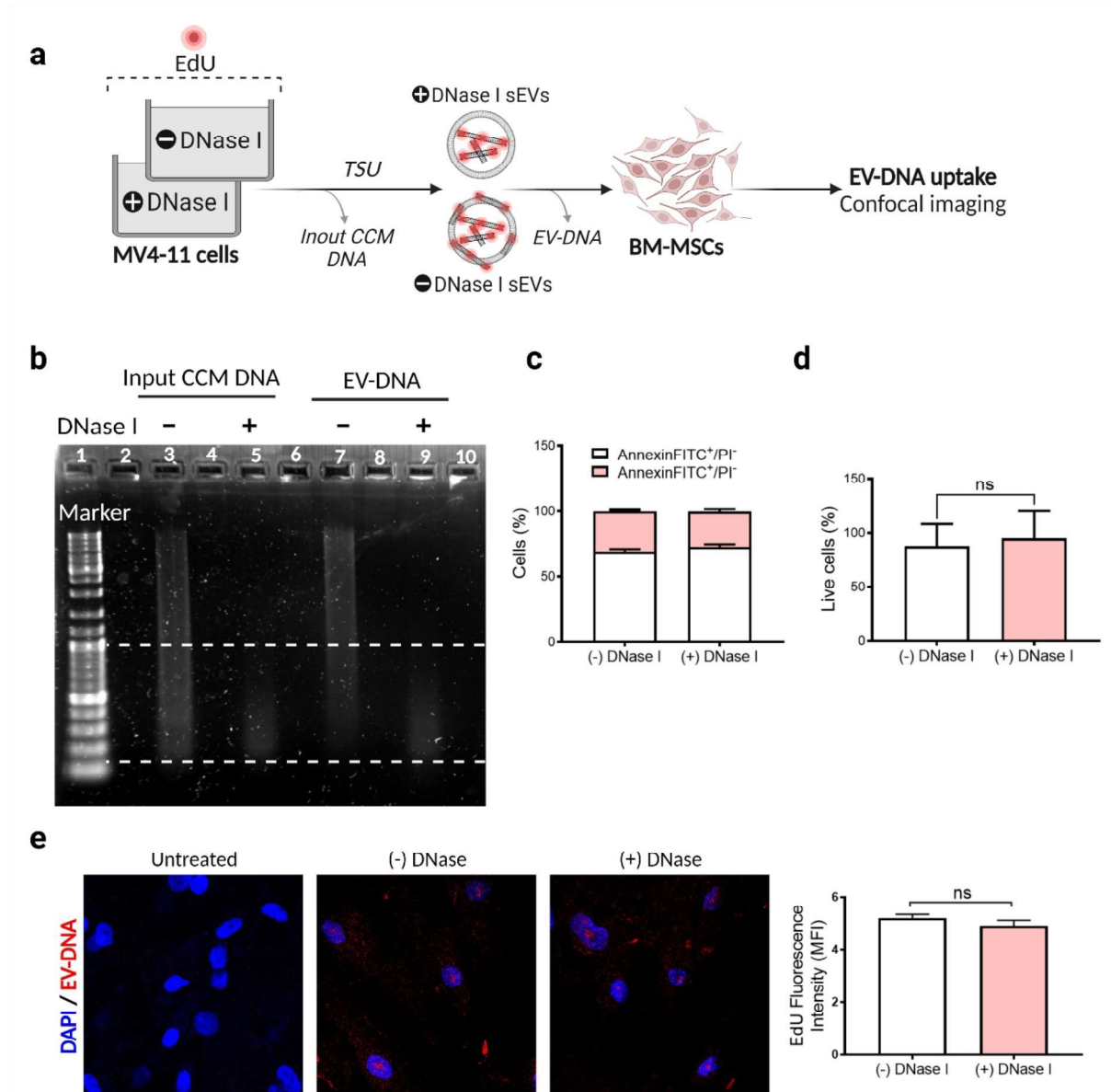
Supplementary Figure S2. Characterization of AML-EV-DNA uptake by BM-MSCs after treatment of MV4-11 cells by DNase I. **(a)** Working flow. **(b)** SYBR™ Gold based detection of DNA extracted from TFF-concentrated CCM from MV4-11 cells cultivated without (lane 3) and with (lane 5) DNase I, and sEVs from MV4-11 cells cultivated without (lane 7) and with (lane 9) DNase I. DNA ladder loaded in lane 1 as the control for MW size in base pairs. The results are representative of three experiments performed independently. Lanes 2, 4, 8, and 10 are empty. **(c)** Apoptosis assay. **(d)** MTT assay showing that DNase I did not affect MV4-11 viability. **(e)** Confocal images and mean EdU fluorescence intensity quantification demonstrate no significant difference in EV-DNA uptake by BM-MSCs, when MV4-11 sEVs with and without DNase I were used.

UniProt n°	EV-chromatin proteins	Expression level
P63261	Actin, cytoplasmic 2	17.88 ± 1.24
O75342	Arachidonate 12 lipoxygenase 12R type	18.675 ± 1.30
A6NMY6	Putative annexin A2-like protein	21.55 ± 0.77
A6NMY6	Annexin A2	21.65 ± 0.91
P05089	Arginase-1	21.45 ± 1.34
P25705	ATP synthase subunit alpha	21.89 ± 1.99
Q13867	Bleomycin hydrolase	20.95 ± 0.77
P31944	Caspase-14	22 ± 1.41
P31944	Caspase-14 subunit p17	22 ± 1.41
P04040	Catalase	16.75 ± 1.06
P81605	Dermcidin-1	23.075 ± 0.81
Q02413	Desmoglein-1	21.95 ± 0.63
P15924	Desmoplakin	21.025 ± 1.37
P68104	Elongation factor 1-alpha	16.25 ± 1.06
P68104	Elongation factor 1-alpha like 3	16.25 ± 1.06
P06733	Alpha-enolase	18.365 ± 0.89
Q01469	Fatty acid binding protein, epidermal	21.25 ± 1.06
P04406	GAPDH	19 ±1.41
P68871	Hemoglobin subunit beta	21.5 ± 0.70
P68871	LVV-hemorphin-7	21.5 ± 0.70
P68871	Spinorphin	21.5 ± 0.70
P14923	Junction plakoglobin	21.875 ± 0.17
Q5T749	Keratinocyte proline-rich protein	21.875 ± 1.23
Q9HC84	Mucin-5B	16.5 ± 0.77
Q13835	Plakophilin-1	18.2 ± 1.18
P29508	Serpin B3	17.65 ± 0.92
P22758	Protein glutamine gamma glutamyltransferase K	18.95 ± 0.62
Q08188	Protein glutamine gamma glutamyltransferase E	17.84 ± 1.18

Supplementary Figure S3. Characterization of chromatin-like in sEVs. (a) Methylation profile of DNA derived from the studied sEVs and cell lines. Data are expressed as mean ± SD. **(b)** Mass Spectrometry analysis of the pulled-down chromatin (with anti-dsDNA), showing EV-chromatin related proteins. **(c)** Immuno blotting against GFP demonstrating the presence of the fused H2B-GFP protein in EV-Chromatin after pull-down using anti-dsDNA. Data are expressed as mean ± SD.
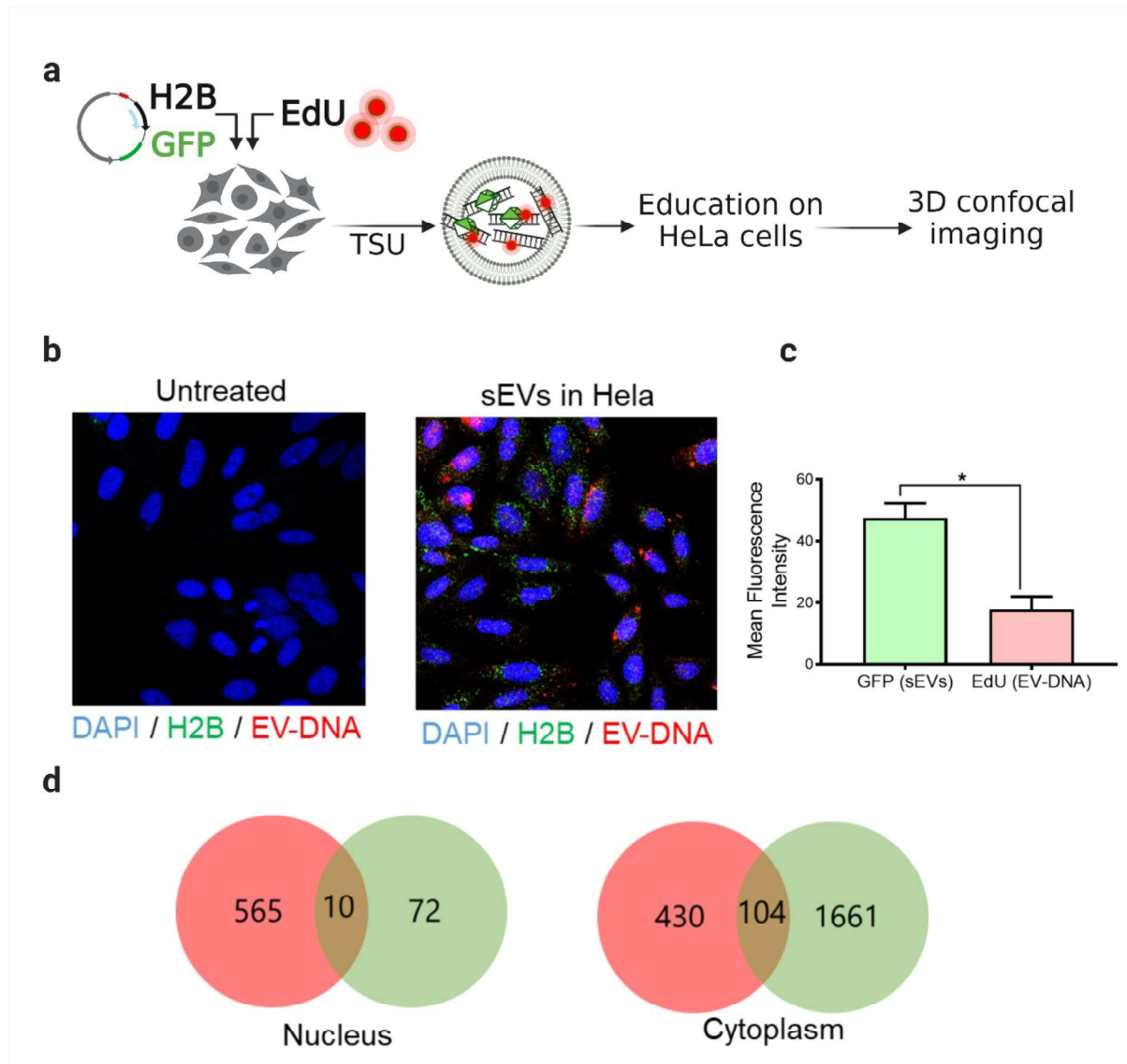
Supplementary Figure S4. EV-DNA and EV-chromatin uptake by recipient cells. **(a)** Schematic illustration showing the education of HeLa cells with sEVs derived from HEK293T cells transfected with H2B-GFP plasmid and labeled with EdU. **(b)** 2D confocal images showing the uptake of EV-DNA (red) and H2B (green) by the recipient cells. **(c)** Quantification of red and green signals in cells treated with labeled sEVs. Data are mean ± SD. **(d)** Venn diagram showing the proportion of EV-DNA and histone H2B co-localization in both cytoplasm and nucleus determined by 3D analysis of the z stack confocal images using Imaris software.
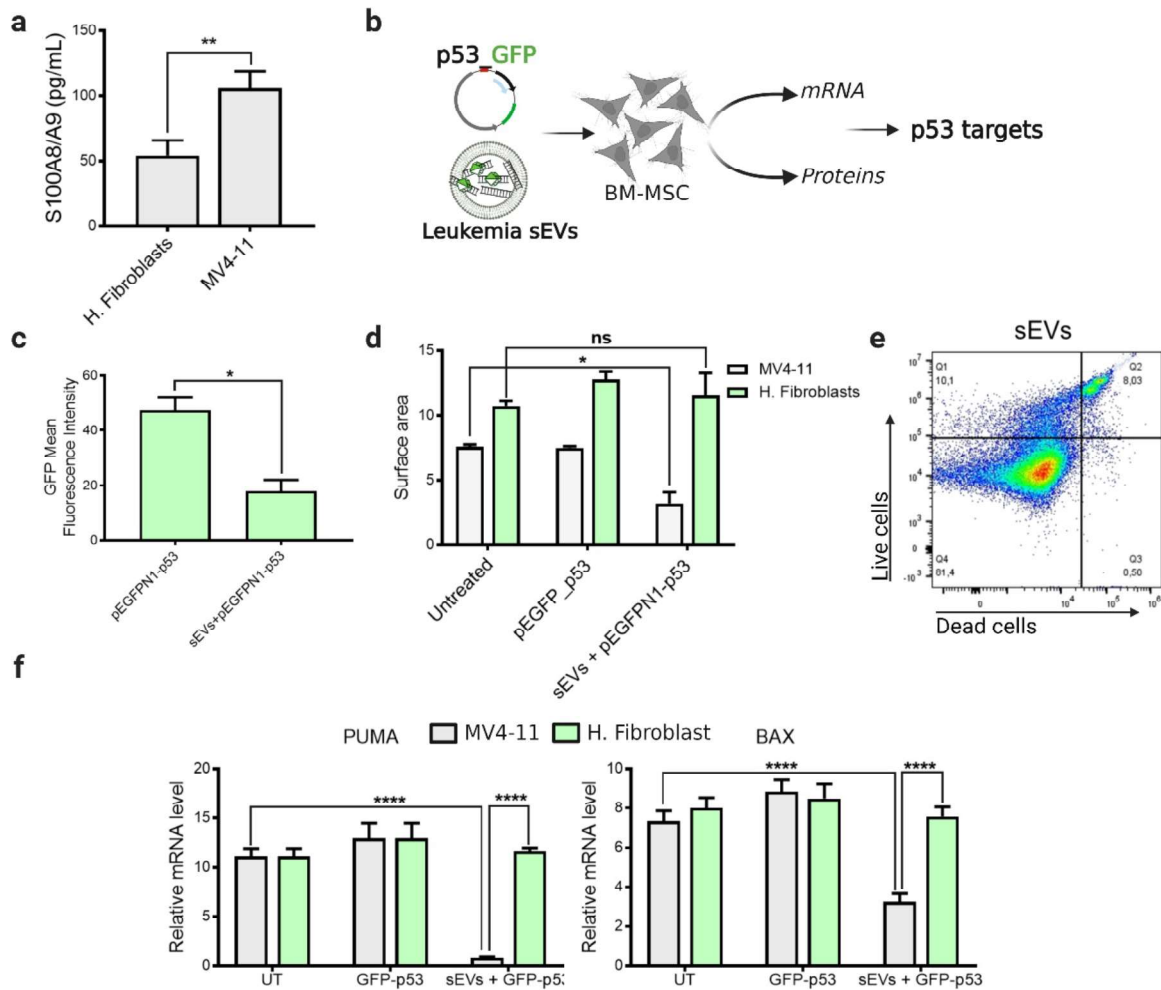
Supplementary Figure S5. Leukemia sEVs downregulate p53-target genes expression but not MDM2 expression. **(a)** S100A8/A9 complex content in sEVs derived from MV4-11 and human fibroblasts cell lines. Data are mean ± SD. **(b)** Schematic illustration of the work flow. **(c)** GFP fluorescence decreases upon treatment of BM-MSCs with leukemic sEVs, indicating a possible p53 degradation. Data are mean ± SD. **(d)** Western blotting band intensity of p53-GFP measured by Image J, revealing a decrease in p53 level upon treatment with leukemic sEVs. Data are mean ± SD. **(e)** Annexin V-FITC/ PI staining of BM-MSCs after treatment with leukemic sEVs. **(f)** Downregulation of p53 target genes PUMA and BAX after treatment of BM-MSC by MV4-11 sEVs, but not human fibroblast sEVs. Data are mean ± SD; the p-value was calculated using unpaired *t*-test or two-way ANOVA followed by Tukey's multiple comparison test. * p < 0.1; **** p < 0.0001; ns, not significant.
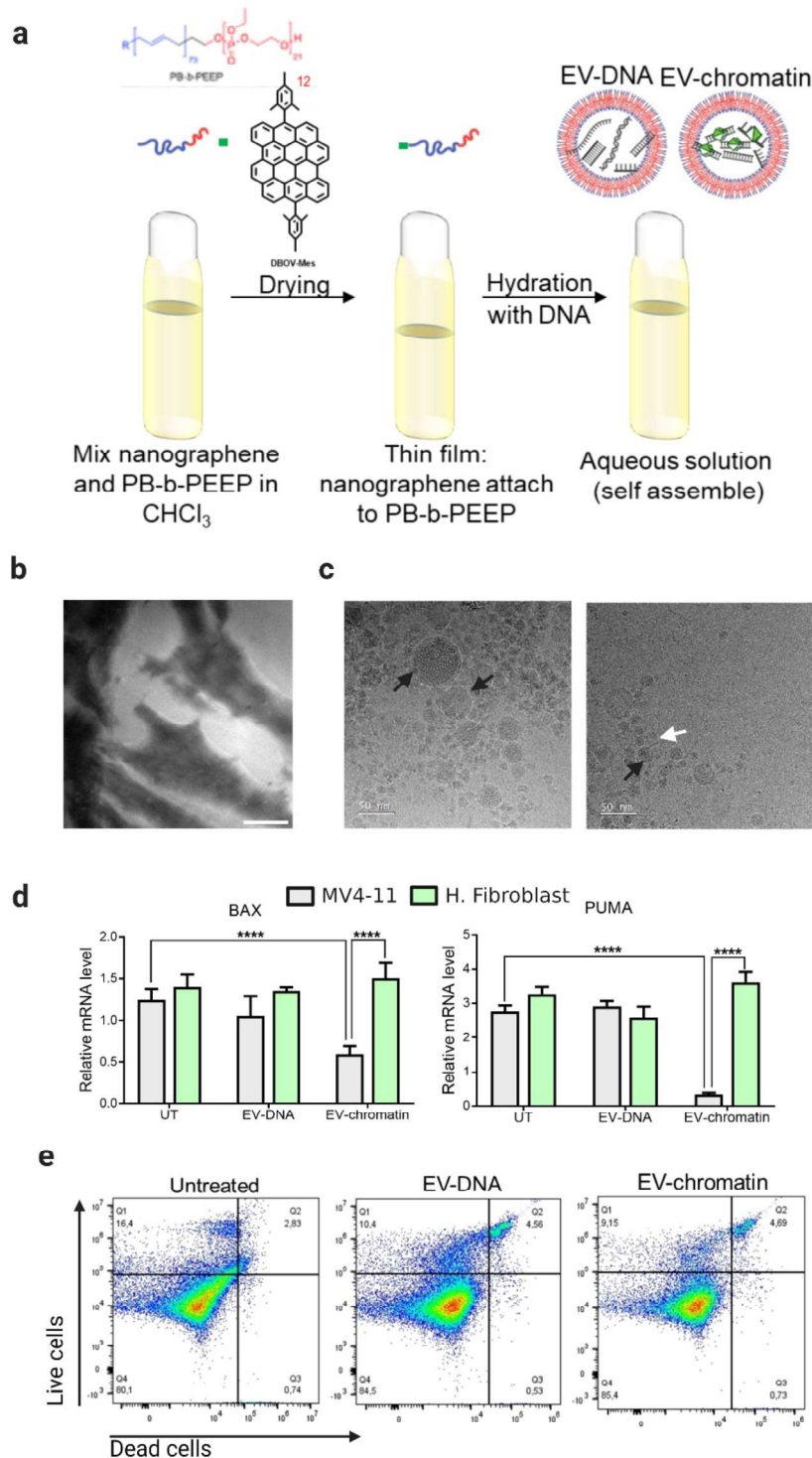
Supplementary Figure S6. EV-chromatin, but not EV-DNA, promotes BM-MSC proliferation. **(a)** Polymersomal formulation of EV-DNA and EV-Chromatin. **(b)** Wide-field images showing the polymersomes uptake. Scale bars- 10 μm. **(c)** Cryo-EM images documenting polymersomes bilayer structure (black arrows) and EV-DNA filaments (white arrows) on the surface. Scale bars- 50 nm. **(d)** Relative expression levels of p53-target genes PUMA and BAX in BM-MSCs (normalized to the internal control). Human fibroblasts derived EV-chromatin had no significant effect on BAX and PUMA expression. Data are mean ± SD. **(e)** Representative flow cytometry plots showing the effect of sEVs, EV-DNA, and EV-chromatin treatment on BM-MCSs viability. p-value was calculated by two-way ANOVA followed by Tukey's multiple comparison test. **** $p < 0.0001$.
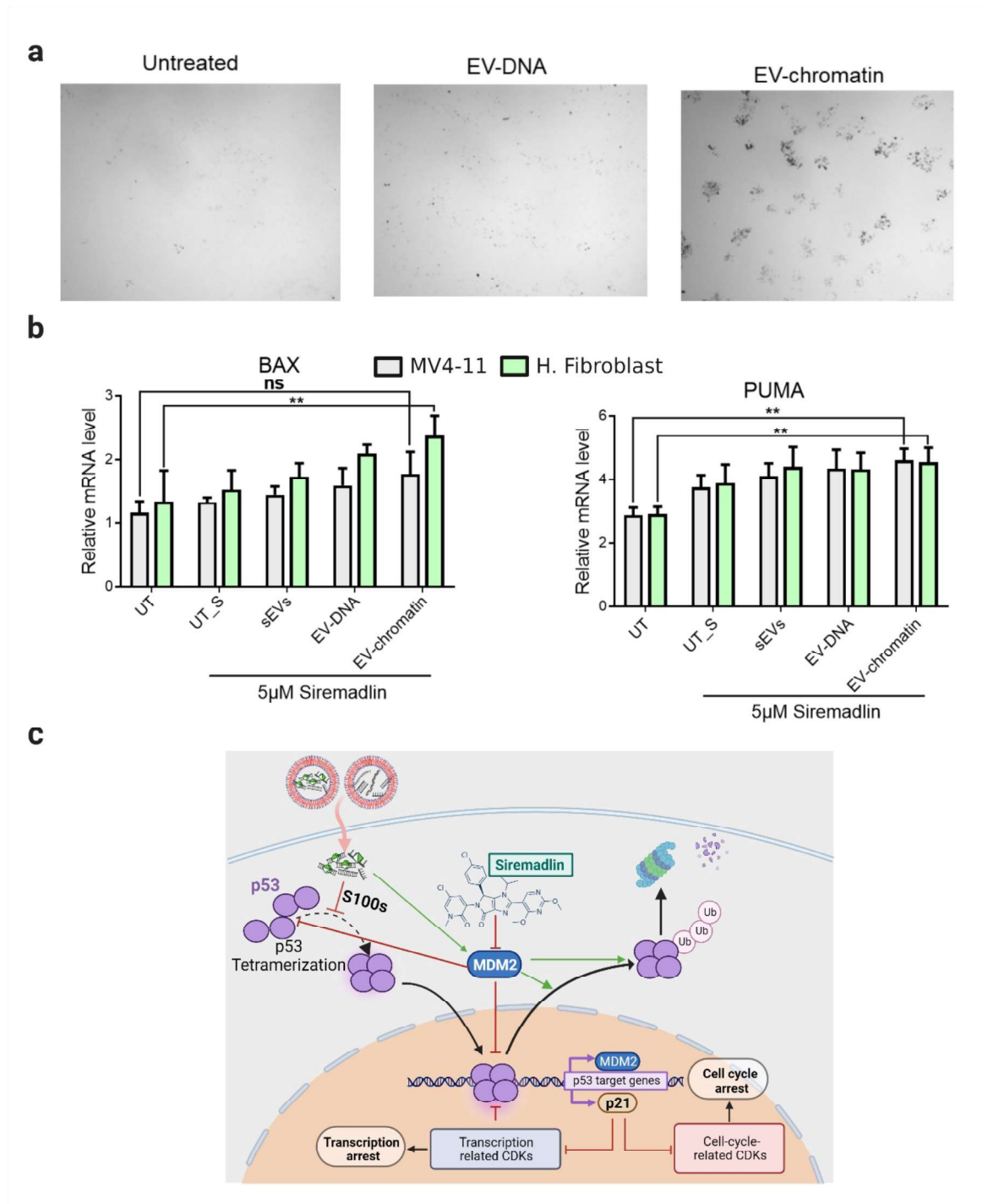
Supplementary Figure S7. Siremadlin reconstitutes the p53 activity in BM-MSC. **(a)** BM-MSC colonies imaging after 7 days. **(b)** Relative expression level of apoptotic genes BAX and PUMA after treatment with 5 μM of Siremadlin. Data are mean ± SD. p-value was calculated by two-way ANOVA followed by Tukey's multiple comparison test. $p < 0.01$; ns, not significant. **(c)** Possible mechanism by which EV-chromatin promotes BM-MSC proliferation. S100 proteins derived from EV-chromatin prevent the tetramerization of p53, which leads to its cytoplasmic accumulation and MDM2-mediated ubiquitination and degradation.
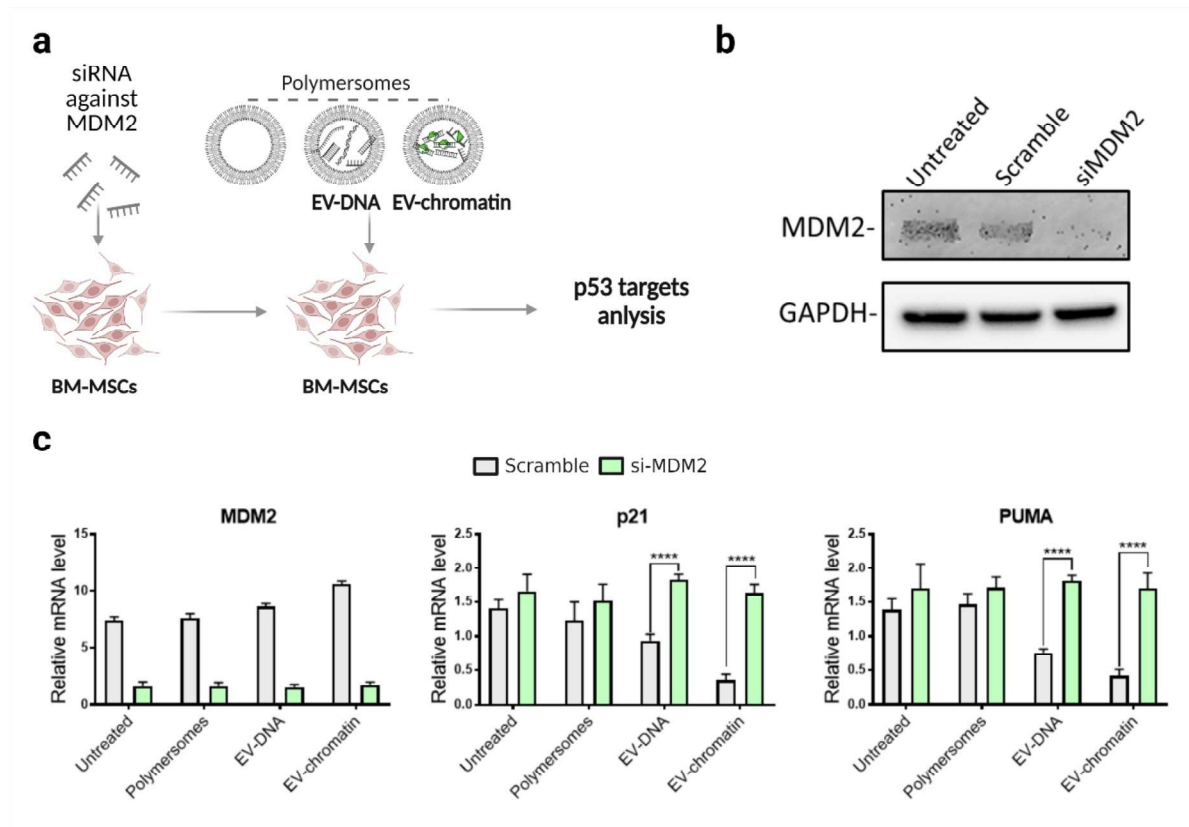
Supplementary Figure S8. MDM2 knockdown rescues the p53 activity in BM-MSC. **(a)** Workflow. **(b)** Immunoblots showing the efficiency of MDM2 gene knockdown. **(c)** Graphs showing the relative expression level of p53 target genes MDM2, p21, and PUMA with and without si-MDM2. Data are represented as mean ± SD. p-value was calculated by two-way ANOVA followed by Tukey's multiple comparison test. **** $p < 0.0001$.

Supplementary Table S1. Antibodies used in this study

Antibody	Source	Catalogue Number	Assay
Anti-Histone H3	Cell Signalling technology	4499T	WB
Anti-Histone H2B	Abcam Biotechnology	ab1790	WB
Anti-Histone H3 (trimethyl K9)	Abcam Biotechnology	Ab8898	WB
Anti-Histone H4	Cell Signalling technology	2935T	WB
Anti-TSG101	Sigma	HPA006161	WB
Anti-Hsp70	System Biosciences	EXOAB-KIT-1	WB
Anti-CD81	Biolegend	349502	WB
Anti-Syntenin	Abcam Biotechnology	ab133267	WB
Anti-Calnexin	Abcam Biotechnology	ab22595	WB
Anti-LC3B	Sigma	L7543	WB
Anti-dsDNA	Abcam Biotechnology	Ab27156	ChIP
Anti-CD81-FITC	Beckman Coulter	B25329	FC
Anti-p53	Cell Signalling technology	2524S	WB
Anti-GFP	Cell Signalling technology	2555S	WB
Anti-MDM2	Merckmillipore	OP46	WB
Anti-GAPDH	Santa Cruz Biotechnology	sc-47724	WB

FC, flow cytometry; WB, Western blotting; ChIP, chromatin immunoprecipitation.

Supplementary Table S2. Primers for human mRNA expression analysis

Gene	Forward primer	Reverse primer
p21	ATGTGTCCTGGTTCCCGTC	CATTGTGGGAGGAGCTGTGA
MDM2	TTCAGTGGGCAGGTTGACT	CCAGCTGGAGACAAGTCAGG
BAX	GTGTCTCAAGCGCATCGGG	GAGGAGTCTCACCCAACCACCCT
PUMA	GACGACCTCAACGCACAGT	CTGGGTAAGGGCAGGAGTC
Bcl-2	ATGTGTGTGGAGAGCGTCA	ACAGTTCCACAAAGGCATCC
CXCL12	TGGGCTCCTACTGTAAGGG	TTGACCCGAAGCTAAAGTGG
SCF	AATCCTCTCGTCAAAACTG	CCATCTCGCTTATCCAACAATGA
COL1A	GTTGAGTTTGGGTTGCTTGT	CCTGTCTGCTTCCTGTAAACT
ANGPT	GCCATCTCCGACTTCATGT	CTGCAGAGAGATGCTCCACA
GAPDH	AATCCCATCACCATCTTCC	TGGACTCCACGACGTACTCA

4. Discussion

Acute myeloid leukemia (AML) is the second most prevalent form of pediatric leukemia. Despite significant progress in AML therapy, how AML cells precisely alter the bone marrow microenvironment (BMM) to facilitate their growth and evade chemotherapy is still not completely understood. Besides genetic abnormalities and extracellular factors, recent studies demonstrated that different proteins and RNA cargoes associated with AML-derived small extracellular vesicles (sEVs) have emerged as crucial players that promote leukemogenesis in BMM (Huan et al. 2015; Kumar et al. 2018; Namburi et al. 2021; Hornick et al. 2016; Huan et al. 2013; Jiang et al. 2022; Baba et al. 2021; Georgievski et al. 2022). Nonetheless, AML blasts also release DNA associated with sEVs (EV-DNA) to maintain homeostasis and viability (Baba et al., 2021). In addition, the functional role of EV-DNA in AML development remains unexplored. Technically, one of the significant limitations in EV-DNA functional studies is the use of suitable methods to isolate sEVs devoid of non-sEV contaminates, such as cell-free DNA (cfDNA) and apoptotic bodies.

TSU provides highly pure sEVs suitable for EV-DNA functional studies
Many studies have already reported the diagnostic and functional role of EV-DNA in various diseases by employing the sEVs obtained using ultracentrifugation (UC) and polymer-based precipitation (PBP) methods (Cambier et al. 2021; Vaidya, Bacchus, and Sugaya 2018; Kahlert et al. 2014; Kontopoulou et al. 2020; Thakur et al. 2014). Although UC and PBP methods provide good sEV yield to execute diagnostic biomarker studies, we assert that these sEVs are not suitable to perform EV-DNA functional studies since these isolation methods are known to co-isolate cell-free DNA (cfDNA) and apoptotic bodies (Sidhom, Obi, and Saleem 2020; Gamez-Valero et al. 2016; Liangsupree, Multia, and Riekkola 2021). Due to this limitation, we cannot ascertain whether the observed biological function is due to EV-DNA alone or not by any other DNA-associated non-sEV components.

To address this limitation, we have successfully established and optimized a simple benchtop sEV isolation method by combining Tangential flow filtration (mechanical concentration), Size exclusion chromatography (size-based fractionation), and Ultrafiltration (further concentration), collectively named "TSU" (Chetty et al. 2022). Various fractions obtained using TSU were characterized according to MISEV2018 guidelines, and we found that the majority of sEVs (30-200 nm) are present only in fraction 2 (F2) and fraction 3 (F3). In addition, TSU sEV fractions F2 and F3 contain significantly less lipoprotein without apoptotic bodies and cfDNA.

Lázaro-Ibáñez et al., 2019 performed the sEVs isolation using UC-based iodixanol density separation and defined two different sEV populations based on EV-DNA content and topology (Lazaro-Ibanez et al. 2019). However, no EV-DNA functional studies were performed afterward to show that radiocontrast agents such as iodixanol would not affect the sEV uptake into the recipient cells. Because in our case, we found that the polyethylene glycol (PEG) utilized in the PSU method influenced the EV-DNA uptake into the recipient cells. In the same study, they also demonstrated that the extracted EV-DNA fragments from these two different sEV populations possess nucleosomal patterns, a common feature of cfDNA. On the other side, using differential UC, Vagner et al., 2018 isolated both small EVs and large EVs (lEVs) from prostate cancer cells and claimed that sEVs contain fewer DNA. In contrast, lEVs are enriched in chromosomal DNA containing large fragments up to 2 million base pairs long. In our case, with TSU sEV isolation, we observed the cfDNA nucleosomal pattern only in fractions such as F4 and F5, which contain fewer sEVs but not in F2 and F3. As the TSU isolation method is mainly based on size fractionation, the EVs obtained in fractions F4 and F5 are probably EVs that are less than 30 nm. Altogether, it indicates that sEVs obtained using UC and PEG precipitation cannot be employed for EV-DNA functional studies. Whereas the TSU isolation method provides sEVs with good yield and the maximum achievable purity suitable to perform EV-DNA functional studies.

Interaction of EV-DNA with endosomal proteins and cytoplasmic DNA sensors

As previously mentioned, we revealed that PEG chemical used in the PSU isolation method for the precipitation of sEVs restricts the entry of EV-DNA into the recipient cells. However, this was not the case with EV-DNA derived from sEVs by TSU, hence only this EV-DNA is considered for further downstream functional analysis (Chetty et al. 2022). Interestingly, after the reconstruction of three dimensional (3D) confocal z-stacks of EV-DNA into the recipient cells using Imaris software, we found that the spatial distribution of EV-DNA in different recipient cellular compartments is not uniform. Indeed, we revealed something distinctive that the recipient cell membrane barrier restricts the major proportion of foreign EV-DNA from entering the recipient cells. Whereas the remaining EV-DNA population overcomes this barrier and localizes in the cytoplasm and nucleus (Chetty et al. 2022). This shows that the proportion of EV-DNA that entered the recipient cells has successfully passed through the cell membrane barrier, possibly through its binding with cell surface receptors that specifically recognized them. On the other hand, it hints that the composition of the substantial proportion of EV-DNA that were restricted at the cell membrane barrier could be different from the ones that were entered.

Many studies reported that sEV uptake and internalization into the endosomal compartment occur in the recipient cells mainly through receptor- and non-receptor-mediated endocytosis, such as clathrin-mediated endocytosis and micropinocytosis, respectively (Rappa et al. 2017; Costa Verdera et al. 2017; Tian et al. 2014). Joshi et al. 2020 demonstrated that endocytosis inhibition in the recipient cells using the dynamin inhibitor dynasore decreased the foreign sEV uptake (Joshi et al. 2020). To further elucidate if any intercellular communication exists between the passenger EV-DNA and the endosomal components in the recipient cells, we checked for the association of EV-DNA with the early endosome marker, Rab5, and late endosome marker, Rab7. Interestingly, we revealed that foreign EV-DNA colocalized with both Rab5 and Rab7 in the recipient cells. Furthermore, we found that EV-DNA colocalized also with the lysosomal marker, Lamp1, which indicates that these EV-DNA molecules are in the process of degradation (phagocytosis) (Chetty et al. 2022). In future studies, it is important to identify the proteins on the sEV membrane that determine the mechanism of EV-DNA uptake and their intracellular distribution in the recipient cells.

As a part of the innate immune defense response against infections, inflammation, and cancer, it has been known that the accumulation of foreign DNA in the cytoplasm from various sources activates the cGAS-STING (cyclic GMP-AMP synthase-stimulator of interferon genes) cytosolic DNA-sensing pathway (Motwani, Pesiridis, and Fitzgerald 2019). Takahashi et al., 2017 demonstrated that the inhibition of exosome secretion in both senescent and non-senescent cells leads to the accumulation of nuclear DNA in the cytoplasm, which ultimately activates the cGAS-STING cytoplasmic DNA sensor pathway (Takahashi et al. 2017). In addition, Torralba et al., 2018 showed that EV-DNA contained in T-cells-derived sEVs is involved in priming dendritic cells by inducing the antiviral inflammatory responses through activating the cGAS/STING/IRF3 signaling pathway (Torralba et al. 2018). In line with these studies, we found that passenger EV-DNA interacted with cGAS and STING in HeLa recipient cells. Nevertheless, we need to evaluate if this interaction plays an essential role in AML. Functionally relevant to AML, we also observed that AML-derived EV-DNA co-localized with healthy bone marrow-derived stem cells (BM-MSCs), which hints that AML-derived EV-DNA may have a role in BMM. Considering the previous publications and the current study, we illustrate that when EV-DNA is internalized in the recipient cells, they take three different routes for intracellular distribution. In the cytoplasm, they interact with 1] endosomal and lysosomal compartment, such as endosomal proteins (Rab5/Rab7) and lysosomes (Lamp1) and 2] cytoplasmic DNA sensors (cGAS/STING). At the same time, some of the EV-DNA population enter 3) the nucleus. Nevertheless, the mechanism of interaction and the functional

consequence involved in these three routes are still unknown and needs to be addressed in future research (Figure 5).
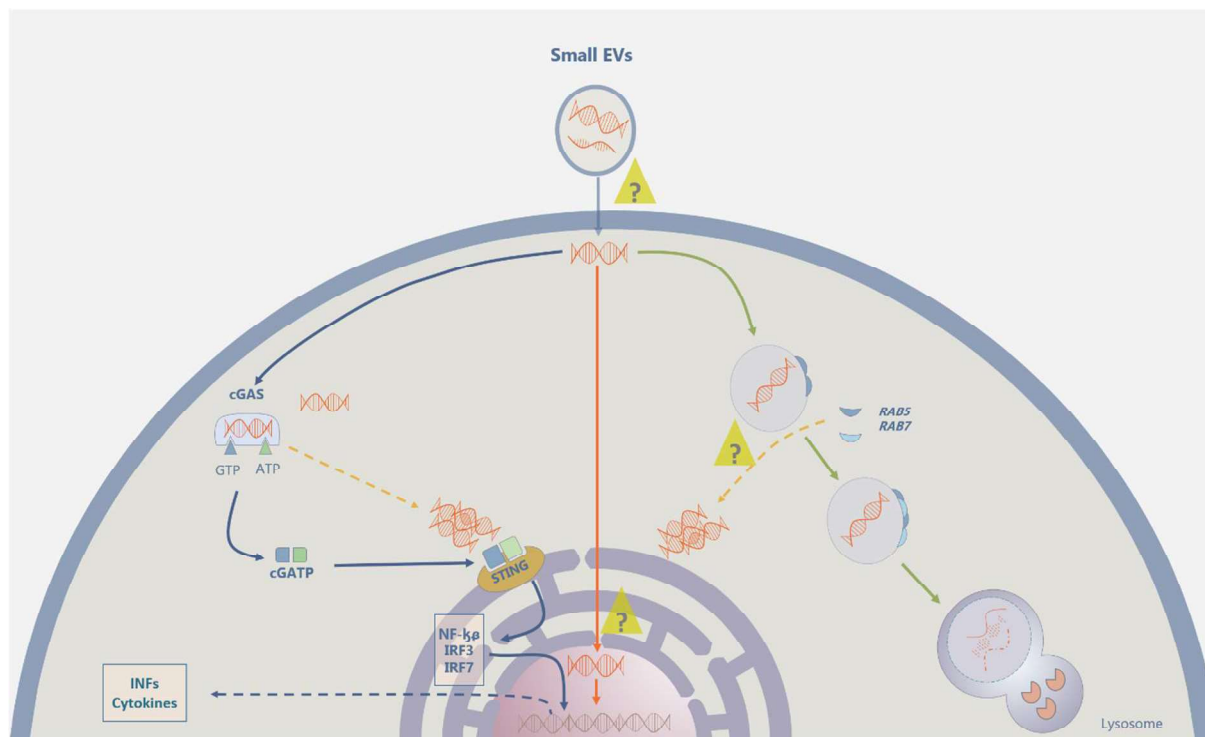

Figure 5. Modes of distribution of EV-DNA in the recipient cells. EV-DNA enters the recipient cells tackling the cell membrane barrier via an unknown mechanism and taking three different routes. **[1]** EV-DNA interacts with endosomal proteins (Rab5 / Rab7) and subsequently undergoes degradation in the lysosome compartment in the cytoplasm (green arrows). **[2]** EV-DNA interacts with DNA-sensing machinery cGAS/STING in the cytoplasm (blue arrows). **[3]** EV-DNA gains entry into the nucleus (orange), but the mechanism behind it is still perplexed.

EV-DNA association with histones and other proteins

Based on the observation of the unequal spatial distribution of EV-DNA associated with sEVs between different compartments of recipient cells, including the nucleus, we started to investigate if the EV-DNA population that overcomes the cell membrane barrier is alone or bound with DNA binding proteins. Although DNA binding proteins such as histones known for chromosome packaging and transcription in the cell nucleus are abundant in sEVs, it was still unknown whether they were free or complexed with EV-DNA (Lazaro-Ibanez et al. 2019; Zhang et al. 2018). Nonetheless, Lázaro-Ibáñez et al. quantified the level of histones in sEVs without characterizing their direct association with EV-DNA (Lazaro-Ibanez et al. 2019). Takahashi et al. have only obscurely mentioned that at least a certain proportion of EV-DNA was bound to histones (Takahashi et al. 2017).

Similarly, we found that histones H2B and H3 are abundant in various sEVs obtained from various cancer and non-cancer cell lines. In addition, we explicitly revealed, using atomic force microscopy (AFM), the presence of chromatin-like structures in pediatric AML cell line (MV4-

11)- derived sEVs, which we termed EV-chromatin. This finding implies that there are some proteins that are closely associated with EV-DNA. Non-targeted mass spectrometry (MS) of the pulled-down AML-derived sEVs-dsDNA revealed that thirty proteins, including core histones (H2B and H4), desmosome proteins, and S100 proteins, were bound with sEV-EV-DNA. Through western blot, the existence of H2B in the pulled-down sEVs-dsDNA sample was further confirmed. These observations clearly proved for the first time that EV-DNA is directly complexed with histones and other proteins (Ghanam et al. (in press)).

It is known that sEVs harbor cell-membrane-associated desmosome proteins, such as dermcidin, desmoglein-1, and desmoplakin. Choi et al., 2012 suggested that the abundance of desmosome-associated proteins in sEVs is highly correlated with the malignancy development of adenocarcinoma (Choi et al. 2012). In addition, Li et al., 2019 identified desmoplakin as a novel telomere-binding protein that localizes in the nucleus and protects the cells from telomere DNA damage and resultant cell apoptosis (Li et al. 2019). It is more likely that desmosome proteins were abundantly prevalent in EV-DNA-protein complex (EV chromatin) due to their telomere maintenance function, possibly post sEV biogenesis. In addition to desmosome proteins, the S100 protein family, including S100A4, S100A16, and S100A8/A9, were highly represented in the protein mixture associated with EV-DNA. Same as histones, S100 proteins were enriched in both MV4-11 and AML patient-derived sEVs (Ghanam et al. (in press)). S100 proteins are calcium-binding proteins that trigger many biological processes through interaction with their targets. Unlike desmosome proteins, S100 proteins are known to localize in different cell compartments, including the nucleus. It could suggest that S100 proteins are complexed with EV-DNA post- and/or pre-sEV biogenesis due to their known functional interactions with transcription factors and nucleic acids (Gonzalez, Garrie, and Turner 2020; Hsieh et al. 2004).

Functional role of EV-DNA and EV-chromatin in BMM

Following the findings discussed above, we attempted to determine whether EV-DNA and EV-chromatin exert the same effect(s) in the BM-MSCs, a critical component of BMM. To start with, sEVs isolated from MV4-11 cells grown in the presence of EdU (to label EV-DNA (Chetty et al. 2022)), and DNase I (to digest cell-free DNA (cfDNA) or extra-vesicular DNA), were incubated with BM-MSCs to check if cfDNA or extra-vesicular DNA influence the EV-DNA uptake. Confocal images demonstrated that the EV-DNA uptake rate was not influenced irrespective of cfDNA or extra-vesicular DNA, suggesting that only intra-vesicular DNA was transferred into BM-MSCs (Ghanam et al. (in press)).

Tumor suppressor protein, p53, is known to play a crucial role in BMM by maintaining normal hematopoiesis through the stabilization of the transcriptional activation of cyclin-dependent kinases inhibitor p21, which induces cell cycle arrest required to maintain the equilibrium between self-renewal and differentiation of bone marrow stromal cells (Ghatak, Das Ghosh, and Roychoudhury 2020; Zhao et al. 2010). Boregowda et al., and Pourebrahimabadi et al., recently showed that basal level expression of p53 in BM-MSCs is necessary to maintain p53 integrity in BMM, through which BM-MSCs control the proliferation and apoptosis of hematopoietic cells (Boregowda et al. 2018; Rasoul Pourebrahimabadi et al. 2019). In this regard, our data demonstrated that AML-sEVs downregulated the expression of p53 and its cell cycle (p21) and apoptosis (BAX and PUMA) related genes in healthy BM-MSCs. Besides, the negative regulator of p53, MDM2 was upregulated in BM-MSCs. To determine whether EV-DNA and/or EV-chromatin exert the same effect(s) in BM-MSCs, EV-DNA and EV-chromatin were packaged in engineered polymersomes, which have a comparable size of sEVs (Ghanam et al. (in press)).

In AML patients with wild-type TP53 alleles, overexpression of MDM2 has been defined as a mechanism by which AML blasts tackle p53's tumor suppressive effects (Quintas-Cardama et al. 2017). Likewise, our results illustrated that MDM2 attributed to the complete and partial degradation of p53 in healthy BM-MSCs treated with AML-EV-chromatin and AML-sEVs, respectively. Nonetheless, the same outcome was not observed on the AML-EV-DNA-treated healthy BM-MSCs. In this instance, it suggested that only EV-chromatin, not EV-DNA, could be the key player in sEVs that induced the MDM2-mediated p53 degradation in BM-MSCs. (Ghanam et al. (in press)). As illustrated before, a certain proportion of EV-DNA interacted with endosomal proteins directed towards lysosomal degradation (RAB5 and RAB7) and cytoplasmic DNA sensors (cGAS and STING) in the recipient cells (Chetty et al. 2022). Michalski et al., 2020 showed that cGAS interacts only with free histones such as H2A and H2B, but not with the chromatin (Michalski et al. 2020). It is more likely that EV-chromatin does not interact with these endosomal proteins and cytoplasmic DNA sensors since it contains a complex of DNA and nuclear proteins, such as histones and S100 proteins, which might prevent them from cytosolic localization and degradation.

Moreover, we have identified S100A4 in EV chromatin, which is known to bind to the p53 tetramerization domain, thereby preventing its nuclear translocation (Fernandez-Fernandez, Veprintsev, and Fersht 2005). On the other hand, it is known that MDM2 promotes p53 ubiquitination by reducing p53 acetylation through histone deacetylase 1 (Xia et al. 2017).

Thus, the EV-chromatin-mediated degradation of p53 could be the cooperative activity of S100 proteins that prevents p53 nuclear translocation and MDM2-mediated p53 ubiquitination, which will be investigated in our lab in the future. As expected, we found that MDM2 inhibition using Siremadlin or siRNA rescued the p53 transcriptional activity, which indicates that S100 proteins in EV-chromatin and MDM2 could be the potential factors for p53 dysfunction in BM-MSCs (Ghanam et al. (in press)). Taken together, our data suggest that AML-derived EV-chromatin downregulates the p53-mediated transcription of p21 and other apoptotic proteins in healthy BM-MSCs.
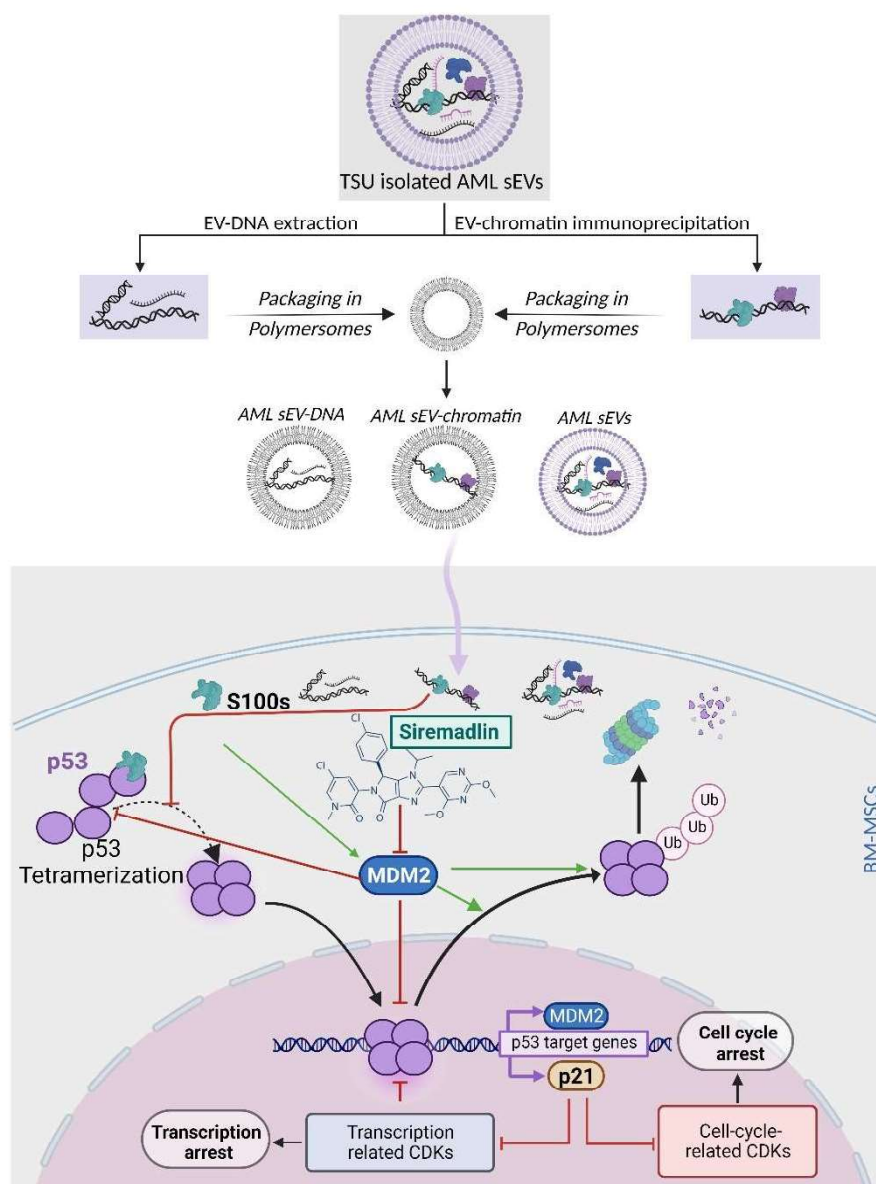
Figure 6. Functional role of AML-derived EV chromatin in BMM. After the isolation of AML-derived sEVs using TSU, both EV-DNA and EV-chromatin were packaged in engineered polymersomes and cocultured with healthy BM-MSCs. AML-derived EV-chromatin downregulates the p53-mediated transcription of p21 and other apoptotic proteins through MDM2 and, probably, S100 proteins. The p53 activity could be rescued after using the MDM2 inhibitor, Siremadlin. Figure modified from Ghanam et al. (Ghanam et al. (in press)).

In summary, the current study showed that the TSU sEV isolation method is well-suitable for EV-DNA functional studies since it provides small extracellular vesicles (sEVs) devoid of cell-free DNA and apoptotic bodies. In addition, it demonstrated that a certain proportion of EV-DNA tackled the recipient cell membrane barrier and interacted with cytoplasmic DNA sensors (cGAS and STING) and endosomal proteins directing towards lysosomal degradation (Rab5, Rab7, and Lamp1) in the cytosol. On the other hand, EV-chromatin caused p53 dysfunction through MDM2 and probably S100 proteins in healthy BM-MSCs, a crucial functional component in the AML bone marrow niche. In the future, targeting the molecular interaction between MDM2 and p53 could be a promising treatment strategy in wild-type TP53 or functional p53 cancers.

5. Future perspectives

In the current study, we revealed that EV-DNA and EV-chromatin associated with small extracellular vesicles (sEVs) have two different functions in the recipient cells. Many studies demonstrated that inflammatory signaling is linked to many aspects of acute myeloid leukemia (AML), such as disease progression, chemoresistance, and myelosuppression (Soyfer and Fleischman 2021; Ignatz-Hoover et al. 2015). Since our results already demonstrated that passenger EV-DNA had overcome the recipient cell membrane barrier and interacted with the cytoplasmic DNA sensor pathway (cGAS-STING) that is known to play an essential role in inflammation (Chetty et al. 2022), we planned to focus on the following topics,

- Coculture of AML-derived EV-DNA packaged in engineered polymerosome with either healthy bone marrow-derived hematopoietic stem cells (BM-HSCs) or mesenchymal stem cells (BM-MSCs) and screening for inflammatory signaling molecules that play an essential role in AML, such as IL-1, IL-6, Toll-like receptors (TLRs), tumor necrosis factor (TNF-α), insulin-like growth factor (IGF-1), type I/II interferon (IFN) and nuclear factor-кappa B (NF-kB) (Recher 2021; Zhong et al. 2022).
- Blocking AML-derived sEVs or EV-DNA delays the inflammation associated with leukemogenesis, ultimately rescuing normal hematopoiesis in BMM.

On the other hand, we demonstrated that EV-Chromatin derived from AML blast (MV4-11) could promote the proliferation of healthy BM-MSCs *in vitro* by increasing MDM2 expression. p53 is highly expressed in hematopoietic stem cells (HSCs), where it maintains and controls their self-renewal, quiescence, and behavior (Liu et al. 2009). However, we do not know whether AML-derived EV-chromatin exerts the same effect (MDM2-mediated p53 degradation) in HSCs, and what would be the consequence of p53 loss on HSCs stemness and hematopoiesis. Furthermore, we need to deepen our knowledge of how AML-sEVs and AML-derived EV-chromatin modulate the molecular pathway mediated by the p53-MDM2 axis to transform BMM into AML growth-permissive microenvironment to unveil novel features of AML pathogenesis. For this, we planned to focus on the following aspects,

- *In vivo* targeting of MDM2 upon treatment with EV-chromatin in TP53 wild-type or functional p53 cancers, using other MDM2 inhibitors like Nutlins.
- Since the transition of HSCs between quiescence and activation states is essential for maintaining hematopoiesis in BMM, exploring the effect of AML-derived sEVs and EV-chromatin on the transcriptional activity of p53 in HSCs and its consequence on stem cell quiescence.

6. List of Figures

7. List of Tables

8. Acknowledgments

Firstly, I would like to thank my scientific supervisor, PD. Dr. Basant Kumar Thakur, Group leader of Cancer Exosomes AG, University Hospital Essen, for providing me with an opportunity to work on this exciting research project. Without his continuous support and excellent research guidance, the completion of this project would not have been possible. Also, I would like to thank Prof. Dr. med. Dirk Reinhardt, Director of Pediatrics III, University Hospital Essen, for his valuable support and suggestions throughout the project. Then, I would like to thank all my present and past colleagues, especially Dr. Jamal Ghanam, Dr. Katarina Reinhardt, Ms. Srishti Anchan, Ms. Laura Reetz, and Mrs. Anja Rieb for their technical support, cooperation, and teamwork in finishing this project successfully. It was always a great pleasure working with them.

Furthermore, I would like to thank our collaborators, PD. Dr. Jadwiga Jablonska and Prof. Dr. Bernd Giebel for providing access to some of the instruments in their lab. A special thanks to Prof. Dr. med. Helmut Hanenberg for his helpful suggestions.

Finally, I would like to express my profound gratitude to all my family members for their constant motivation and unwavering belief in my abilities, particularly my lovely mother, Mrs. Savithri Murugasan, and wonderful sisters, Mrs. Saranya Saravanan and Mrs. Revathi Naveen.

9. References

Abels, E. R., and X. O. Breakefield. 2016. 'Introduction to Extracellular Vesicles: Biogenesis, RNA Cargo Selection, Content, Release, and Uptake', *Cell Mol Neurobiol*, 36: 301-12.

Abhange, K., A. Makler, Y. Wen, N. Ramnauth, W. Mao, W. Asghar, and Y. Wan. 2021. 'Small extracellular vesicles in cancer', *Bioact Mater*, 6: 3705-43.

Admyre, C., S. M. Johansson, K. R. Qazi, J. J. Filen, R. Lahesmaa, M. Norman, E. P. Neve, A. Scheynius, and S. Gabrielsson. 2007. 'Exosomes with immune modulatory features are present in human breast milk', *J Immunol*, 179: 1969-78.

Aga, M., G. L. Bentz, S. Raffa, M. R. Torrisi, S. Kondo, N. Wakisaka, T. Yoshizaki, J. S. Pagano, and J. Shackelford. 2014. 'Exosomal HIF1alpha supports invasive potential of nasopharyngeal carcinoma-associated LMP1-positive exosomes', *Oncogene*, 33: 4613-22.

Alberro, A., L. Iparraguirre, A. Fernandes, and D. Otaegui. 2021. 'Extracellular Vesicles in Blood: Sources, Effects, and Applications', *Int J Mol Sci*, 22.

Anand, S., M. Samuel, and S. Mathivanan. 2021. 'Exomeres: A New Member of Extracellular Vesicles Family', *Subcell Biochem*, 97: 89-97.

Anderson, D., P. Skut, A. M. Hughes, E. Ferrari, J. Tickner, J. Xu, B. H. Mullin, D. Tang, S. Malinge, U. R. Kees, R. S. Kotecha, T. Lassmann, and L. C. Cheung. 2020. 'The bone marrow microenvironment of pre-B acute lymphoblastic leukemia at single-cell resolution', *Sci Rep*, 10: 19173.

Armstrong, D., and D. E. Wildman. 2018. 'Extracellular Vesicles and the Promise of Continuous Liquid Biopsies', *J Pathol Transl Med*, 52: 1-8.

Asada, S., T. Fujino, S. Goyama, and T. Kitamura. 2019. 'The role of ASXL1 in hematopoiesis and myeloid malignancies', *Cell Mol Life Sci*, 76: 2511-23.

Asai, T., Y. Liu, N. Bae, and S. D. Nimer. 2011. 'The p53 tumor suppressor protein regulates hematopoietic stem cell fate', *J Cell Physiol*, 226: 2215-21.

Baba, T., T. Yoshida, Y. Tanabe, T. Nishimura, S. Morishita, N. Gotoh, A. Hirao, R. Hanayama, and N. Mukaida. 2021. 'Cytoplasmic DNA accumulation preferentially triggers cell death of myeloid leukemia cells by interacting with intracellular DNA sensing pathway', *Cell Death Dis*, 12: 322.

Balaj, L., R. Lessard, L. Dai, Y. J. Cho, S. L. Pomeroy, X. O. Breakefield, and J. Skog. 2011. 'Tumour microvesicles contain retrotransposon elements and amplified oncogene sequences', *Nat Commun*, 2: 180.

Benedikter, B. J., F. G. Bouwman, T. Vajen, A. C. A. Heinzmann, G. Grauls, E. C. Mariman, E. F. M. Wouters, P. H. Savelkoul, C. Lopez-Iglesias, R. R. Koenen, G. G. U. Rohde, and F. R. M. Stassen. 2017. 'Ultrafiltration combined with size exclusion chromatography efficiently isolates extracellular vesicles from cell culture media for compositional and functional studies', *Sci Rep*, 7: 15297.

Bernardi, S., and M. Farina. 2021. 'Exosomes and Extracellular Vesicles in Myeloid Neoplasia: The Multiple and Complex Roles Played by These "Magic Bullets"', *Biology (Basel)*, 10.

Boregowda, S. V., V. Krishnappa, J. Strivelli, C. L. Haga, C. N. Booker, and D. G. Phinney. 2018. 'Basal p53 expression is indispensable for mesenchymal stem cell integrity', *Cell Death Differ*, 25: 679-92.

Boussadia, Z., J. Lamberti, F. Mattei, E. Pizzi, R. Puglisi, C. Zanetti, L. Pasquini, F. Fratini, L. Fantozzi, F. Felicetti, K. Fecchi, C. Raggi, M. Sanchez, S. D'Atri, A. Care, M. Sargiacomo, and I. Parolini. 2018. 'Acidic microenvironment plays a key role in human melanoma progression through a sustained exosome mediated transfer of clinically relevant metastatic molecules', *J Exp Clin Cancer Res*, 37: 245.

Butler, J. T., S. Abdelhamed, and P. Kurre. 2018. 'Extracellular vesicles in the hematopoietic microenvironment', *Haematologica*, 103: 382-94.

Cai, J., Y. Han, H. Ren, C. Chen, D. He, L. Zhou, G. M. Eisner, L. D. Asico, P. A. Jose, and C. Zeng. 2013. 'Extracellular vesicle-mediated transfer of donor genomic DNA to recipient cells is a novel mechanism for genetic influence between cells', *J Mol Cell Biol*, 5: 227-38.

Cambier, L., K. Stachelek, M. Triska, R. Jubran, M. Huang, W. Li, J. Zhang, J. Li, and D. Cobrinik. 2021. 'Extracellular vesicle-associated repetitive element DNAs as candidate osteosarcoma biomarkers', *Sci Rep*, 11: 94.

Campanella, C., C. Caruso Bavisotto, M. Logozzi, A. Marino Gammazza, D. Mizzoni, F. Cappello, and S. Fais. 2019. 'On the Choice of the Extracellular Vesicles for Therapeutic Purposes', *Int J Mol Sci*, 20.

Camussi, G., M. C. Deregibus, S. Bruno, V. Cantaluppi, and L. Biancone. 2010. 'Exosomes/microvesicles as a mechanism of cell-to-cell communication', *Kidney Int*, 78: 838-48.

Chen, J. 2016. 'The Cell-Cycle Arrest and Apoptotic Functions of p53 in Tumor Initiation and Progression', *Cold Spring Harb Perspect Med*, 6: a026104.

Chen, J., and C. L. Glasser. 2020. 'New and Emerging Targeted Therapies for Pediatric Acute Myeloid Leukemia (AML)', *Children (Basel)*, 7.

Chetty, V. K., J. Ghanam, S. Anchan, K. Reinhardt, A. Brenzel, M. Gelleri, C. Cremer, E. Grueso-Navarro, M. Schneider, N. von Neuhoff, D. Reinhardt, J. Jablonska, I. Nazarenko, and B. K. Thakur. 2022. 'Efficient Small Extracellular Vesicles (EV) Isolation Method and Evaluation of EV-Associated DNA Role in Cell-Cell Communication in Cancer', *Cancers (Basel)*, 14.

Choi, D., L. Montermini, H. Jeong, S. Sharma, B. Meehan, and J. Rak. 2019. 'Mapping Subpopulations of Cancer Cell-Derived Extracellular Vesicles and Particles by Nano-Flow Cytometry', *ACS Nano*, 13: 10499-511.

Choi, D. S., D. Y. Choi, B. S. Hong, S. C. Jang, D. K. Kim, J. Lee, Y. K. Kim, K. P. Kim, and Y. S. Gho. 2012. 'Quantitative proteomics of extracellular vesicles derived from human primary and metastatic colorectal cancer cells', *J Extracell Vesicles*, 1.

Choi, D. S., J. Lee, G. Go, Y. K. Kim, and Y. S. Gho. 2013. 'Circulating extracellular vesicles in cancer diagnosis and monitoring: an appraisal of clinical potential', *Mol Diagn Ther*, 17: 265-71.

Cocucci, E., G. Racchetti, and J. Meldolesi. 2009. 'Shedding microvesicles: artefacts no more', *Trends Cell Biol*, 19: 43-51.

Costa Verdera, H., J. J. Gitz-Francois, R. M. Schiffelers, and P. Vader. 2017. 'Cellular uptake of extracellular vesicles is mediated by clathrin-independent endocytosis and macropinocytosis', *J Control Release*, 266: 100-08.

De Carolis, S., G. Storci, C. Ceccarelli, C. Savini, L. Gallucci, P. Sansone, D. Santini, R. Seracchioli, M. Taffurelli, F. Fabbri, F. Romani, G. Compagnone, C. Giuliani, P.

Garagnani, M. Bonafe, and M. Cricca. 2019. 'HPV DNA Associates With Breast Cancer Malignancy and It Is Transferred to Breast Cancer Stromal Cells by Extracellular Vesicles', *Front Oncol*, 9: 860.

de Rooij, J. D., C. M. Zwaan, and M. van den Heuvel-Eibrink. 2015. 'Pediatric AML: From Biology to Clinical Management', *J Clin Med*, 4: 127-49.

Deddens, J. C., K. R. Vrijsen, J. M. Colijn, M. I. Oerlemans, C. H. Metz, E. J. van der Vlist, E. N. Nolte-'t Hoen, K. den Ouden, S. J. Jansen Of Lorkeers, T. I. van der Spoel, S. Koudstaal, G. J. Arkesteijn, M. H. Wauben, L. W. van Laake, P. A. Doevendans, S. A. Chamuleau, and J. P. Sluijter. 2016. 'Circulating Extracellular Vesicles Contain miRNAs and are Released as Early Biomarkers for Cardiac Injury', *J Cardiovasc Transl Res*, 9: 291-301.

Diamond, J. M., C. Vanpouille-Box, S. Spada, N. P. Rudqvist, J. R. Chapman, B. M. Ueberheide, K. A. Pilones, Y. Sarfraz, S. C. Formenti, and S. Demaria. 2018. 'Exosomes Shuttle TREX1-Sensitive IFN-Stimulatory dsDNA from Irradiated Cancer Cells to DCs', *Cancer Immunol Res*, 6: 910-20.

Ding, L., T. L. Saunders, G. Enikolopov, and S. J. Morrison. 2012. 'Endothelial and perivascular cells maintain haematopoietic stem cells', *Nature*, 481: 457-62.

Doyle, L. M., and M. Z. Wang. 2019. 'Overview of Extracellular Vesicles, Their Origin, Composition, Purpose, and Methods for Exosome Isolation and Analysis', *Cells*, 8.

Duarte, D., E. D. Hawkins, and C. Lo Celso. 2018. 'The interplay of leukemia cells and the bone marrow microenvironment', *Blood*, 131: 1507-11.

Fei, C., Y. Zhao, J. Guo, S. Gu, X. Li, and C. Chang. 2014. 'Senescence of bone marrow mesenchymal stromal cells is accompanied by activation of p53/p21 pathway in myelodysplastic syndromes', *Eur J Haematol*, 93: 476-86.

Fernandez-Fernandez, M. R., D. B. Veprintsev, and A. R. Fersht. 2005. 'Proteins of the S100 family regulate the oligomerization of p53 tumor suppressor', *Proc Natl Acad Sci U S A*, 102: 4735-40.

Fischer, S., K. Cornils, T. Speiseder, A. Badbaran, R. Reimer, D. Indenbirken, A. Grundhoff, B. Brunswig-Spickenheier, M. Alawi, and C. Lange. 2016. 'Indication of Horizontal DNA Gene Transfer by Extracellular Vesicles', *PLoS One*, 11: e0163665.

Gamez-Valero, A., M. Monguio-Tortajada, L. Carreras-Planella, Ml Franquesa, K. Beyer, and F. E. Borras. 2016. 'Size-Exclusion Chromatography-based isolation minimally alters Extracellular Vesicles' characteristics compared to precipitating agents', *Sci Rep*, 6: 33641.

Georgievski, A., A. Michel, C. Thomas, Z. Mlamla, J. P. Pais de Barros, S. Lemaire-Ewing, C. Garrido, and R. Quere. 2022. 'Acute lymphoblastic leukemia-derived extracellular vesicles affect quiescence of hematopoietic stem and progenitor cells', *Cell Death Dis*, 13: 337.

Ghanam, J, V.K Chetty, S Anchan, L Reetz, Q Yang, E Rideau, X Liu, I Lieberwirth, A Wrobeln, P Hoyer, D Reinhardt, and B.K. Thakur. (in press). 'Extracellular vesicles transfer chromatin-like structures that induce non-mutational dysfunction of p53 in bone marrow stem cells ', *Cell Discovery*.

Ghanam, J., V. K. Chetty, L. Barthel, D. Reinhardt, P. F. Hoyer, and B. K. Thakur. 2022. 'DNA in extracellular vesicles: from evolution to its current application in health and disease', *Cell Biosci*, 12: 37.

35

Ghatak, D., D. Das Ghosh, and S. Roychoudhury. 2020. 'Cancer Stemness: p53 at the Wheel', *Front Oncol*, 10: 604124.

Gonzalez, L. L., K. Garrie, and M. D. Turner. 2020. 'Role of S100 proteins in health and disease', *Biochim Biophys Acta Mol Cell Res*, 1867: 118677.

Goulard, M., C. Dosquet, and D. Bonnet. 2018. 'Role of the microenvironment in myeloid malignancies', *Cell Mol Life Sci*, 75: 1377-91.

Greenbaum, A., Y. M. Hsu, R. B. Day, L. G. Schuettpelz, M. J. Christopher, J. N. Borgerding, T. Nagasawa, and D. C. Link. 2013. 'CXCL12 in early mesenchymal progenitors is required for haematopoietic stem-cell maintenance', *Nature*, 495: 227-30.

Guescini, M., S. Genedani, V. Stocchi, and L. F. Agnati. 2010. 'Astrocytes and Glioblastoma cells release exosomes carrying mtDNA', *J Neural Transm (Vienna)*, 117: 1-4.

Hanahan, D., and L. M. Coussens. 2012. 'Accessories to the crime: functions of cells recruited to the tumor microenvironment', *Cancer Cell*, 21: 309-22.

Harding, C., J. Heuser, and P. Stahl. 1983. 'Receptor-mediated endocytosis of transferrin and recycling of the transferrin receptor in rat reticulocytes', *J Cell Biol*, 97: 329-39.

Harmati, M., M. Bukva, T. Boroczky, K. Buzas, and E. Gyukity-Sebestyen. 2021. 'The role of the metabolite cargo of extracellular vesicles in tumor progression', *Cancer Metastasis Rev*, 40: 1203-21.

Hornick, N. I., B. Doron, S. Abdelhamed, J. Huan, C. A. Harrington, R. Shen, X. A. Cambronne, S. Chakkaramakkil Verghese, and P. Kurre. 2016. 'AML suppresses hematopoiesis by releasing exosomes that contain microRNAs targeting c-MYB', *Sci Signal*, 9: ra88.

Hoshino, A., B. Costa-Silva, T. L. Shen, G. Rodrigues, A. Hashimoto, M. Tesic Mark, H. Molina, S. Kohsaka, A. Di Giannatale, S. Ceder, S. Singh, C. Williams, N. Soplop, K. Uryu, L. Pharmer, T. King, L. Bojmar, A. E. Davies, Y. Ararso, T. Zhang, H. Zhang, J. Hernandez, J. M. Weiss, V. D. Dumont-Cole, K. Kramer, L. H. Wexler, A. Narendran, G. K. Schwartz, J. H. Healey, P. Sandstrom, K. J. Labori, E. H. Kure, P. M. Grandgenett, M. A. Hollingsworth, M. de Sousa, S. Kaur, M. Jain, K. Mallya, S. K. Batra, W. R. Jarnagin, M. S. Brady, O. Fodstad, V. Muller, K. Pantel, A. J. Minn, M. J. Bissell, B. A. Garcia, Y. Kang, V. K. Rajasekhar, C. M. Ghajar, I. Matei, H. Peinado, J. Bromberg, and D. Lyden. 2015. 'Tumour exosome integrins determine organotropic metastasis', *Nature*, 527: 329-35.

Hristov, M., W. Erl, S. Linder, and P. C. Weber. 2004. 'Apoptotic bodies from endothelial cells enhance the number and initiate the differentiation of human endothelial progenitor cells in vitro', *Blood*, 104: 2761-6.

Hsieh, H. L., B. W. Schafer, B. Weigle, and C. W. Heizmann. 2004. 'S100 protein translocation in response to extracellular S100 is mediated by receptor for advanced glycation endproducts in human endothelial cells', *Biochem Biophys Res Commun*, 316: 949-59.

Hsu, Y. L., J. Y. Hung, W. A. Chang, Y. S. Lin, Y. C. Pan, P. H. Tsai, C. Y. Wu, and P. L. Kuo. 2017. 'Hypoxic lung cancer-secreted exosomal miR-23a increased angiogenesis and vascular permeability by targeting prolyl hydroxylase and tight junction protein ZO-1', *Oncogene*, 36: 4929-42.

Huan, J., N. I. Hornick, N. A. Goloviznina, A. N. Kamimae-Lanning, L. L. David, P. A. Wilmarth, T. Mori, J. R. Chevillet, A. Narla, C. T. Roberts, Jr., M. M. Loriaux, B. H.

Chang, and P. Kurre. 2015. 'Coordinate regulation of residual bone marrow function by paracrine trafficking of AML exosomes', *Leukemia*, 29: 2285-95.

Huan, J., N. I. Hornick, M. J. Shurtleff, A. M. Skinner, N. A. Goloviznina, C. T. Roberts, Jr., and P. Kurre. 2013. 'RNA trafficking by acute myelogenous leukemia exosomes', *Cancer Res*, 73: 918-29.

Huang, F., P. Guang, F. Li, X. Liu, W. Zhang, and W. Huang. 2020. 'AML, ALL, and CML classification and diagnosis based on bone marrow cell morphology combined with convolutional neural network: A STARD compliant diagnosis research', *Medicine (Baltimore)*, 99: e23154.

Ignatz-Hoover, J. J., H. Wang, S. A. Moreton, A. Chakrabarti, M. K. Agarwal, K. Sun, K. Gupta, and D. N. Wald. 2015. 'The role of TLR8 signaling in acute myeloid leukemia differentiation', *Leukemia*, 29: 918-26.

Janas, A. M., K. Sapon, T. Janas, M. H. Stowell, and T. Janas. 2016. 'Exosomes and other extracellular vesicles in neural cells and neurodegenerative diseases', *Biochim Biophys Acta*, 1858: 1139-51.

Jeppesen, D. K., A. M. Fenix, J. L. Franklin, J. N. Higginbotham, Q. Zhang, L. J. Zimmerman, D. C. Liebler, J. Ping, Q. Liu, R. Evans, W. H. Fissell, J. G. Patton, L. H. Rome, D. T. Burnette, and R. J. Coffey. 2019. 'Reassessment of Exosome Composition', *Cell*, 177: 428-45 e18.

Jiang, D., X. Wu, X. Sun, W. Tan, X. Dai, Y. Xie, A. Du, and Q. Zhao. 2022. 'Bone mesenchymal stem cell-derived exosomal microRNA-7-5p inhibits progression of acute myeloid leukemia by targeting OSBPL11', *J Nanobiotechnology*, 20: 29.

Joshi, B. S., M. A. de Beer, B. N. G. Giepmans, and I. S. Zuhorn. 2020. 'Endocytosis of Extracellular Vesicles and Release of Their Cargo from Endosomes', *ACS Nano*, 14: 4444-55.

Kahlert, C., S. A. Melo, A. Protopopov, J. Tang, S. Seth, M. Koch, J. Zhang, J. Weitz, L. Chin, A. Futreal, and R. Kalluri. 2014. 'Identification of double-stranded genomic DNA spanning all chromosomes with mutated KRAS and p53 DNA in the serum exosomes of patients with pancreatic cancer', *J Biol Chem*, 289: 3869-75.

Kalluri, R., and V. S. LeBleu. 2020. 'The biology, function, and biomedical applications of exosomes', *Science*, 367.

Kanada, M., M. H. Bachmann, J. W. Hardy, D. O. Frimannson, L. Bronsart, A. Wang, M. D. Sylvester, T. L. Schmidt, R. L. Kaspar, M. J. Butte, A. C. Matin, and C. H. Contag. 2015. 'Differential fates of biomolecules delivered to target cells via extracellular vesicles', *Proc Natl Acad Sci U S A*, 112: E1433-42.

King, H. W., M. Z. Michael, and J. M. Gleadle. 2012. 'Hypoxic enhancement of exosome release by breast cancer cells', *BMC Cancer*, 12: 421.

Kitai, Y., T. Kawasaki, T. Sueyoshi, K. Kobiyama, K. J. Ishii, J. Zou, S. Akira, T. Matsuda, and T. Kawai. 2017. 'DNA-Containing Exosomes Derived from Cancer Cells Treated with Topotecan Activate a STING-Dependent Pathway and Reinforce Antitumor Immunity', *J Immunol*, 198: 1649-59.

Konig, L., S. Kasimir-Bauer, A. K. Bittner, O. Hoffmann, B. Wagner, L. F. Santos Manvailer, R. Kimmig, P. A. Horn, and V. Rebmann. 2017. 'Elevated levels of extracellular vesicles are associated with therapy failure and disease progression in breast cancer patients undergoing neoadjuvant chemotherapy', *Oncoimmunology*, 7: e1376153.

Kontopoulou, E., S. Strachan, K. Reinhardt, F. Kunz, C. Walter, B. Walkenfort, H. Jastrow, M. Hasenberg, B. Giebel, N. von Neuhoff, D. Reinhardt, and B. K. Thakur. 2020. 'Evaluation of dsDNA from extracellular vesicles (EVs) in pediatric AML diagnostics', *Ann Hematol*, 99: 459-75.

Kubbutat, M. H., S. N. Jones, and K. H. Vousden. 1997. 'Regulation of p53 stability by Mdm2', *Nature*, 387: 299-303.

Kumar, B., M. Garcia, J. L. Murakami, and C. C. Chen. 2016. 'Exosome-mediated microenvironment dysregulation in leukemia', *Biochim Biophys Acta*, 1863: 464-70.

Kumar, B., M. Garcia, L. Weng, X. Jung, J. L. Murakami, X. Hu, T. McDonald, A. Lin, A. R. Kumar, D. L. DiGiusto, A. S. Stein, V. A. Pullarkat, S. K. Hui, N. Carlesso, Y. H. Kuo, R. Bhatia, G. Marcucci, and C. C. Chen. 2018. 'Acute myeloid leukemia transforms the bone marrow niche into a leukemia-permissive microenvironment through exosome secretion', *Leukemia*, 32: 575-87.

Kunz, F., E. Kontopoulou, K. Reinhardt, M. Soldierer, S. Strachan, D. Reinhardt, and B. K. Thakur. 2019. 'Detection of AML-specific mutations in pediatric patient plasma using extracellular vesicle-derived RNA', *Ann Hematol*, 98: 595-603.

Lagunas-Rangel, F. A., V. Chavez-Valencia, M. A. Gomez-Guijosa, and C. Cortes-Penagos. 2017. 'Acute Myeloid Leukemia-Genetic Alterations and Their Clinical Prognosis', *Int J Hematol Oncol Stem Cell Res*, 11: 328-39.

Lai, C. P., E. Y. Kim, C. E. Badr, R. Weissleder, T. R. Mempel, B. A. Tannous, and X. O. Breakefield. 2015. 'Visualization and tracking of tumour extracellular vesicle delivery and RNA translation using multiplexed reporters', *Nat Commun*, 6: 7029.

Lazaro-Ibanez, E., C. Lasser, G. V. Shelke, R. Crescitelli, S. C. Jang, A. Cvjetkovic, A. Garcia-Rodriguez, and J. Lotvall. 2019. 'DNA analysis of low- and high-density fractions defines heterogeneous subpopulations of small extracellular vesicles based on their DNA cargo and topology', *J Extracell Vesicles*, 8: 1656993.

Lee, T. H., S. Chennakrishnaiah, E. Audemard, L. Montermini, B. Meehan, and J. Rak. 2014. 'Oncogenic ras-driven cancer cell vesiculation leads to emission of double-stranded DNA capable of interacting with target cells', *Biochem Biophys Res Commun*, 451: 295-301.

Lee, Y. R., G. Kim, W. Y. Tak, S. Y. Jang, Y. O. Kweon, J. G. Park, H. W. Lee, Y. S. Han, J. M. Chun, S. Y. Park, and K. Hur. 2019. 'Circulating exosomal noncoding RNAs as prognostic biomarkers in human hepatocellular carcinoma', *Int J Cancer*, 144: 1444-52.

Li, P., Y. Meng, Y. Wang, J. Li, M. Lam, L. Wang, and L. J. Di. 2019. 'Nuclear localization of Desmoplakin and its involvement in telomere maintenance', *Int J Biol Sci*, 15: 2350-62.

Liangsupree, T., E. Multia, and M. L. Riekkola. 2021. 'Modern isolation and separation techniques for extracellular vesicles', *J Chromatogr A*, 1636: 461773.

Lipner, Maxine. 2022. 'Acute and chronic myeloid leukemia', verywellhealth.

Liu, C., S. Yu, K. Zinn, J. Wang, L. Zhang, Y. Jia, J. C. Kappes, S. Barnes, R. P. Kimberly, W. E. Grizzle, and H. G. Zhang. 2006. 'Murine mammary carcinoma exosomes promote tumor growth by suppression of NK cell function', *J Immunol*, 176: 1375-85.

Liu, J., Y. Chen, F. Pei, C. Zeng, Y. Yao, W. Liao, and Z. Zhao. 2021. 'Extracellular Vesicles in Liquid Biopsies: Potential for Disease Diagnosis', *Biomed Res Int*, 2021: 6611244.

Liu, Y., S. E. Elf, T. Asai, Y. Miyata, Y. Liu, G. Sashida, G. Huang, S. Di Giandomenico, A. Koff, and S. D. Nimer. 2009. 'The p53 tumor suppressor protein is a critical regulator of hematopoietic stem cell behavior', *Cell Cycle*, 8: 3120-4.

Lobb, R. J., M. Becker, S. W. Wen, C. S. Wong, A. P. Wiegmans, A. Leimgruber, and A. Moller. 2015. 'Optimized exosome isolation protocol for cell culture supernatant and human plasma', *J Extracell Vesicles*, 4: 27031.

Logozzi, M., A. De Milito, L. Lugini, M. Borghi, L. Calabro, M. Spada, M. Perdicchio, M. L. Marino, C. Federici, E. Iessi, D. Brambilla, G. Venturi, F. Lozupone, M. Santinami, V. Huber, M. Maio, L. Rivoltini, and S. Fais. 2009. 'High levels of exosomes expressing CD63 and caveolin-1 in plasma of melanoma patients', *PLoS One*, 4: e5219.

Losche, W., T. Scholz, U. Temmler, V. Oberle, and R. A. Claus. 2004. 'Platelet-derived microvesicles transfer tissue factor to monocytes but not to neutrophils', *Platelets*, 15: 109-15.

Lotvall, J., and H. Valadi. 2007. 'Cell to cell signalling via exosomes through esRNA', *Cell Adh Migr*, 1: 156-8.

Maia, J., S. Caja, M. C. Strano Moraes, N. Couto, and B. Costa-Silva. 2018. 'Exosome-Based Cell-Cell Communication in the Tumor Microenvironment', *Front Cell Dev Biol*, 6: 18.

Maire, C. L., M. M. Fuh, K. Kaulich, K. D. Fita, I. Stevic, D. H. Heiland, J. A. Welsh, J. C. Jones, A. Gorgens, T. Ricklefs, L. Duhrsen, T. Sauvigny, S. A. Joosse, G. Reifenberger, K. Pantel, M. Glatzel, A. G. Miklosi, J. H. Felce, M. Caselli, V. Pereno, R. Reimer, H. Schluter, M. Westphal, U. Schuller, K. Lamszus, and F. L. Ricklefs. 2021. 'Genome-wide methylation profiling of glioblastoma cell-derived extracellular vesicle DNA allows tumor classification', *Neuro Oncol*.

Matsumoto, A., Y. Takahashi, M. Nishikawa, K. Sano, M. Morishita, C. Charoenviriyakul, H. Saji, and Y. Takakura. 2017. 'Accelerated growth of B16BL6 tumor in mice through efficient uptake of their own exosomes by B16BL6 cells', *Cancer Sci*, 108: 1803-10.

McKelvey, K. J., K. L. Powell, A. W. Ashton, J. M. Morris, and S. A. McCracken. 2015. 'Exosomes: Mechanisms of Uptake', *J Circ Biomark*, 4: 7.

Menard, J. A., M. Cerezo-Magana, and M. Belting. 2018. 'Functional role of extracellular vesicles and lipoproteins in the tumour microenvironment', *Philos Trans R Soc Lond B Biol Sci*, 373.

Michalski, S., C. C. de Oliveira Mann, C. A. Stafford, G. Witte, J. Bartho, K. Lammens, V. Hornung, and K. P. Hopfner. 2020. 'Structural basis for sequestration and autoinhibition of cGAS by chromatin', *Nature*, 587: 678-82.

Mittelbrunn, M., C. Gutierrez-Vazquez, C. Villarroya-Beltri, S. Gonzalez, F. Sanchez-Cabo, M. A. Gonzalez, A. Bernad, and F. Sanchez-Madrid. 2011. 'Unidirectional transfer of microRNA-loaded exosomes from T cells to antigen-presenting cells', *Nat Commun*, 2: 282.

Motwani, M., S. Pesiridis, and K. A. Fitzgerald. 2019. 'DNA sensing by the cGAS-STING pathway in health and disease', *Nat Rev Genet*, 20: 657-74.

Muller, L., C. S. Hong, D. B. Stolz, S. C. Watkins, and T. L. Whiteside. 2014. 'Isolation of biologically-active exosomes from human plasma', *J Immunol Methods*, 411: 55-65.

Nahi, H., S. Lehmann, S. Bengtzen, M. Jansson, L. Mollgard, C. Paul, and M. Merup. 2008. 'Chromosomal aberrations in 17p predict in vitro drug resistance and short overall survival in acute myeloid leukemia', *Leuk Lymphoma*, 49: 508-16.

Namburi, S., H. E. Broxmeyer, C. S. Hong, T. L. Whiteside, and M. Boyiadzis. 2021. 'DPP4(+) exosomes in AML patients' plasma suppress proliferation of hematopoietic progenitor cells', *Leukemia*, 35: 1925-32.

Nazarenko, I., S. Rana, A. Baumann, J. McAlear, A. Hellwig, M. Trendelenburg, G. Lochnit, K. T. Preissner, and M. Zoller. 2010. 'Cell surface tetraspanin Tspan8 contributes to molecular pathways of exosome-induced endothelial cell activation', *Cancer Res*, 70: 1668-78.

Ozaki, T., and A. Nakagawara. 2011. 'Role of p53 in Cell Death and Human Cancers', *Cancers (Basel)*, 3: 994-1013.

Pan, B. T., and R. M. Johnstone. 1983. 'Fate of the transferrin receptor during maturation of sheep reticulocytes in vitro: selective externalization of the receptor', *Cell*, 33: 967-78.

Patel, G. K., M. A. Khan, A. Bhardwaj, S. K. Srivastava, H. Zubair, M. C. Patton, S. Singh, M. Khushman, and A. P. Singh. 2017. 'Exosomes confer chemoresistance to pancreatic cancer cells by promoting ROS detoxification and miR-155-mediated suppression of key gemcitabine-metabolising enzyme, DCK', *Br J Cancer*, 116: 609-19.

Pimenta, D. B., V. A. Varela, T. S. Datoguia, V. B. Caraciolo, G. H. Lopes, and W. O. Pereira. 2021. 'The Bone Marrow Microenvironment Mechanisms in Acute Myeloid Leukemia', *Front Cell Dev Biol*, 9: 764698.

Pulliero, A., L. Pergoli, L. A. Maestra S, R. T. Micale, A. Camoirano, V. Bollati, A. Izzotti, and D. E. Flora S. 2019. 'Extracellular vesicles in biological fluids. A biomarker of exposure to cigarette smoke and treatment with chemopreventive drugs', *J Prev Med Hyg*, 60: E327-E36.

Qin, X., S. Yu, L. Zhou, M. Shi, Y. Hu, X. Xu, B. Shen, S. Liu, D. Yan, and J. Feng. 2017. 'Cisplatin-resistant lung cancer cell-derived exosomes increase cisplatin resistance of recipient cells in exosomal miR-100-5p-dependent manner', *Int J Nanomedicine*, 12: 3721-33.

Qu, J. L., X. J. Qu, M. F. Zhao, Y. E. Teng, Y. Zhang, K. Z. Hou, Y. H. Jiang, X. H. Yang, and Y. P. Liu. 2009. 'Gastric cancer exosomes promote tumour cell proliferation through PI3K/Akt and MAPK/ERK activation', *Dig Liver Dis*, 41: 875-80.

Quintas-Cardama, A., C. Hu, A. Qutub, Y. H. Qiu, X. Zhang, S. M. Post, N. Zhang, K. Coombes, and S. M. Kornblau. 2017. 'p53 pathway dysfunction is highly prevalent in acute myeloid leukemia independent of TP53 mutational status', *Leukemia*, 31: 1296-305.

Raimondo, S., L. Saieva, C. Corrado, S. Fontana, A. Flugy, A. Rizzo, G. De Leo, and R. Alessandro. 2015. 'Chronic myeloid leukemia-derived exosomes promote tumor growth through an autocrine mechanism', *Cell Commun Signal*, 13: 8.

Ramos-Garcia, V., I. Ten-Domenech, A. Albiach-Delgado, M. Gomez-Ferrer, P. Sepulveda, A. Parra-Llorca, L. Campos-Berga, A. Moreno-Gimenez, G. Quintas, and J. Kuligowski. 2023. 'Isolation and Lipidomic Screening of Human Milk Extracellular Vesicles', *Methods Mol Biol*, 2571: 177-88.

Raposo, G., and W. Stoorvogel. 2013. 'Extracellular vesicles: exosomes, microvesicles, and friends', *J Cell Biol*, 200: 373-83.

Rappa, G., M. F. Santos, T. M. Green, J. Karbanova, J. Hassler, Y. Bai, S. H. Barsky, D. Corbeil, and A. Lorico. 2017. 'Nuclear transport of cancer extracellular vesicle-derived

biomaterials through nuclear envelope invagination-associated late endosomes', *Oncotarget*, 8: 14443-61.

Recher, C. 2021. 'Clinical Implications of Inflammation in Acute Myeloid Leukemia', *Front Oncol*, 11: 623952.

Reinhardt, D., E. Antoniou, and K. Waack. 2022. 'Pediatric Acute Myeloid Leukemia-Past, Present, and Future', *J Clin Med*, 11.

Rubnitz, J. E., B. Gibson, and F. O. Smith. 2010. 'Acute myeloid leukemia', *Hematol Oncol Clin North Am*, 24: 35-63.

Sansone, P., C. Savini, I. Kurelac, Q. Chang, L. B. Amato, A. Strillacci, A. Stepanova, L. Iommarini, C. Mastroleo, L. Daly, A. Galkin, B. K. Thakur, N. Soplop, K. Uryu, A. Hoshino, L. Norton, M. Bonafe, M. Cricca, G. Gasparre, D. Lyden, and J. Bromberg. 2017. 'Packaging and transfer of mitochondrial DNA via exosomes regulate escape from dormancy in hormonal therapy-resistant breast cancer', *Proc Natl Acad Sci U S A*, 114: E9066-E75.

Schepers, K., E. M. Pietras, D. Reynaud, J. Flach, M. Binnewies, T. Garg, A. J. Wagers, E. C. Hsiao, and E. Passegue. 2013. 'Myeloproliferative neoplasia remodels the endosteal bone marrow niche into a self-reinforcing leukemic niche', *Cell Stem Cell*, 13: 285-99.

Seifert, H., B. Mohr, C. Thiede, U. Oelschlagel, U. Schakel, T. Illmer, S. Soucek, G. Ehninger, M. Schaich, and Leukemia Study Alliance. 2009. 'The prognostic impact of 17p (p53) deletion in 2272 adults with acute myeloid leukemia', *Leukemia*, 23: 656-63.

Sendker, S., K. Waack, and D. Reinhardt. 2021. 'Far from Health: The Bone Marrow Microenvironment in AML, A Leukemia Supportive Shelter', *Children (Basel)*, 8.

Shu, S., Y. Yang, C. L. Allen, E. Hurley, K. H. Tung, H. Minderman, Y. Wu, and M. S. Ernstoff. 2020. 'Purity and yield of melanoma exosomes are dependent on isolation method', *J Extracell Vesicles*, 9: 1692401.

Sidhom, K., P. O. Obi, and A. Saleem. 2020. 'A Review of Exosomal Isolation Methods: Is Size Exclusion Chromatography the Best Option?', *Int J Mol Sci*, 21.

Sison, E. A., and P. Brown. 2011. 'The bone marrow microenvironment and leukemia: biology and therapeutic targeting', *Expert Rev Hematol*, 4: 271-83.

Song, S., Y. Zhang, T. Ding, N. Ji, and H. Zhao. 2020. 'The Dual Role of Macropinocytosis in Cancers: Promoting Growth and Inducing Methuosis to Participate in Anticancer Therapies as Targets', *Front Oncol*, 10: 570108.

Soyfer, E. M., and A. G. Fleischman. 2021. 'Inflammation in Myeloid Malignancies: From Bench to Bedside', *J Immunother Precis Oncol*, 4: 160-67.

Stahl, A. L., K. Johansson, M. Mossberg, R. Kahn, and D. Karpman. 2019. 'Exosomes and microvesicles in normal physiology, pathophysiology, and renal diseases', *Pediatr Nephrol*, 34: 11-30.

Szczepanski, M. J., M. Szajnik, A. Welsh, T. L. Whiteside, and M. Boyiadzis. 2011. 'Blast-derived microvesicles in sera from patients with acute myeloid leukemia suppress natural killer cell function via membrane-associated transforming growth factor-beta1', *Haematologica*, 96: 1302-9.

Takahashi, A., R. Okada, K. Nagao, Y. Kawamata, A. Hanyu, S. Yoshimoto, M. Takasugi, S. Watanabe, M. T. Kanemaki, C. Obuse, and E. Hara. 2017. 'Exosomes maintain cellular homeostasis by excreting harmful DNA from cells', *Nat Commun*, 8: 15287.

Thakur, B. K., H. Zhang, A. Becker, I. Matei, Y. Huang, B. Costa-Silva, Y. Zheng, A. Hoshino, H. Brazier, J. Xiang, C. Williams, R. Rodriguez-Barrueco, J. M. Silva, W. Zhang, S. Hearn, O. Elemento, N. Paknejad, K. Manova-Todorova, K. Welte, J. Bromberg, H. Peinado, and D. Lyden. 2014. 'Double-stranded DNA in exosomes: a novel biomarker in cancer detection', *Cell Res*, 24: 766-9.

Thery, C., S. Amigorena, G. Raposo, and A. Clayton. 2006. 'Isolation and characterization of exosomes from cell culture supernatants and biological fluids', *Curr Protoc Cell Biol*, Chapter 3: Unit 3 22.

Thery, C., K. W. Witwer, E. Aikawa, M. J. Alcaraz, J. D. Anderson, R. Andriantsitohaina, A. Antoniou, T. Arab, F. Archer, G. K. Atkin-Smith, D. C. Ayre, J. M. Bach, D. Bachurski, H. Baharvand, L. Balaj, S. Baldacchino, N. N. Bauer, A. A. Baxter, M. Bebawy, C. Beckham, A. Bedina Zavec, A. Benmoussa, A. C. Berardi, P. Bergese, E. Bielska, C. Blenkiron, S. Bobis-Wozowicz, E. Boilard, W. Boireau, A. Bongiovanni, F. E. Borras, S. Bosch, C. M. Boulanger, X. Breakefield, A. M. Breglio, M. A. Brennan, D. R. Brigstock, A. Brisson, M. L. Broekman, J. F. Bromberg, P. Bryl-Gorecka, S. Buch, A. H. Buck, D. Burger, S. Busatto, D. Buschmann, B. Bussolati, E. I. Buzas, J. B. Byrd, G. Camussi, D. R. Carter, S. Caruso, L. W. Chamley, Y. T. Chang, C. Chen, S. Chen, L. Cheng, A. R. Chin, A. Clayton, S. P. Clerici, A. Cocks, E. Cocucci, R. J. Coffey, A. Cordeiro-da-Silva, Y. Couch, F. A. Coumans, B. Coyle, R. Crescitelli, M. F. Criado, C. D'Souza-Schorey, S. Das, A. Datta Chaudhuri, P. de Candia, E. F. De Santana, O. De Wever, H. A. Del Portillo, T. Demaret, S. Deville, A. Devitt, B. Dhondt, D. Di Vizio, L. C. Dieterich, V. Dolo, A. P. Dominguez Rubio, M. Dominici, M. R. Dourado, T. A. Driedonks, F. V. Duarte, H. M. Duncan, R. M. Eichenberger, K. Ekstrom, S. El Andaloussi, C. Elie-Caille, U. Erdbrugger, J. M. Falcon-Perez, F. Fatima, J. E. Fish, M. Flores-Bellver, A. Forsonits, A. Frelet-Barrand, F. Fricke, G. Fuhrmann, S. Gabrielsson, A. Gamez-Valero, C. Gardiner, K. Gartner, R. Gaudin, Y. S. Gho, B. Giebel, C. Gilbert, M. Gimona, I. Giusti, D. C. Goberdhan, A. Gorgens, S. M. Gorski, D. W. Greening, J. C. Gross, A. Gualerzi, G. N. Gupta, D. Gustafson, A. Handberg, R. A. Haraszti, P. Harrison, H. Hegyesi, A. Hendrix, A. F. Hill, F. H. Hochberg, K. F. Hoffmann, B. Holder, H. Holthofer, B. Hosseinkhani, G. Hu, Y. Huang, V. Huber, S. Hunt, A. G. Ibrahim, T. Ikezu, J. M. Inal, M. Isin, A. Ivanova, H. K. Jackson, S. Jacobsen, S. M. Jay, M. Jayachandran, G. Jenster, L. Jiang, S. M. Johnson, J. C. Jones, A. Jong, T. Jovanovic-Talisman, S. Jung, R. Kalluri, S. I. Kano, S. Kaur, Y. Kawamura, E. T. Keller, D. Khamari, E. Khomyakova, A. Khvorova, P. Kierulf, K. P. Kim, T. Kislinger, M. Klingeborn, D. J. Klinke, 2nd, M. Kornek, M. M. Kosanovic, A. F. Kovacs, E. M. Kramer-Albers, S. Krasemann, M. Krause, I. V. Kurochkin, G. D. Kusuma, S. Kuypers, S. Laitinen, S. M. Langevin, L. R. Languino, J. Lannigan, C. Lasser, L. C. Laurent, G. Lavieu, E. Lazaro-Ibanez, S. Le Lay, M. S. Lee, Y. X. F. Lee, D. S. Lemos, M. Lenassi, A. Leszczynska, I. T. Li, K. Liao, S. F. Libregts, E. Ligeti, R. Lim, S. K. Lim, A. Line, K. Linnemannstons, A. Llorente, C. A. Lombard, M. J. Lorenowicz, A. M. Lorincz, J. Lotvall, J. Lovett, M. C. Lowry, X. Loyer, Q. Lu, B. Lukomska, T. R. Lunavat, S. L. Maas, H. Malhi, A. Marcilla, J. Mariani, J. Mariscal, E. S. Martens-Uzunova, L. Martin-Jaular, M. C. Martinez, V. R. Martins, M. Mathieu, S. Mathivanan, M. Maugeri, L. K. McGinnis, M. J. McVey, D. G. Meckes, Jr., K. L. Meehan, I. Mertens, V. R. Minciacchi, A. Moller, M. Moller Jorgensen, A. Morales-Kastresana, J. Morhayim, F. Mullier, M.

Muraca, L. Musante, V. Mussack, D. C. Muth, K. H. Myburgh, T. Najrana, M. Nawaz, I. Nazarenko, P. Nejsum, C. Neri, T. Neri, R. Nieuwland, L. Nimrichter, J. P. Nolan, E. N. Nolte-'t Hoen, N. Noren Hooten, L. O'Driscoll, T. O'Grady, A. O'Loghlen, T. Ochiya, M. Olivier, A. Ortiz, L. A. Ortiz, X. Osteikoetxea, O. Ostergaard, M. Ostrowski, J. Park, D. M. Pegtel, H. Peinado, F. Perut, M. W. Pfaffl, D. G. Phinney, B. C. Pieters, R. C. Pink, D. S. Pisetsky, E. Pogge von Strandmann, I. Polakovicova, I. K. Poon, B. H. Powell, I. Prada, L. Pulliam, P. Quesenberry, A. Radeghieri, R. L. Raffai, S. Raimondo, J. Rak, M. I. Ramirez, G. Raposo, M. S. Rayyan, N. Regev-Rudzki, F. L. Ricklefs, P. D. Robbins, D. D. Roberts, S. C. Rodrigues, E. Rohde, S. Rome, K. M. Rouschop, A. Rughetti, A. E. Russell, P. Saa, S. Sahoo, E. Salas-Huenuleo, C. Sanchez, J. A. Saugstad, M. J. Saul, R. M. Schiffelers, R. Schneider, T. H. Schoyen, A. Scott, E. Shahaj, S. Sharma, O. Shatnyeva, F. Shekari, G. V. Shelke, A. K. Shetty, K. Shiba, P. R. Siljander, A. M. Silva, A. Skowronek, O. L. Snyder, 2nd, R. P. Soares, B. W. Sodar, C. Soekmadji, J. Sotillo, P. D. Stahl, W. Stoorvogel, S. L. Stott, E. F. Strasser, S. Swift, H. Tahara, M. Tewari, K. Timms, S. Tiwari, R. Tixeira, M. Tkach, W. S. Toh, R. Tomasini, A. C. Torrecilhas, J. P. Tosar, V. Toxavidis, L. Urbanelli, P. Vader, B. W. van Balkom, S. G. van der Grein, J. Van Deun, M. J. van Herwijnen, K. Van Keuren-Jensen, G. van Niel, M. E. van Royen, A. J. van Wijnen, M. H. Vasconcelos, I. J. Vechetti, Jr., T. D. Veit, L. J. Vella, E. Velot, F. J. Verweij, B. Vestad, J. L. Vinas, T. Visnovitz, K. V. Vukman, J. Wahlgren, D. C. Watson, M. H. Wauben, A. Weaver, J. P. Webber, V. Weber, A. M. Wehman, D. J. Weiss, J. A. Welsh, S. Wendt, A. M. Wheelock, Z. Wiener, L. Witte, J. Wolfram, A. Xagorari, P. Xander, J. Xu, X. Yan, M. Yanez-Mo, H. Yin, Y. Yuana, V. Zappulli, J. Zarubova, V. Zekas, J. Y. Zhang, Z. Zhao, L. Zheng, A. R. Zheutlin, A. M. Zickler, P. Zimmermann, A. M. Zivkovic, D. Zocco, and E. K. Zuba-Surma. 2018. 'Minimal information for studies of extracellular vesicles 2018 (MISEV2018): a position statement of the International Society for Extracellular Vesicles and update of the MISEV2014 guidelines', *J Extracell Vesicles*, 7: 1535750.

Tian, T., Y. L. Zhu, Y. Y. Zhou, G. F. Liang, Y. Y. Wang, F. H. Hu, and Z. D. Xiao. 2014. 'Exosome uptake through clathrin-mediated endocytosis and macropinocytosis and mediating miR-21 delivery', *J Biol Chem*, 289: 22258-67.

Tian, Y., M. Gong, Y. Hu, H. Liu, W. Zhang, M. Zhang, X. Hu, D. Aubert, S. Zhu, L. Wu, and X. Yan. 2020. 'Quality and efficiency assessment of six extracellular vesicle isolation methods by nano-flow cytometry', *J Extracell Vesicles*, 9: 1697028.

Torralba, D., F. Baixauli, C. Villarroya-Beltri, I. Fernandez-Delgado, A. Latorre-Pellicer, R. Acin-Perez, N. B. Martin-Cofreces, A. L. Jaso-Tamame, S. Iborra, I. Jorge, G. Gonzalez-Aseguinolaza, J. Garaude, M. Vicente-Manzanares, J. A. Enriquez, M. Mittelbrunn, and F. Sanchez-Madrid. 2018. 'Priming of dendritic cells by DNA-containing extracellular vesicles from activated T cells through antigen-driven contacts', *Nat Commun*, 9: 2658.

Tsilioni, I., and T. C. Theoharides. 2018. 'Extracellular vesicles are increased in the serum of children with autism spectrum disorder, contain mitochondrial DNA, and stimulate human microglia to secrete IL-1beta', *J Neuroinflammation*, 15: 239.

Umezu, T., H. Tadokoro, K. Azuma, S. Yoshizawa, K. Ohyashiki, and J. H. Ohyashiki. 2014. 'Exosomal miR-135b shed from hypoxic multiple myeloma cells enhances angiogenesis by targeting factor-inhibiting HIF-1', *Blood*, 124: 3748-57.

Vaidya, M., M. Bacchus, and K. Sugaya. 2018. 'Differential sequences of exosomal NANOG DNA as a potential diagnostic cancer marker', *PLoS One*, 13.

Valadi, H., K. Ekstrom, A. Bossios, M. Sjostrand, J. J. Lee, and J. O. Lotvall. 2007. 'Exosome-mediated transfer of mRNAs and microRNAs is a novel mechanism of genetic exchange between cells', *Nat Cell Biol*, 9: 654-9.

Waclawiczek, A., A. Hamilton, K. Rouault-Pierre, A. Abarrategi, M. G. Albornoz, F. Miraki-Moud, N. Bah, J. Gribben, J. Fitzgibbon, D. Taussig, and D. Bonnet. 2020. 'Mesenchymal niche remodeling impairs hematopoiesis via stanniocalcin 1 in acute myeloid leukemia', *J Clin Invest*, 130: 3038-50.

Waldenstrom, A., N. Genneback, U. Hellman, and G. Ronquist. 2012. 'Cardiomyocyte microvesicles contain DNA/RNA and convey biological messages to target cells', *PLoS One*, 7: e34653.

Willms, E., C. Cabanas, I. Mager, M. J. A. Wood, and P. Vader. 2018. 'Extracellular Vesicle Heterogeneity: Subpopulations, Isolation Techniques, and Diverse Functions in Cancer Progression', *Front Immunol*, 9: 738.

Wollert, T., and J. H. Hurley. 2010. 'Molecular mechanism of multivesicular body biogenesis by ESCRT complexes', *Nature*, 464: 864-9.

Wu, M., C. Chen, Z. Wang, H. Bachman, Y. Ouyang, P. H. Huang, Y. Sadovsky, and T. J. Huang. 2019. 'Separating extracellular vesicles and lipoproteins via acoustofluidics', *Lab Chip*, 19: 1174-82.

Xavier, C. P. R., H. R. Caires, M. A. G. Barbosa, R. Bergantim, J. E. Guimaraes, and M. H. Vasconcelos. 2020. 'The Role of Extracellular Vesicles in the Hallmarks of Cancer and Drug Resistance', *Cells*, 9.

Xia, C., Z. Braunstein, A. C. Toomey, J. Zhong, and X. Rao. 2017. 'S100 Proteins As an Important Regulator of Macrophage Inflammation', *Front Immunol*, 8: 1908.

Xu, J., R. Camfield, and S. M. Gorski. 2018. 'The interplay between exosomes and autophagy - partners in crime', *J Cell Sci*, 131.

Yanez-Mo, M., P. R. Siljander, Z. Andreu, A. B. Zavec, F. E. Borras, E. I. Buzas, K. Buzas, E. Casal, F. Cappello, J. Carvalho, E. Colas, A. Cordeiro-da Silva, S. Fais, J. M. Falcon-Perez, I. M. Ghobrial, B. Giebel, M. Gimona, M. Graner, I. Gursel, M. Gursel, N. H. Heegaard, A. Hendrix, P. Kierulf, K. Kokubun, M. Kosanovic, V. Kralj-Iglic, E. M. Kramer-Albers, S. Laitinen, C. Lasser, T. Lener, E. Ligeti, A. Line, G. Lipps, A. Llorente, J. Lotvall, M. Mancek-Keber, A. Marcilla, M. Mittelbrunn, I. Nazarenko, E. N. Nolte-'t Hoen, T. A. Nyman, L. O'Driscoll, M. Olivan, C. Oliveira, E. Pallinger, H. A. Del Portillo, J. Reventos, M. Rigau, E. Rohde, M. Sammar, F. Sanchez-Madrid, N. Santarem, K. Schallmoser, M. S. Ostenfeld, W. Stoorvogel, R. Stukelj, S. G. Van der Grein, M. H. Vasconcelos, M. H. Wauben, and O. De Wever. 2015. 'Biological properties of extracellular vesicles and their physiological functions', *J Extracell Vesicles*, 4: 27066.

Yao, Y., F. Li, J. Huang, J. Jin, and H. Wang. 2021. 'Leukemia stem cell-bone marrow microenvironment interplay in acute myeloid leukemia development', *Exp Hematol Oncol*, 10: 39.

Yu, D., Y. Li, M. Wang, J. Gu, W. Xu, H. Cai, X. Fang, and X. Zhang. 2022. 'Exosomes as a new frontier of cancer liquid biopsy', *Mol Cancer*, 21: 56.

Zaborowski, M. P., L. Balaj, X. O. Breakefield, and C. P. Lai. 2015. 'Extracellular Vesicles: Composition, Biological Relevance, and Methods of Study', *Bioscience*, 65: 783-97.

Zebrowska, A., A. Skowronek, A. Wojakowska, P. Widlak, and M. Pietrowska. 2019. 'Metabolome of Exosomes: Focus on Vesicles Released by Cancer Cells and Present in Human Body Fluids', *Int J Mol Sci*, 20.

Zeng, Y. L., Z. Y. Guo, H. Z. Su, F. D. Zhong, K. Q. Jiang, and G. D. Yuan. 2019. 'Diagnostic and prognostic value of lncRNA cancer susceptibility candidate 9 in hepatocellular carcinoma', *World J Gastroenterol*, 25: 6902-15.

Zhang, H., D. Freitas, H. S. Kim, K. Fabijanic, Z. Li, H. Chen, M. T. Mark, H. Molina, A. B. Martin, L. Bojmar, J. Fang, S. Rampersaud, A. Hoshino, I. Matei, C. M. Kenific, M. Nakajima, A. P. Mutvei, P. Sansone, W. Buehring, H. Wang, J. P. Jimenez, L. Cohen-Gould, N. Paknejad, M. Brendel, K. Manova-Todorova, A. Magalhaes, J. A. Ferreira, H. Osorio, A. M. Silva, A. Massey, J. R. Cubillos-Ruiz, G. Galletti, P. Giannakakou, A. M. Cuervo, J. Blenis, R. Schwartz, M. S. Brady, H. Peinado, J. Bromberg, H. Matsui, C. A. Reis, and D. Lyden. 2018. 'Identification of distinct nanoparticles and subsets of extracellular vesicles by asymmetric flow field-flow fractionation', *Nat Cell Biol*, 20: 332-43.

Zhang, Q., D. K. Jeppesen, J. N. Higginbotham, R. Graves-Deal, V. Q. Trinh, M. A. Ramirez, Y. Sohn, A. C. Neininger, N. Taneja, E. T. McKinley, H. Niitsu, Z. Cao, R. Evans, S. E. Glass, K. C. Ray, W. H. Fissell, S. Hill, K. L. Rose, W. J. Huh, M. K. Washington, G. D. Ayers, D. T. Burnette, S. Sharma, L. H. Rome, J. L. Franklin, Y. A. Lee, Q. Liu, and R. J. Coffey. 2021. 'Supermeres are functional extracellular nanoparticles replete with disease biomarkers and therapeutic targets', *Nat Cell Biol*, 23: 1240-54.

Zhang, Y., Y. Liu, H. Liu, and W. H. Tang. 2019. 'Exosomes: biogenesis, biologic function and clinical potential', *Cell Biosci*, 9: 19.

Zhao, Z., J. Zuber, E. Diaz-Flores, L. Lintault, S. C. Kogan, K. Shannon, and S. W. Lowe. 2010. 'p53 loss promotes acute myeloid leukemia by enabling aberrant self-renewal', *Genes Dev*, 24: 1389-402.

Zhong, F. M., F. Y. Yao, J. Liu, H. B. Zhang, M. Y. Li, J. Y. Jiang, Y. M. Xu, W. M. Yang, S. Q. Li, J. Zhang, Y. Cheng, S. Xu, B. Huang, and X. Z. Wang. 2022. 'Inflammatory response mediates cross-talk with immune function and reveals clinical features in acute myeloid leukemia', *Biosci Rep*, 42.

The curriculum vitae is not included in the online version for data protection reasons.

Declaration:

In accordance with § 6 (para. 2, clause g) of the Regulations Governing the Doctoral Proceedings of the Faculty of Biology for awarding the doctoral degree Dr. rer. nat., I hereby declare that I represent the field to which the topic *"Functional role of small extracellular vesicles associated DNA and chromatin in pediatric acute myeloid leukemia (AML)"* is assigned in research and teaching and that I support the application of *Mr. Venkatesh Kumar Chetty.*

Essen, date 12|12|2022 PD.Dr.Basant Kumar Thakur

Name of the scientific	Signature of the supervisor/
supervisor/member of the	member of the University of Duisburg-Essen
University of Duisburg-Essen	

Declaration:

In accordance with § 7 (para. 2, clause d and f) of the Regulations Governing the Doctoral Proceedings of the Faculty of Biology for awarding the doctoral degree Dr. rer. nat., I hereby declare that I have written the herewith submitted dissertation independently using only the materials listed, and have cited all sources taken over verbatim or in content as such.

Essen, date 12|12|2022

Signature of the doctoral candidate

Declaration:

In accordance with § 7 (para. 2, clause e and g) of the Regulations Governing the Doctoral Proceedings of the Faculty of Biology for awarding the doctoral degree Dr. rer. nat., I hereby declare that I have undertaken no previous attempts to attain a doctoral degree, that the current work has not been rejected by any other faculty, and that I am submitting the dissertation only in this procedure.

Essen, date 12|12|2022

Signature of the doctoral candidate